UNIVERSITA' DEGLI STUDI DI PADOVA

Dipartimento di Scienze Chimiche

Dottorato di Ricerca in Scienze Chimiche

XX CICLO

3_{10}-HELICAL PEPTIDES AS SPACERS AND TEMPLATES FOR SPECTROSCOPIC STUDIES AND ORGANIC SYNTHESES

Coordinatore: Ch.mo Prof. Maurizio Casarin

Supervisore: Ch.mo Prof. Fernando Formaggio

Dottorando: Ivan Guryanov

31 gennaio 2008

INDEX

RIASSUNTO

Per comprendere in dettaglio sistemi naturali molto complicati, con diverse relazioni inter- ed intramolecolari, oppure per creare nuovi nanosistemi con proprietà di riconoscimento molecolare e conservazione d'informazione è necessario poter progettare e sintetizzare molecole modello di complessità ridotta, con struttura tridimensionale ben definita. In questa Tesi di Dottorato è stato deciso di applicare la capacità degli α-amminoacidi C^{α}-tetrasostituiti di formare strutture peptidiche 3_{10}-elicoidali particolarmente stabili, al fine di poter progettare templati e spaziatori rigidi per studi spettroscopici e fotofisici e per applicazioni in sintesi organica.

1. Peptidi 3_{10}-elicoidali come templati per studi fotofisici

In questa parte del lavoro è stata studiata l'influenza del dipolo macroscopico dell'elica peptidica 3_{10} sul trasferimento elettronico tra i cromofori azulenico e pirenico, cambiando la loro posizione nella sequenza. I nostri studi fotofisici hanno mostrato la notevole differenza sia del tempo di vita dello stato eccitato ché dell'efficienza del quenching. Questi dati indicano che il momento del dipolo dell'elica 3_{10} potrebbe effettivamente influenzare la velocità del trasferimento elettronico. Se il trasferimento elettronico va in direzione opposta a quella del momento del dipolo, l'efficienza del quenching aumenta e la vita dello stato eccitato diminuisce. Studi di questo tipo possono anche aiutare a comprendere i processi primari coinvolti nella fotosintesi.

2. Peptidi 3_{10}-elicoidali come spaziatori per studi spettroscopici CD

Un problema importante degli studi delle conformazioni dei biopolimeri è lo sviluppo di nuovi metodi per determinare accuratamente la loro struttura 3D e la conseguente disposizione relativa di eventuali sonde presenti in tali biopolimeri. A tale scopo la spettroscopia CD basata sul fenomeno dell'*exciton coupling* di opportuni cromofori, come ad esempio le porfirine, è una tecnica sensibile e molto promettente. In questo lavoro abbiamo esaminato con tale tecnica spettroscopica una serie di sette sistemi molecolari, progettati e sintetizzati in modo da contenere due unità porfiriniche legate covalentemente alle estremità di spaziatori peptidici rigidi (formanti β-turn o strutture 3_{10}-elicoidali). E' stato mostrato che non solo la distanza, ma anche l'orientamento tra le

direzioni dei momenti di transizione di due cromofori influenza l'intensità del segnale dicroico di *exciton coupling*.

3. Peptidi 3_{10}-elicoidali per studi di assorbimento IR

La spettroscopia di assorbimento IR di peptidi e proteine isotopicamente marcate è un metodo estremamente efficace per studiare la loro conformazione e le loro eventuali transizioni strutturali. Abbiamo mostrato l'utilità di questo metodo per indagare l'elica peptidica 3_{10}. E' stata sintetizzata una serie di esapeptidi contenenti due gruppi carbossilici vicinali marcati con ^{13}C al C carbonilico. Per confronto, sono stati preparati anche i corrispondenti peptidi non marcati isotopicamente. Nell'elica 3_{10} formata da tali peptidi abbiamo potuto distinguere la banda ammide I del residuo marcato da quella degli altri residui. Questo dato dimostra l'utilità della marcatura isotopica per identificare selettivamente il comportamento di una singola unità ammidica.

4. Peptidi 3_{10}-elicoidali come templati per sintesi organiche (*ring-closing metathesis* intramolecolare)

Un'altra parte del lavoro è stata dedicata a peptidi 3_{10}-elicoidali in grado di fungere da templati per sintesi organiche. La stabilità della struttura secondaria è stata aumentata mediante un *molecular stapler* (un catalizzatore della metatesi olefinica basato sul rutenio), che ha consentito di collegare covalentemente e intramolecolarmente due ripiegamenti dell'elica. Abbiamo mostrato usando le tecniche di cristallografia ai raggi X, CD e NMR che la struttura secondaria elicoidale rimane pressoché intatta anche dopo ciclizzazione. Per indagare l'influenza della posizione dei residui coinvolti nella reazione di ciclizzazione e per bloccare in una conformazione 3_{10}-elicoidale anche i peptidi contenenti amminoacidi proteici, sono stati sintetizzati tre peptidi basati sia su Aib ché su Ala, aventi due residui di hhMag in diverse posizioni reciproche lungo la catena. I risultati ottenuti confermano l'importanza di avere una giusta disposizione spaziale delle catene olefiniche sottoposte alla reazione di metatesi. Inoltre, viene anche confermata l'adozione di strutture elcoidali 3_{10} da parte dei peptidi sintetizzati, in quanto solo quelli con i due gruppi allilici nelle posizioni $i \rightarrow i+3$ (l'uno sopra l'altro ad un giro d'elica) sono in grado di chiudere covalentemente un ciclo mediante reazione di metatesi tra le due catene alliliche. Si è anche osservata la formazione di dimeri in

peptidi ricchi di Aib, forse a motivo dell'ingombro sterico e della notevole rigidità di tali strutture elicoidali.

ABSTRACT

In order to understand in detail very complex natural systems with different inter- and intramolecular interactions and to create nanosystems with the new properties of molecular recognition and information storage, it is often necessary to design model compounds of reduced complexity with well defined geometry. In this Ph.D. thesis it was decided to apply the property of C^{α}-tetrasubstituted α-amino acids to form particularly stable, peptide 3_{10}-helical structures for the design of rigid templates and spacers for different spectroscopic and photophysical studies as well as for organic syntheses.

1. 3_{10}-Helical peptides as templates for photophysical studies

In this part of the work the influence of the macroscopic dipole of the peptide 3_{10}-helix on the electron transfer between the azulene and pyrene chromophoric moieties, by exchanging their place in the sequence, was investigated. Our photophysical study showed a noticeable difference both in the life time of the excited state and in the quenching efficiency. This finding seems to indicate that the dipole moment of the 3_{10}-helix might indeed influence the electron transfer rate. When the electron transfer takes place in a direction that is opposite to that of the dipole moment, the quenching efficiency becomes higher and the lifetime of the excited state decreases. Such experiments can give valuable information on our understanding of the primary processes which take place during photosynthesis.

2. 3_{10}-Helical peptides as spacers for CD spectroscopic studies

An important problem in studying the overall conformation of large biopolymers is the development of new tools for the determination of their precise 3D-structure and the relative spatial disposition of specific probes. CD spectroscopy based on exciton coupling of highly absorbing chromophores, such as porphyrins, is a sensitive technique for this purpose. In this work we examined by the exciton coupled CD method the combined distance and angular dependencies, generated by the seven conformationally restricted β-turn and 3_{10}-helical spacer peptides -L-Ala-[L-(αMe)Val]$_n$- (n = 1-7), in a system formed by two intramolecularly interacting 5-carbamido-5,10,15,20-tetraphenylporphyrin chromophores. A net decrease of the intensity of the CD bands with an increase in the length of the spacer between the two chromophores was seen. It

was shown that not only the distance, but the spatial orientation between the directions of the effective transition moments of the two chromophores as well, influences the onset of the induced, exciton coupled, bisignate CD curve.

3. 3_{10}-Helical peptides for IR absorption spectroscopy studies

Isotope edited infrared absorption spectroscopy is a powerful tool for determining the secondary structure and conformational changes of peptides and proteins. We demonstrated the possibility to use this method for the peptide 3_{10}-helix. To this end, a series of hexapeptides, both unlabelled and containing a ^{13}C label at two vicinal carbonyl groups, was synthesized. The labels were incorporated at the N-terminus, at the C-terminus, and at central positions. In the 3_{10}-helix we were able to distinguish the amide I carbonyl stretching band of the given labelled residue from the main band of the peptide.

4. 3_{10}-Helical peptides as templates for organic synthesis (intramolecular ring-closing metathesis)

Another part of this thesis is devoted to 3_{10}-helical peptides as templates for organic synthesis and to enhancement of the helical stability by using a "molecular stapler" (a ruthenium-based olefin metathesis catalyst) *via* intramolecular RCM macrocyclization between neighbouring turns of the helix. By X-ray crystallographic and CD and NMR analyses of both the uncyclized peptides and the peptides after cyclization we demonstrated the feasibility of such a modification since the regularity of the helix remains substantially unchanged. To investigate the influence of the positions of the residues which takes part in the cyclization reaction and to fix the 3_{10}-helical conformation in the peptides containing protein amino acids, three peptides, based both on Aib and Ala with different positionings of hhMag were synthesized. The results obtained confirmed the difficulty in macrocyclizing a sterical hindered RCM peptide substrate. It was also shown that cyclic dimer formation can take place.

ABBREVIATIONS

Ac = acetyl
Aib = α-aminoisobutyric acid
Ala = alanine
Api = 4-aminopiperidine-4-carboxylic acid
Asn = asparagine
Azu = azulene
Boc = *tert*-butyloxycarbonyl
Bzl = benzyl
CD = circular dichroism
DIEA = N,N-diisopropylethylamine
DMSO = dimethylsulphoxyde
EDC = N-ethyl-N'-(3-dimethylamino)propyl-carbodiimide
EP = petroleum ether
Et_2O = diethyl ether
ESI = electron-spray ionization
FT-IR = Fourier transform infrared spectroscopy
Glu = glutamic acid
hhMag = C^{α}-methyl-, C^{α}-homo-homo-allylglycine
HOAt = 1-hydroxy-7-aza-1,2,3-benzotriazol
HPLC = high performance liquid chromatography
IR = infrared absorption
*i*Pr = isopropyl
Iva = isovaline
NMM = N-methylmorpholine
NMR = nuclear magnetic resonance
OMe = methoxy
OEt = ethoxy
OSu = 1-oxysuccinimide
O*t*Bu = *tert*-butoxy
Phe = phenylalanine

ppm = parts *per* million
Pro = proline
Pyr = pyrenyl
R_f = retention coefficient
RCM = ring-closing metathesis
Ser = serine
TFA = trifluoracetic acid
TLC = thin layer chromatography
TPP = 5-(4-carboxy)-5,10,15,20-tetraphenylporphyrin
Tyr = tyrosine
UV-*Vis* = ultraviolet-visible
Val = valine
Z = benzyloxycarbonyl

P.S. The chiral amino acids are in the configuration L (S) if not otherwise specified.

CHAPTER 1

INTRODUCTION

The study of novel phenomena and processes at the molecular level provides useful information for the design of a wide range of tools, materials, devices and systems with unique characteristics. Nanostructured materials and nanodevices are irreplaceable in biomedical research and technologies because of their numerous and diverse applications[1]. To be able to synthesize and process complex nanomaterials with enhanced properties it is overwhelmingly important to have in hand structures of reduced complexity. Such model structures should be conformationally constrained in given conditions, such as solvent, temperature, pH, etc. This property is relevant for a correct assessment of the distances and relative orientations of the molecular groups under study or the functional parts of a nanodevice. To this end, numerous pathways inspired by biological systems have been adopted, including the design of molecular rulers based on α-amino acids[2]. Peptides as self-assembling smart materials have an enormous potential. Sequence manipulations enable the design of a number of different structures that can be developed for many important applications, including tissue repair, miniaturized solar cells, and optical and electronic devices. Peptides offer attractive features, principally because of our acceptable knowledge of their ability to fold into specific structures, and of the rich chemistry with which their 3D-structure and function can be manipulated. Peptides also offer the ability to incorporate non-coded amino acids or non-peptidic moieties, which is a particularly valuable feature for the inclusion of function and/or smartness in the scaffold (i.e. a photoswitch or a non-peptide ligand). Notwithstanding the evident advantages of peptides for this purpose, it is not very easy to predict the structure of a peptide formed by protein α-amino acids. Another drawback of these amino acids is the requirement of rather long main-chain length for the formation and full development of a given polypeptide structure. The ability to form highly rigid and well developed 3_{10}-helices by C^{α}-tetrasubstituted α-amino acids (**Fig. 1**) under appropriate conditions is very useful for creating short and precisely conformationally tunable peptide scaffolds.

Besides the classical α-helix, β-sheet and β-turn conformations, the 3_{10}-helix represents the fourth principal structural element occurring in globular proteins and has been described at atomic resolution in model peptides and in peptaibol antibiotics[3].

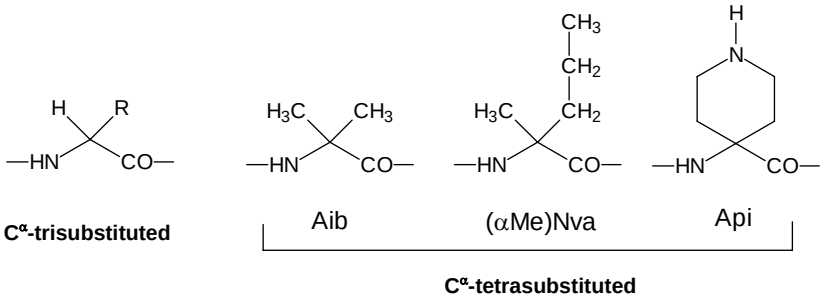

Fig. 1. Chemical structures of selected α-amino acids.

The helical conformations differ by the number of residues per turn, the pitch, the φ, ψ, ω torsion angles in the peptide backbone[4, 5] (**Fig. 2**), and the number of the atoms in the *pseudo*-rings formed by the C=O···N-N intramolecular H-bonds.

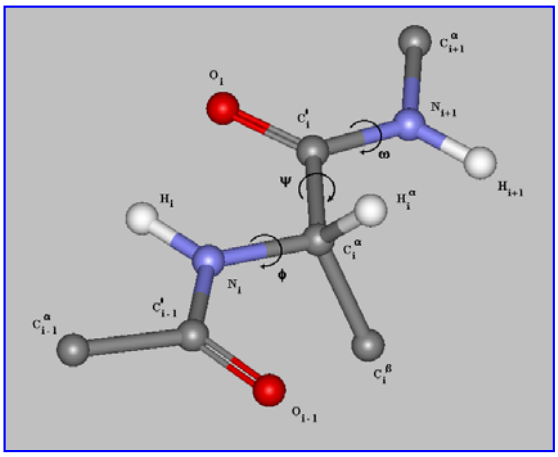

Fig. 2. Representation of a segment of polypeptide chain in the fully-extended conformation ($\phi_i = \psi_i = \omega_i = 180°$).

The α-helix is characterized by 3.63 residues per turn and it is stabilized by intramolecular H-bonds between the carbonyl group of a residue at position *i* and the N-H group at the *i* + 4 position, forming the *pseudo*-rings of 13 atoms (α-turns or C_{13}-structures)[6]. The 3_{10}-helical structure has 3.24 residues per turn. The intramolecular H-bonds are formed between the oxygen of the carbonyl group at position *i* and the N-H group at position *i* + 3 with the onset of *pseudo*-rings of 10 atoms (β-turns or C_{10}-structures) (**Table 1**). Thus, the average conformational parameters of the 3_{10}-helix are close to those of the α-helix, but the former helix is slightly tighter and more elongated (**Fig. 3**).

A 3_{10}-helix formed by C^{α}-trisubstituted (protein) α-amino acids is less stable than the α-helix due to the larger distortion of the H-bonds and some unfavorable van der Waals interactions[7-9]. Though the 3_{10}-helical structure would not be widespread, nevertheless it is not rare. The recent improvements in analytical techniques allowed to identify the 3_{10}-helical patterns in numerous natural proteins[10-12]. A statistical analysis of the X-ray diffraction structures of 57 globular proteins revealed the presence of 71 3_{10}-helical motifs of different length. Interestingly, in most cases such structures were found at the N- and C-termini of α-helices.

Table 1. Structural parameters for the α- and 3_{10}-helical conformations[6].

Parameter	3_{10}-Helix	α-Helix
Φ	-57°	-63°
Ψ	-30°	-42°
number of residues per turn	3.24	3.63
pitch	6.29 Å	5.67Å

The main β-turn patterns were classified by Venkatachalam[13] as types I, II, and III (**Fig. 4**), depending on the values of the φ, ψ torsion angles of the *i* + 1 and *i* + 2

residues (**Table 2**). Repeating type III β-turns leads to the formation of the right-handed 3_{10}-helical structure, while the other two types of β-turns are not helix forming.

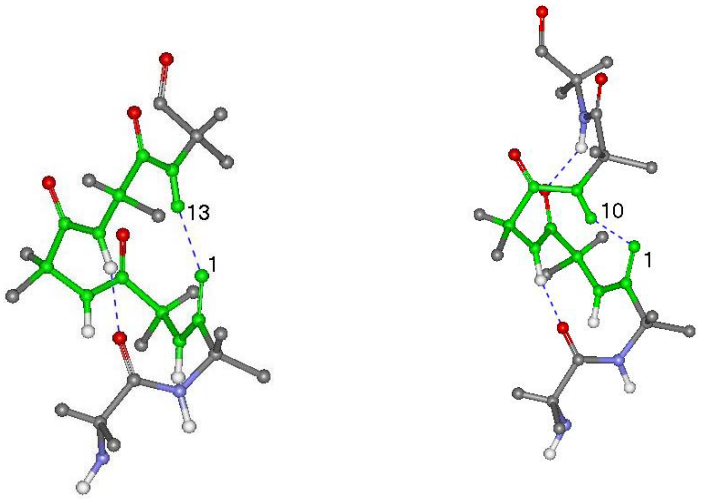

right-handed α-helix right-handed 3_{10}-helix.

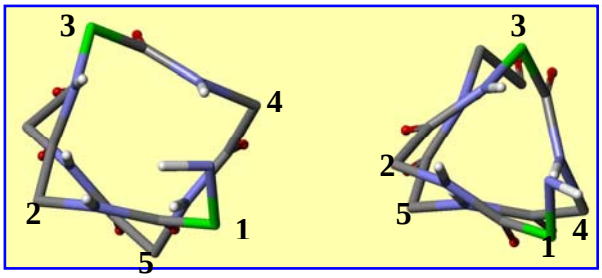

α-helix **3_{10}-helix**

Fig. 3. Models of the α- and 3_{10}-helical conformations (top: side view; bottom: view along helix axis).

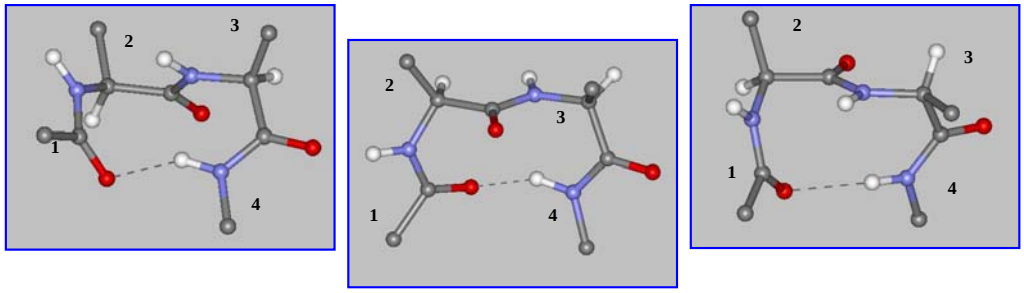

I **II** **III**

Fig. 4. Representation of the β-turn (type I, II and III) structure with the central amide bond in the *trans* conformation.

Table 2. Torsion angle values for the three types of β-turns

β-Turn	φ (*i* + *1*)	ψ (*i* + *1*)	φ (*i* + *2*)	ψ (*i* + *2*)
Type I	-60°	-30°	-90°	0°
Type II	-60°	+120°	+80°	0°
Type III	-60°	-30°	-60°	-30°

In contrast to the C^{α}-trisubstituted (protein) α-amino acids, the C^{α}-tetrasubstituted α-amino acids are extremely strong promoters of 3_{10}-helical structures. The study of the conformational preferences of the peptides rich in different C^{α}-tetrasubstituted amino acids and their possible applications have been the main subjects of the work of the research group headed by Prof. C. Toniolo (University of Padova) since 1980[14-17].

C^{α}-Tetrasubstituted amino acids differ from protein amino acids by the substitution of the hydrogen at the α-carbon atom by an alkyl or an aryl group. The noticeable sterical hindrance induced by these substituents drastically limits the N-C^{α} and C^{α}-C' (φ and ψ torsion angles, respectively) bond rotations[18, 19].

In the case of the peptides containing the simplest C^{α}-tetrasubstituted α-amino acid (Aib, α-amino isobutyric acid) and protein amino acids as well, in the crystal state only helical structures of the α-, 3_{10}- or α/3_{10}-"mixed" type were found[20, 21]. For the Aib-based oligopeptides also the second longest 3_{10}-helix known so far [(*p*BrBz-$(Aib)_{10}$-O*t*Bu)] was obtained in the Padova laboratory (**Fig. 5**). The main factors which bias the peptide conformational preference toward a specific type of helix are the length of the polypeptide chain, the Aib content, and the amino acid sequence. In general, the α-helix formation tends to be favored when the main chain is lengthened and the number of Aib residues is decreased. Very short peptides (up to 6 residues) with a large amount of Aib residues show a strong tendency for 3_{10}-helix formation[22].

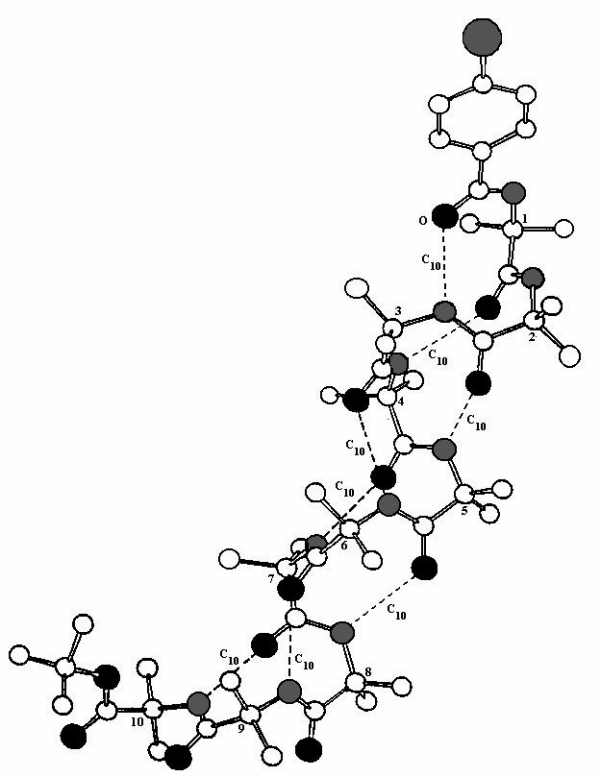

Fig. 5. X-ray diffraction structure of *p*BrBz-$(Aib)_{10}$-O*t*Bu (intramolecular C=O···H-N H-bonds are shown as dashed lines).

Being achiral the Aib residue does not induce any preferred sense of spiralization in the peptide. As in the case of protein amino acids, in the peptides based on C^{α}-tetrasubstituted α-amino acids the helix sence is strongly influenced by the nature of side-chains. In the peptides containing C^{α}-tetrasubstituted α-amino acids with linear or β- or δ-branched side chains, the sense of spiralization follows the common rules of protein amino acids (L-residues induce a right-handed helix), while γ-branched side-chains tend to promote the opposite handedness. An exception is C^{α}-methyl isovaline (with one methyl and one ethyl side chain), which does not show any noticeable screw sense preference.

In the case of the study of the homo-octapeptide Ac-[L-(αMe)Val]$_8$-O*t*Bu[23] it was obtained the first CD spectrum of a 3_{10}-helix[24] (**Fig. 6**), which was close to that theoretically predicted by Woody *et al.*[25] Moreover, it was discovered that this peptide can undergo a conformational transformation from the 3_{10}-helix to the α-helix (and vice versa) in a solvent dependent manner[26-28]. This is one of the very few peptides known, constituted exclusively by C^{α}-tetrasubstituted α-amino acids which can form an α-helical structure.

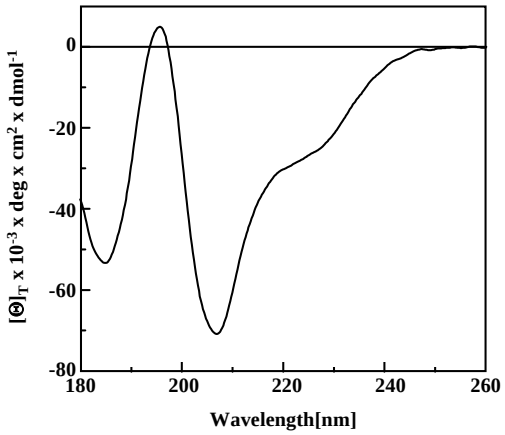

Fig. 6. CD spectrum of Ac-[L-(αMe)Val]$_8$-O*t*Bu in TFE solution.

Highly ordered 3_{10}-helical structures are very promising tools for detailed studies of a variety of different biochemical and biophysical fundamental processes. In these cases, the rigid helices can be used as templates or spacers[29], which serve to direct and orient two or more labels into desired topologies. It is worth reminding that a spacer is a linear system which allows the regulation of the distance between two labels in the molecule, while a template is a linear (or a cyclic) system which directs the two labels into a desired spatial separation/orientation (**Fig. 7**).

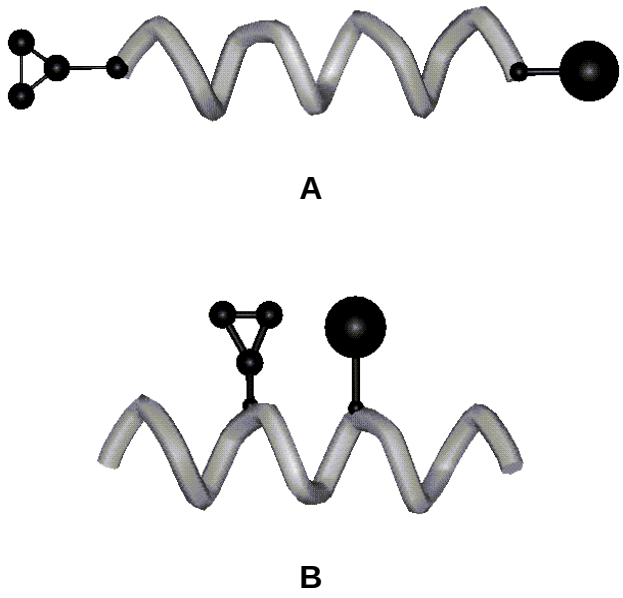

Fig. 7. Schematic representation of a spacer (**A**) and a template (**B**).

In this Ph.D. thesis it was decided to apply the property of C^{α}-tetrasubstituted α-amino acids to form particularly stable 3_{10}-helical structures for the design of the rigid spacers and templates for different spectroscopic and photophysical studies as well as for organic syntheses. In particular, such peptides are thought to be used as rigid templates for the investigation of the influence of the macroscopic dipole of the 3_{10}-helix on the rate of energy transfer between two appropriate chromophoric moieties by studying the fluorescence quenching effect between the donor and the acceptor. 3_{10}-Helical structures have also been applied for the investigations of the exciton coupled CD between two porphyrin chromophores and the isotope edited IR spectroscopy, as well as for the synthesis of helices with enhanced stability.

CHAPTER 2

3_{10}-HELICAL PEPTIDES AS TEMPLATES FOR PHOTOPHYSICAL STUDIES

Many biological phenomena, such as photosynthesis and cell respiration[30, 31] are related to electron and energy transfer from donor to acceptor molecules through different molecular structures. A detailed understanding of the principles governing natural photosynthesis has evolved in parallel with the study of artificial molecular systems, designed to mimic charge separation, the retardation of charge recombination, and electron transfer. Molecular electronic devices, such as molecular wires[32], optoelectronic gates[33, 34] switches[35, 36], that control electronic response *via* external stimuli, have been suggested as an application of basic principles of transfer processes in such systems (**Fig. 8**).

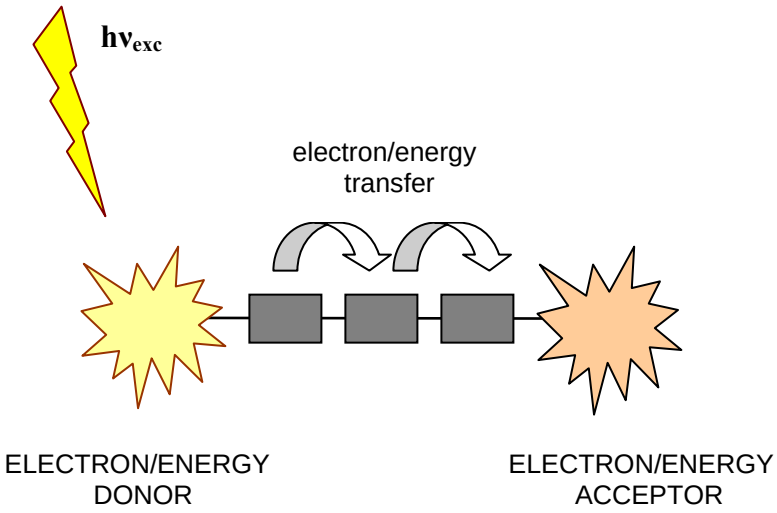

Fig. 8. Principle of the work of a molecular device based on energy or electron transfer.

It is shown experimentally that in biological systems transferred electron covers distances of order 30-70 Å. It is unlikely that electron transfer covering such large distances is realized *via* a simple mechanism of tunnelling[37]. One of the possible ways of explanation of this process is related to the idea that the transfer is facilitated by the participation of protein molecules. Possible subsequent cleavage of C-N bonds may occur [38]. In the work of Ichinose *et al.*[39] it was supposed the electron can be transferred through the H-bonded chain of an α-helical protein molecule. The storage and transport mechanisms would involve keto-enol transition of the H-bonding backbone structure. Another way of energy transfer was suggested by Clarke and Collins[40]. By classical simulation of a section of the α-helical peptide poly(L-Ala) it was demonstrated a mechanism by which N-H stretching quanta are coherently transported along a chain of H-bonded peptide groups through highly efficient vibrational energy propagation.

Synthetic donor-acceptor molecules could provide a decisive means for a systematic study of the energy and electron transfer mechanisms[41, 42]. The highly organized arrangement of the reaction centre during photosynthesis strongly suggests the importance of the separation between the energy/electron donor and acceptor and their spatial orientation. Long-range energy transfer occurs not only when the emission spectrum of the donor overlaps the absorption spectrum of the acceptor but also when the emission and absorption dipoles of the donor and acceptor molecules are at a certain distance and properly oriented. When explaining the molecular mechanism of electron transfer it is extremely important to know the spatial arrangement of the chromophores. Flexibility and length of the spacer or linker between the energy donor and acceptor has significant effects on the mechanisms and rates of energy transfer and quenching[43]. Compounds with flexible linker groups, such as methylenic[44] (**Fig. 9**) and ester[45] linkages suffer from reduced transfer efficiency due to variable chromophore orientation and spacing. Rigid spacers can control the orientation of the chromophores[46-48], which can be very important for optimum electron/energy transfer even when the edge-to-edge distance between the donor and the acceptor remains practically constant[49].

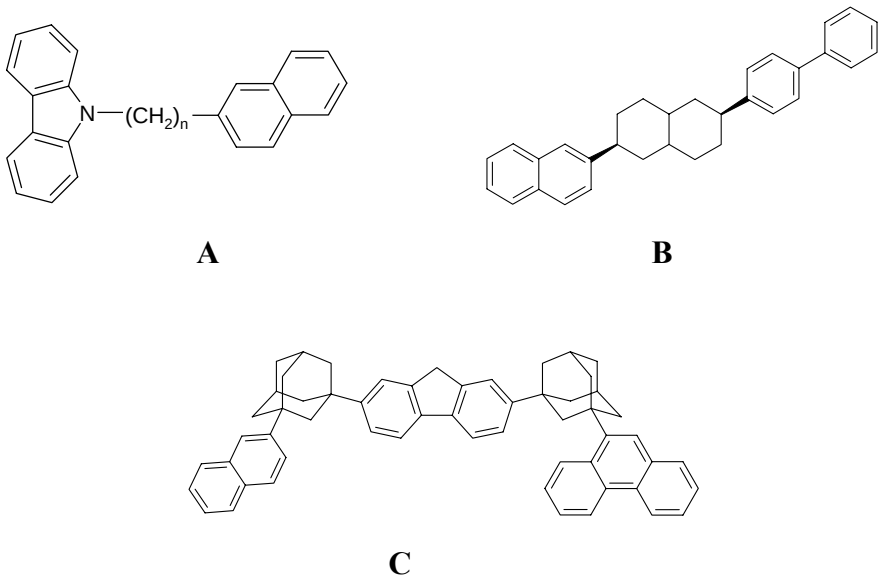

Fig. 9. Examples of spacers and linkers used in ref. [44] (**A**), [46] (**B**), and [47] (**C**).

Transfer processes between two chromophores are thought to be through-space in molecules with larger chromophore separations and through-bond in peptides with smaller interchromophore distances. In addition to linker rigidity and its effect on through-bond transfer efficiency, interchromophore separation is also a determining factor on the rate and mechanism of energy transfer. At small interchromophore distances, energy transfer can occur by both the exchange mechanism (Dexter) *via* overlap of electron clouds which requires collision between the molecules, and the dipole-induced dipole mechanism (Förster), where oscillation of the excited state donor dipole induces oscillations in the acceptor's dipole. In this case the transition occurs *via* the electromagnetic field and does not require physical contact of the interacting partners. The efficiency of the energy transfer through Dexter mechanism drops off exponentially, whereas in the dipole-induced dipole mechanism it is related to the inverse sixth power of intercromophore distance. At larger interchromophore distances, only the dipole-induced dipole mechanism is operative.

Peptide scaffolds offer several advantages for studying and controlling energy transfer [50, 51]. The α-helical peptides may serve as ideal molecular structures that transport an electron from one molecule to another or from one part of the molecule to another one, as it

was shown in the work of Toniolo *et al.*[52], where the phthaloyl end of the peptide acted as an electron-transfer antenna, inducing peroxyester disruption followed by rapid intramolecular electron transfer through the rigid, 3_{10}-helical peptide bridge (electron capture dissociation[53]). In the work of Sisido *et al.*[54] α-helical structures were used as templates for studying the distance dependence of photoinduced electron transfer between the pyrenyl and nitrophenyl chromophores upon excitation of the pyrene chromophore:

H-Glu(OBzl)$_n$-Ala(Pyr)-Glu(OChx)$_m$-Phe(*p*-NO_2)-Glu(OBzl)$_4$-NH_2 **P*m*T**
(*m* = 0-8, n varied from 32 to 54)

The pyrenyl fluorescence was significantly quenched by the incorporation of the nitrophenyl group, and both the quenching efficiency and the rates of electron transfer strongly depended on the number of spacer units between pyrenylalanine and nitrophenylalanine and therefore on the distance between the chromophores (**Fig. 10**). One of the reasons of the complex behavior of the rates of electron transfer and its deviation from linear dependence at *m* = 2 and 6 was thought to be caused by the closer spatial orientation of the chromophores at these two positions caused by peculiarities of the α-helical structure. Another reason supposed was the possibility of the simple through-bond electron transfer mechanism.

Oligo-L-proline bridges to separate the electron donor and acceptor pair were proven to be useful for studying rapid energy and electron transfer processes, because oligo-L-proline spacers may take a fairly stable helical conformation and the intramolecular energy and electron transfer can be readily monitored by various physico-chemical techniques[55]. A photoexcited zinc(II) porphyrin as an energy and electron donor, and a metal-free porphyrin and an iron (III) porphyrin as an energy and electron acceptor were used (**Fig. 11**).

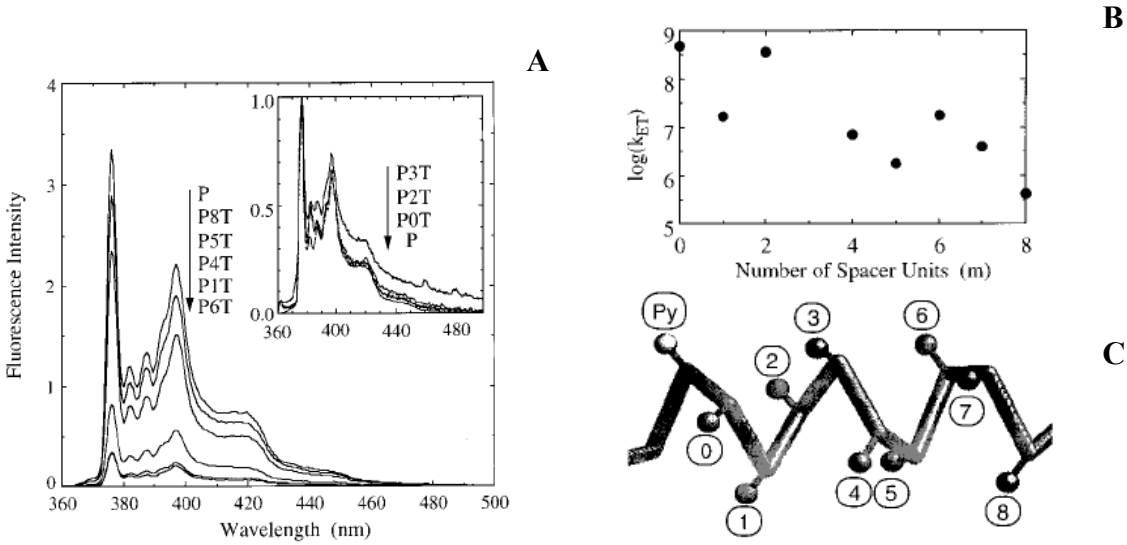

Fig. 10. Steady-state fluorescence spectra (**A**) and electron transfer rate constants of the P*m*T polypeptides plotted against the number of spacer units between the pyrenyl and nitrophenyl groups (**B**). A simplified molecular model showing the helix geometry (**C**)[54].

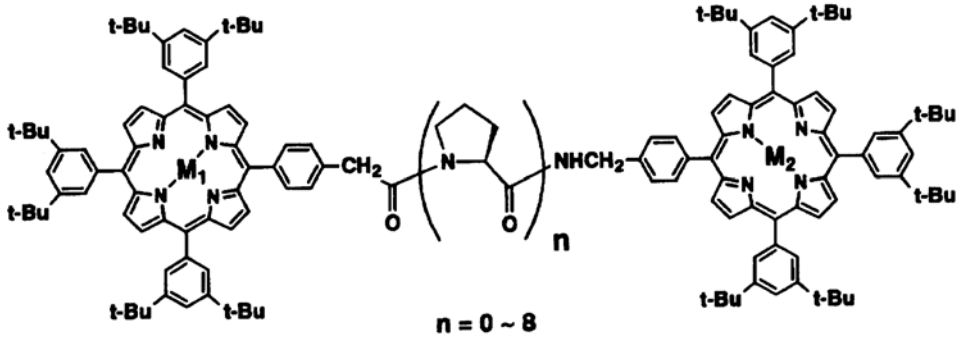

		M_1	M_2
ZnP-CO-Pro$_n$-NH-H$_2$P	(**Z-n-H**)	Zn(II)	H_2
H$_2$P-CO-Pro$_n$-NH-ZnP	(**H-n-Z**)	H_2	Zn(II)
ZnP-CO-Pro$_n$-NH-FeP	(**Z-n-F**)	Zn(II)	Fe(III)Cl
FeP-CO-Pro$_n$-NH-ZnP	(**F-n-Z**)	Fe(III)Cl	Zn(II)

Fig. 11. Synthetic oligo-L-proline-bridged porphyrin donor-acceptor conjugates studied in ref. [55].

In both the series of the donor-acceptor molecules the relative fluorescence intensities increased with an increase in the number of proline units in the spacer, and quenching *via* an energy transfer was reduced in concomitance with the increase in *n*, suggesting that the average spatial distance between the two chromophores in the molecule should increase with an increase in *n*. An intramolecular energy transfer occurred from a photoexcited zinc porphyrin N-terminal moiety to a metal-free porphyrin moiety at the C-terminus with the same efficiency as from the Zn porphyrin at the C-terminus to the N-terminal metal-free porphyrin. The independence of the direction of the spacer on the electron transfer was observed also in the case of an iron(III) porphyrin in the molecule. In addition, a weak change in the intramolecular electron-transfer efficiency with the distance between the zinc and iron porphyrins suggested that the electron should move through the peptide bonds in the oligoproline spacer and the direction of the bonds should not be important in a bond-mediated electron-transfer process.

A series of rigid 3_{10}-helical peptides of different length (3, 6, 9, 12 and 15 residues of Aib) with chromophores, which were directly bound to the ends of the backbone chain, were used by Pispisa *et al.*[56] to study the distance dependence of the photoexcited transfer processes between naphthyl and protoporphyrin chromophores. Such lengths of the peptides allowed the chromophores to lie on the same side of the helix with a distance from one to five turns, respectively (**Fig. 12**). A substantial quenching of the naphthyl chromophore fluorescence by the bound protoporphyrin moiety took place with corresponding increase in length of the peptide spacer (**Table 3**).

The photophysical study allowed to make another conclusion about the occurrence of a competitive mechanism of donor fluorescence quenching, involving electron transfer from porphyrin to naphthalene chromophore, and, therefore, a competition between energy and electron transfer is likely to occur in the case of the longest peptide spacers of the series, resulting from a complex interplay of electronic and topological factors.

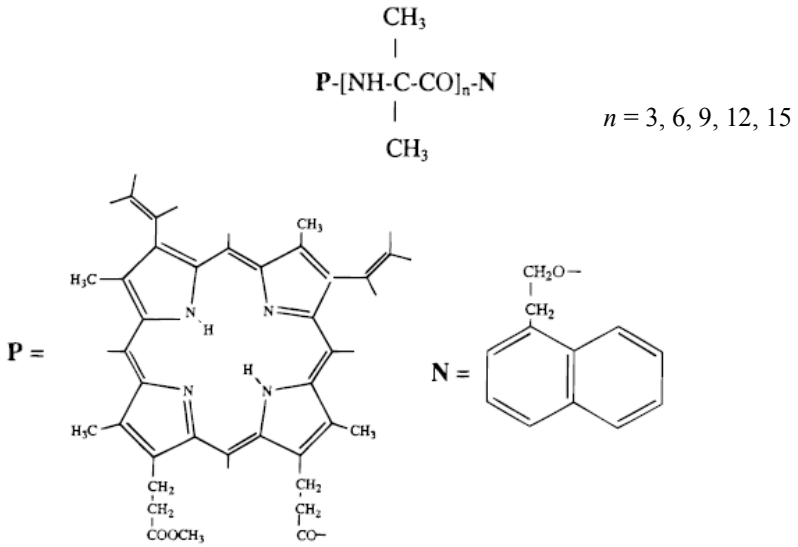

Fig. 12. Peptide conjugates studied in ref. [56].

Table 3. Steady-state fluorescence of P(Aib)$_n$N in methanol solution.

Peptides	Quenching efficiency
P(Aib)$_3$N	0.99
P(Aib)$_6$N	0.96
P(Aib)$_9$N	0.90
P(Aib)$_{12}$N	0.84
P(Aib)$_{15}$N	0.40

While studying the energy and electron processes in the systems with peptide-bridged chromophores one should take into consideration the dipole moment of the peptide chain more or less noticeable for each conformation and H-bonding pattern, especially for a helical structure. In the helix the peptide bond dipoles (about 3.5 D per bond) are aligned along the helix axis, producing an effective positive charge at the N- end and an effective negative charge at the C-end (**Fig. 13**). Polarization effects due to H-bonding increase the dipole moment per residue to about 5.2 D for the α-helix[57] (**Table 4**). In contrast, in a 3_{10}-

helix the H-bonds are not perfectly aligned with respect to the helical axis, and hence the resulting total molecular dipole is smaller than in the α-helix (about 4.6 D per residue).

Table 4. Orientation of the peptide C=O group with respect to the helical axis and its effect on the molecular dipole moment in different secondary structures[57].

Structure	Angle (deg)	Dipole/residue (D)
α-helix	13	5.16
polyproline II	70	1.54
3_{10}-helix	28	4.57
polyproline I	144	-4.10
β-strand	78	0.25

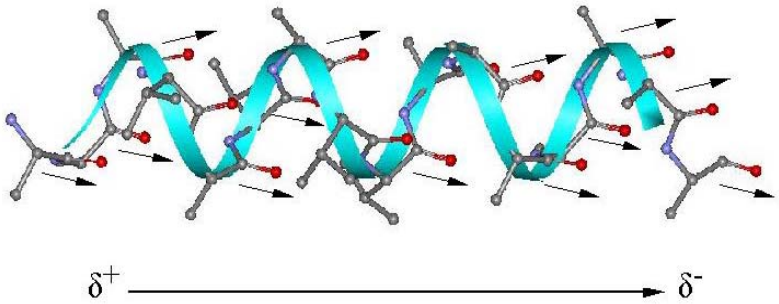

Fig. 13. Macroscopic dipole of a helical conformation.

The resulting macroscopic dipole generates an electrostatic potential, estimated to be up to 109 V/m in an α-helix[58], plays an important role in the structure and functions of proteins, and probably also influences the primary electron transfer event in the photosynthesis. Hence, the different H-bonding patterns in the two (α- and 3_{10}-helical

conformations could influence the electronic coupling between donor and acceptor moieties linked to the peptide chain, as was supposed by Fox and Galoppini[59] by studying α-helical structures **(Fig. 14)**.

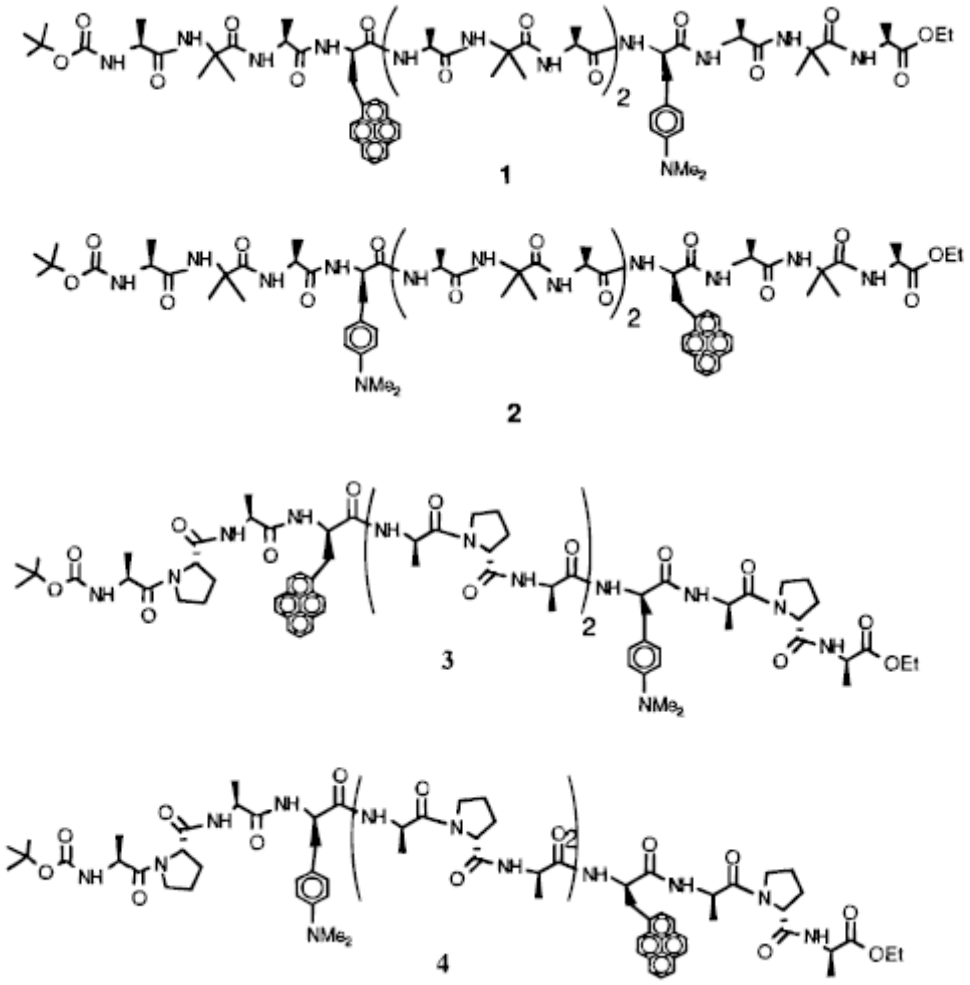

Fig. 14. Chromophore-bearing peptides studied in ref. [59].

From an analysis of the measurements of time-resolved pyrene fluorescence, the rates of electron transfer were shown to be 5-27 times faster in **2**, where the electron transfer took place in the direction opposite to the direction of helical macrodipole, which is an electrostatically more favored process. However, bi-exponential decays in **1** and **2** were observed, which is a clear indication of multiple conformations in the oligopeptides, probably caused by the flexibility of the methylene units that link each of the chromophores to the backbone.

In the helix-disrupting solvents the electron transfer rates of **1** and **2** were identical. Moreover, electron transfer rates in peptides **3** and **4**, where the helical structure and the related electric field along the helix are perturbed because of the disruption of the intramolecular H-bonding pattern, were identical to those obtained for the peptides **1** and **2** in the solvents where they are random coil. All of the differences in electron transfer rates between **3** and **4** in different solvents could be attributed to the flexibility of the backbone chain. All these results apparently confirm the influence of the helical macrodipole on the photophysical processes which can take place between two chromophores.

The rate constant of electron transfer (k_{ET}) from a donor (D) to an acceptor (A) at a fixed distance in terms of the Marcus theory is described by the following equation:

$$k_{ET} = \sqrt{\frac{4\pi^3}{h^2 \lambda k_B T}} H_{DA}^2 \exp\left[-\frac{\left(\Delta G^0 + \lambda\right)^2}{4\lambda k_B T} \right]$$

$$H_{DA}^2 = \left(H_{DA}^0\right)^2 \exp\left(-\beta r\right)$$

where h is Planck's constant, λ is the reorganization energy, k_B is the Boltzmann's constant, T is the absolute temperature, H_{DA}^2 is the electronic coupling strength between donor and acceptor, $(H_{AD}^0)^2$ is the coupling strength at the closest contact, ΔG^0 is the driving force for the electron transfer reaction, β is the tunnelling parameter for the medium and r is the edge-to-edge donor-acceptor distance. Therefore, the electron transfer rate must depend on the positioning of the donor and acceptor with respect to the peptide helical dipole.

Due to the importance of the interchromophore separation on transfer rates and also due to the fact that in most systems based on helical peptides conformational flexibility results in a wide distribution of interchromophore separations, we have undertaken the study of electron/energy transfer in a system that should possess sufficient conformational rigidity to limit the range of interchromophore separation in order to verify if the helical macrodipole actually influences the transfer rats for the case of the 3_{10}-helix.

For this purpose we sinthesized three terminally-blocked octapeptides with the following sequence:

Z-Aib-Api(***Pyr***)-L-(αMe)Nva-Aib-L-(αMe)Nva-L-(αMe)Nva-Aib-Api(Boc)-NH*t*Bu **P2**
Z-Aib-Api(***Pyr***)-L-(αMe)Nva-Aib-L-(αMe)Nva-L-(αMe)Nva-Aib-Api(***Azu***)-NH*t*Bu **P2A8**
Z-Aib-Api(***Azu***)-L-(αMe)Nva-Aib-L-(αMe)Nva-L-(αMe)Nva-Aib-Api(***Pyr***)-NH*t*Bu **A2P8**

For the synthesis, only C^{α}-tetrasubstituted α-amino acids were used for supporting well formed 3_{10}-helical structure, and therefore a narrow distribution of conformers of the peptide compounds. In addition, we have designed a more rigid system than in the work of Fox and Galoppini[59] by anchoring the two chromophores (azulene and pyrene) to the peptide backbone through the cyclic, non rotable side chain of the C^{α}-tetrasubstituted amino acid Api (**Fig. 15**). By introducing the amide group at the C-terminus it was possible to make an octapeptide equivalent to a nonapeptide due to the additional H-bond forming ability of the C-terminal NH group.

The **P2A8** and **A2P8** oligopeptides, having as an electron donor pyrene and as an electron acceptor the azulene chromophore, differ only in the relative positions of the donor-acceptor pair along the helix dipole. Thus, the photoinduced electron transfer process between donor and acceptor should be affected by the orientation of the electric field determined by the helix dipole, which is directed from N-terminus to C-terminus. The alignment of the electric field with respect to the direction of the photoinduced electron transfer should induce a faster electron transfer rate in **A2P8** than in **P2A8**. In contrast, the back electron transfer charge recombination process should be relatively favored in **P2A8**.

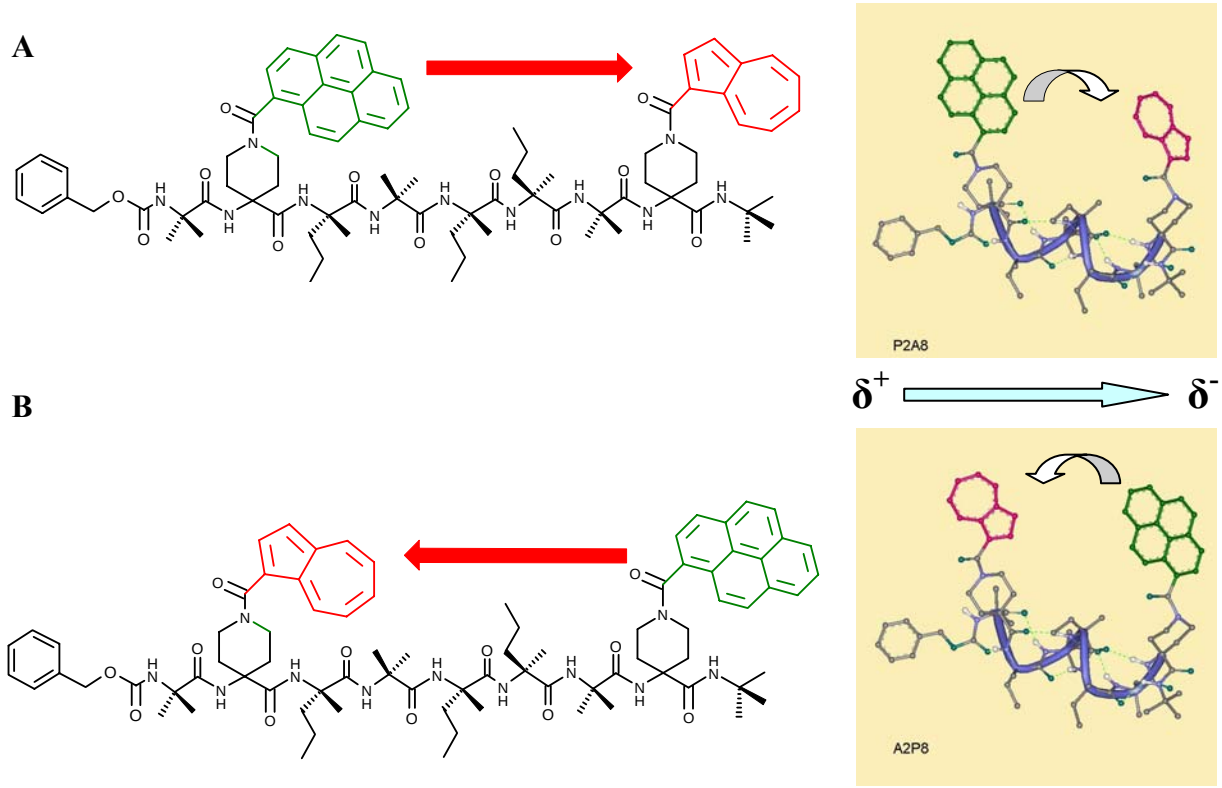

Fig. 15. Chemical structures of the peptides **P2A8** (**A**) and **A2P8** (**B**).

The peptides were obtained by classical synthesis in solution, because sterically hindered C^{α}-tetrasubstituted amino acids do not allow using the faster solid-phase synthesis. The design and the synthesis of peptides **P2A8** and **P2** have been already described[60]. A second template, **A2P8**, had to be prepared. Since in our experience the Azu group is not resistant toward a catalytic hydrogenation (unlike pyrene), for the preparation of **A2P8** we were forced to modify the scheme adopted for the synthesis of the abovementioned peptides and use both fragment condensation and step-by-step synthesis with introduction of the azulene fragment at the last step (**Fig. 16-19**). We first prepared the C-terminal pentapeptide **5BC** by condensating the C-terminally deprotected tripeptide

segment **3B** with the N-deprotected dipeptide **2C**. The octapeptide **8'** was synthesized from **5BC** by three successive steps using Z-L-(αMe)Nva-OH, Z-Api(Boc)-OH, and Z-Aib-OH. In the last step the side-chain protecting Boc group of Api was removed and the resulting octapeptide was reacted with Azu-COOH/EDC/HOAt to afford the desired compound **A2P8**.

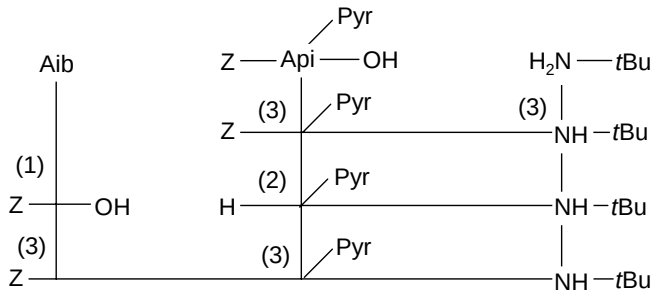

(1): Z-OSu/Et_3N in CH_3CN/H_2O; (2): H_2/Pd/MeOH; (3): EDC/HOAt/NMM

Fig. 16. Scheme of synthesis for Z-Aib-Api(Pyr)-NH*t*Bu (fragment **2C**).

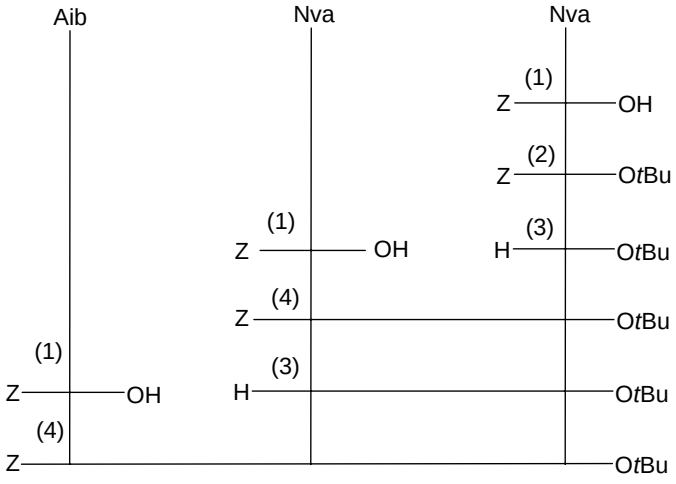

(1): Z-OSu / Et_3N in CH_3CN/H_2O; (2): isobutene/H_2SO_4; (3): H_2/Pd/MeOH; (4): **E**DC/HOAt/NMM

Fig. 17. Scheme of synthesis for Z-Aib-L-(αMe)Nva-L-(αMe)Nva-O*t*Bu (fragment **3B**).

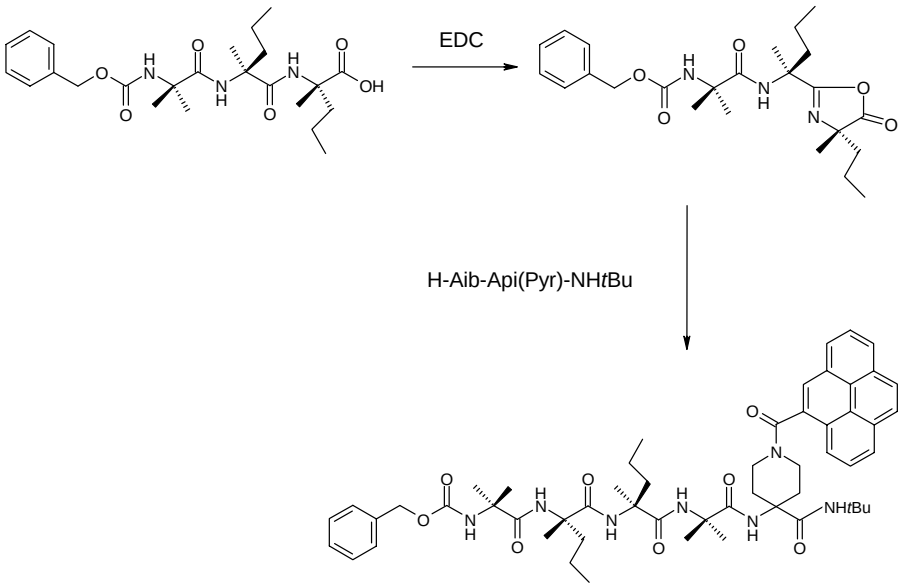

Fig. 18. Scheme of synthesis for Z-Aib-L-(αMe)Nva-L-(αMe)Nva-Aib-Api(Pyr)-NH*t*Bu (fragment **5BC**).

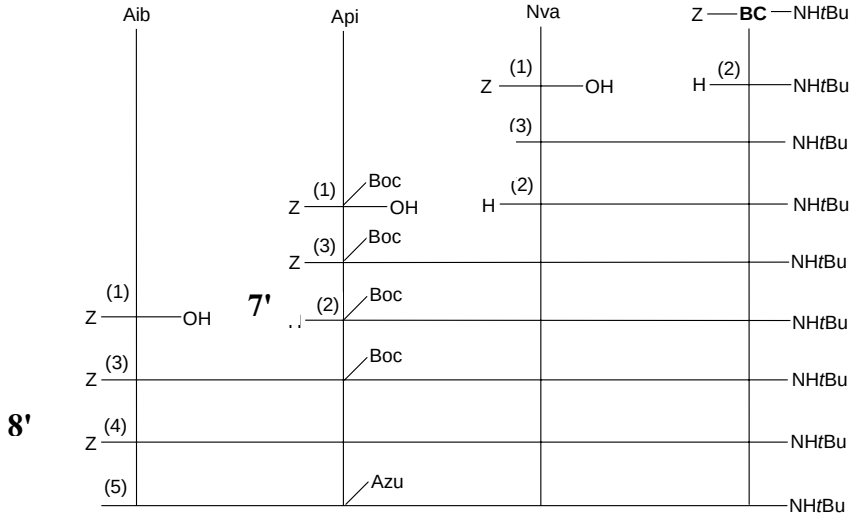

BC = Z-Aib-L-(αMe)Nva-L-(αMe)Nva-Aib-Api(Pyr)-NH*t*Bu

(1): Z-OSu/Et_3N in CH_3CN/H_2O; (2): H_2/Pd/MeOH; (3): EDC/HOAt/NMM; (4): 3.3 N HCl/EtOAc; (5): AzuCOOH/HOAt/EDC/NMM

Fig. 19. Scheme of synthesis for Z-Aib-Api(Azu)-L-(αMe)Nva-Aib-L-(αMe)Nva-L-(αMe)Nva-Aib-Api(Pyr)-NH*t*Bu (**A2P8**).

The UV absorption spectra of the **P2A8** and **A2P8** peptides are very similar to each other and exhibit a combination of the same absorption bands of the pyrenyl and azulenyl components of the reference compounds, containing only the pyrene (peptide **P2**) or the azulene [Z-Api(Azu)-OH] chromophore, indicating the absence of any strong ground-state interaction between donor and acceptor in both peptides (**Fig. 20**).

The FT-IR absorption spectra of the peptides show an increased intensity of the band at 3380-3320 cm^{-1} (NH groups involved in the H-bonds) with increasing peptide main-chain length. The intensity of this band is independent on peptide concentration in the range $1\times10^{-3} - 1\times10^{-4}$ (**Fig. 21**). In addition, the CD spectra of **P2**, **P2A8** and **A2P8** in CH_3CN solution exhibit an intense negative maximum around 202-205 nm, a pattern typical of peptides attaining a right-handed 3_{10}-helical conformation. In the 230-250 nm range some differences among the three peptides may be noted, probably due to an induced CD resulting from electronic transitions of the aromatic side chains (pyrene and azulene) caused by the nearest-neighbour peptide groups. Taken together, these results support the view that **A2P8** and **P2A8** adopt in solution the 3_{10}-helical structure, stabilized by intramolecular H-bonds.

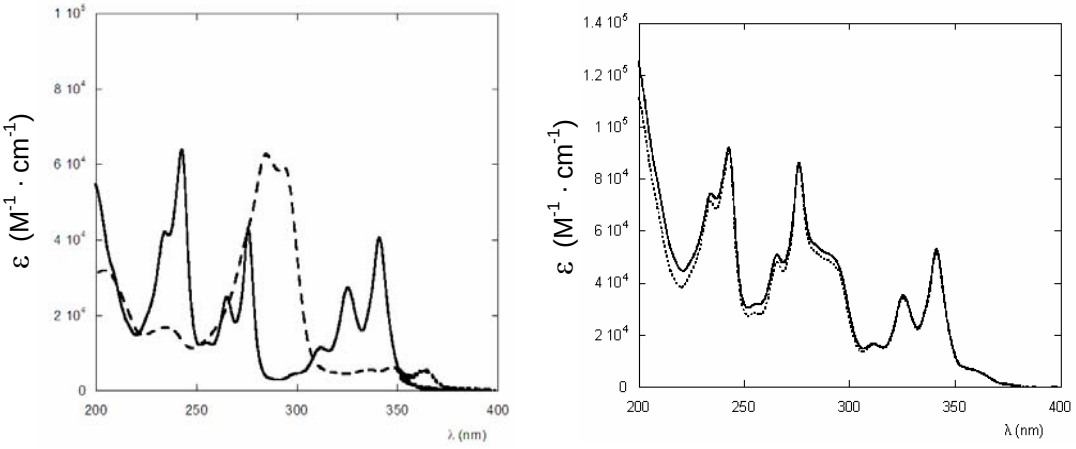

Fig. 20. Absorption spectra of **P2** (solid line) and Z-Api(Azu)-OH (dashed line) (*left*), and of **P2A8** (dotted line) and **A2P8** (solid line) (*right*) in CH_3CN solution.

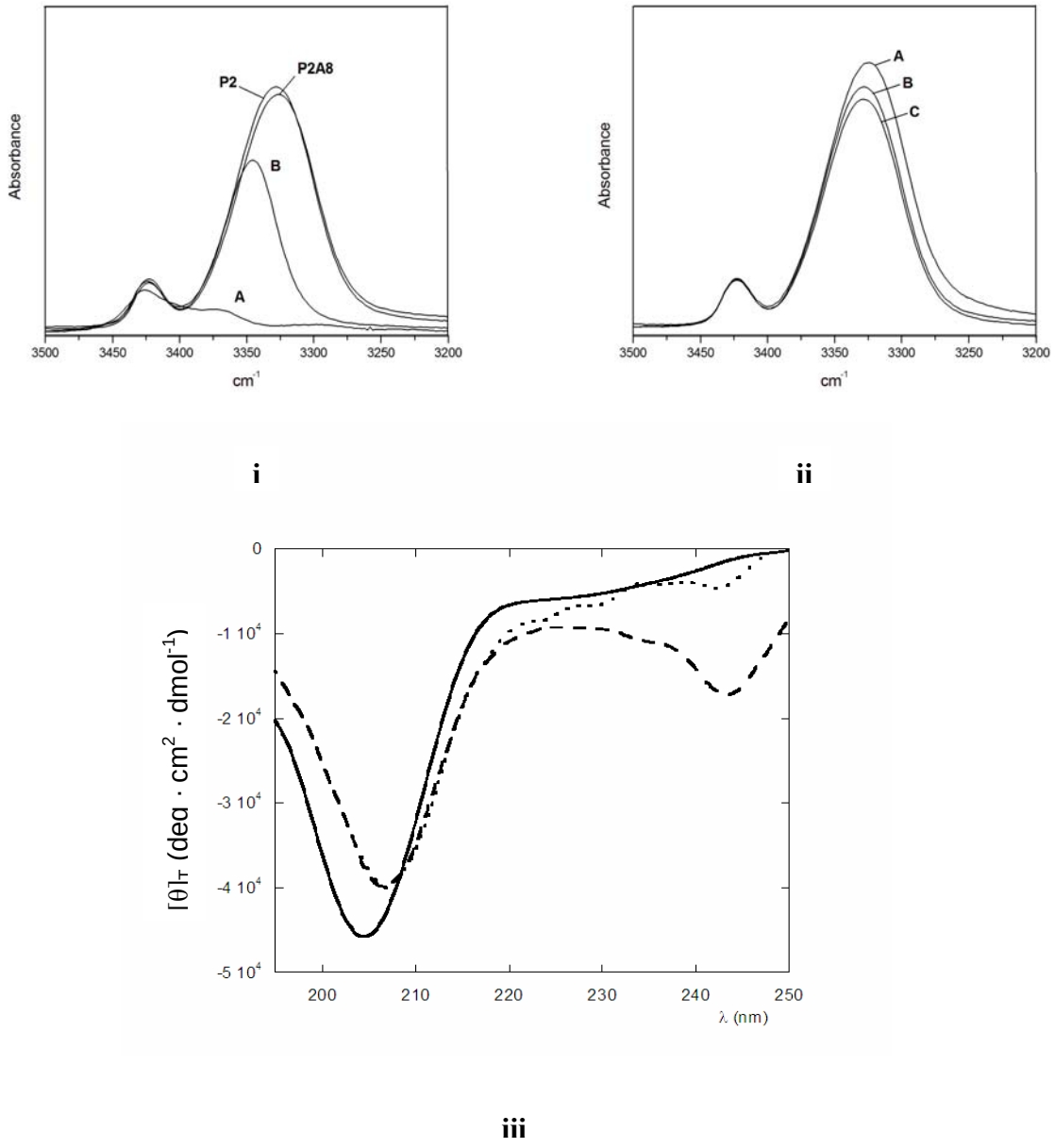

Fig. 21. (**i**): FT-IR absorption spectra of the Z-Aib-Api(Pyr)-L-(αMe)Nva-O*t*Bu (**A**), Z-Aib-Api(Pyr)-L-(αMe)Nva-Aib-L-(αMe)Nva-L-(αMe)Nva-OtBu (**B**), **P2** and **P2A8** peptides in $CDCl_3$ solution in the 3500-3200 cm^{-1} region. Peptide concentration: 1×10^{-3} M. (**ii**): FT-IR absorption spectra of **P2** (1×10^{-2} M, **A**; 1×10^{-3} M, **B**; 1×10^{-4} M, **C**). (**iii**): Far-UV CD spectra of the **P2** (full line), **P2A8** (dotted line), and **A2P8** (dashed line) in CH_3CN solution. Peptide concentration: 1×10^{-4} M.

A NMR conformational analysis of **A2P8** (as well as **P2A8**) (**Fig. 22**) has revealed that a *cis* ⇄ *trans* isomerism in the two side-chain, tertiary amide bonds, characterizing Api(Azu) and Api(Pyr), could be present. Indeed, the mono-dimensional ^{1}H NMR spectrum in the -CONH- region is simplified by raising the temperature (when the *cis* ⇄ *trans* interconvertion is faster). This finding should be taken into account when considering the results of the electron/energy transfer experiments.

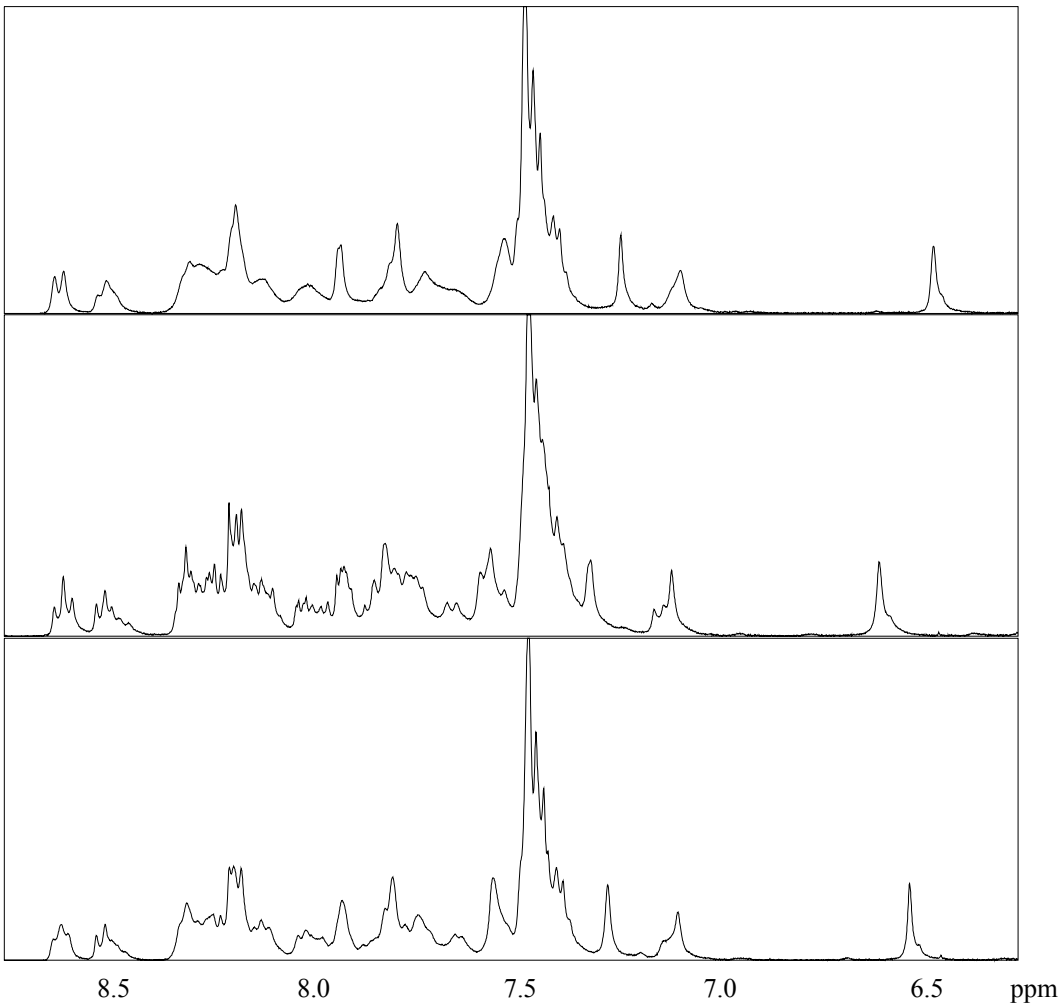

Fig. 22. ^{1}H NMR spectrum of the octapeptide **A2P8** at 25 °C, 50 °C and 70 °C (from bottom to top) (1×10^{-3} M in CH_3CN solution).

A detailed steady-state and time-resolved photophysical study of the bis-chromophoric peptides as well as of the peptide without the azulene moiety, used as a "blank" compound, was performed in the laboratory of Prof. M. Venanzi (Department of Chemical Sciences and Technologies, University of Rome "Tor Vergata").

Steady-state fluorescence experiments in CH_3CN solution upon excitation of the pyrene chromophore at 341 nm showed a substantial quenching of the pyrene emission by azulene for both **A2P8** and **P2A8**, as illustrated in **Figure 23**. Interestingly, the **P2A8** quantum yield was slightly greater than that of **A2P8**, indicating a somewhat more efficient quenching in the latter peptide. It should be noted that the azulene emission is negligible and the fluorescence quantum yield of the pyrenyl peptide **P2** (ϕ = 0.063) is much lower than that of pyrene (ϕ = 0.72), probably because of the α-carbonyl derivatization[61].

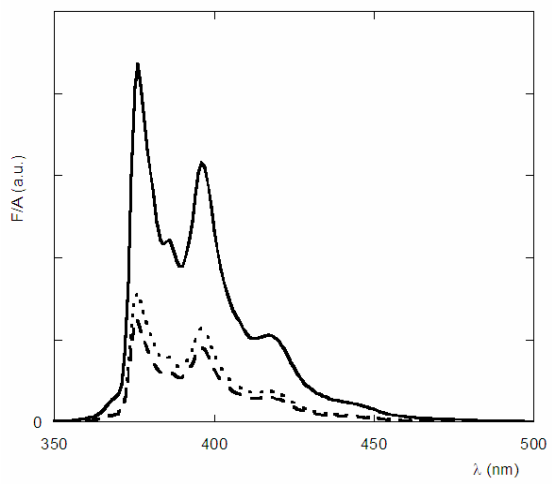

Peptide	ϕ
P2	0.063
P2A8	0.022
A2P8	0.017

Fig. 23. Steady-state fluorescence spectra of **P2** (full line), **P2A8** (dotted line), and **A2P8** (dashed line) in CH_3CN solution (λ_{ex}= 341 nm). Corresponding quantum yields (ϕ) are reported.

The results of the time-resolved fluorescence experiments (**Fig. 24**) are in agreement with the steady-state results: the average fluorescence lifetime $<\tau>$ of the **P2** peptide (11.7 ns) is much shorter than that of the pyrene molecule in solution (200 ns), and both **A2P8** and **P2A8** are significantly quenched with respect to the **P2** reference compound.

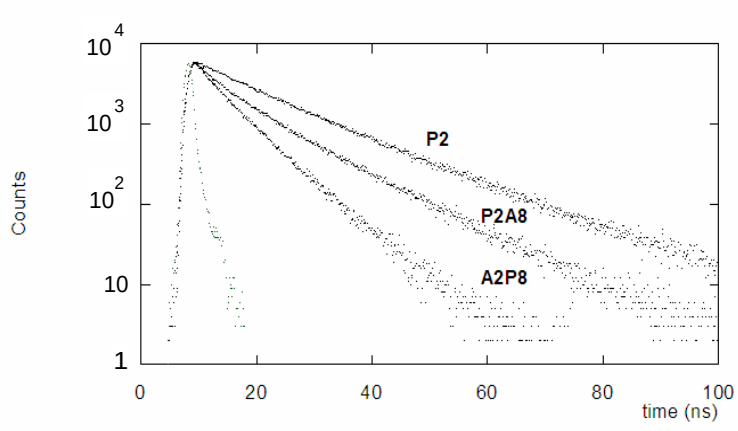

CH_3CN solution

Peptide	<τ> (ns)	$<k_{ET}>$ ($10^{-8}s^{-1}$)
P2	11.7	
P2A8	6.4	0.7
A2P8	4.8	1.2

DMSO solution

Peptide	<τ> (ns)	$<k_{ET}>$ ($10^{-8}s^{-1}$)
P2	5.0	
P2A8	3.6	0.8
A2P8	3.1	1.2

Fig. 24. Time-resolved fluorescence spectra of the peptides **P2**, **P2A8**, and **A2P8** (λ_{ex}= 341 nm, λ_{em}= 410 nm, CH_3CN solution). The lamp profile is also shown (*left*). Average lifetimes <τ> and dynamic quenching rate constants (k_{ET}) of the peptides (*right*).

All time decays can be reproduced by a multi-exponential fitting function, suggesting the existence of several ground-state conformers. This quenching effect could be explained in terms of an intramolecular photoinduced electron transfer, but resonance energy transfer is very likely taking place as well, since the absorption spectrum of the azulene chromophore partially overlaps with the emission spectrum of the pyrene moiety.

The total quenching rate constants were calculated from the average lifetimes of the pyrenyl group in the peptides (<τ>) and in the reference compound **P2** (<τ_0>), as given by:

$$< k_{ET} >= \frac{1}{< \tau >} - \frac{1}{< \tau_0 >}$$

In agreement with the steady-state results, the quenching rate constant of **A2P8** is greater than that of **P2A8** (**Fig. 24**).

Since the net dipole of an unordered peptide is zero, the photophysical studies using secondary structure disrupting solvents, such as DMSO, should provide a valuable information about the influence of the helical dipole on the measured decay rates. For this reason, time-resolved fluorescence experiments were also performed in DMSO. No significant differences were observed in the quenching rates with respect to those obtained in CH_3CN solution, suggesting that DMSO is not able to unfold the extremely stable 3_{10}-helix based on eight consecutive C^{α}-tetrasubstituted amino acids (**Fig. 24**). Unfortunately, CD experiments to confirm this conclusion could not be performed in this solvent, because of its strong absorption in the peptide spectral region (195-250 nm).

A better insight in the electron transfer process can be derived from the transient absorption experiments (**Table 5**).

Table 5. Transient absorption results for the peptides **P2**, **P2A8** and **A2P8** in CH_3CN solution.

Peptide	$\Delta A_{tot}/A$ [a)]	k_T [b)] ($\times 10^{-4}$) s^{-1}	$\Delta A_T/A$ [c)]	α_T [d)]	k_c [e)] ($\times 10^{-5}$) s^{-1}	$\Delta A_C/A$ [f)]	α_C [g)]
P2	0.289	0.6±0.1	0.098	0.34	1.82±0.05	0.191	0.66
P2A8	0.095	2.7±0.2	0.021	0.26	6.9±0.2	0.059	0.74
A2P8	0.100	4.9±0.5	0.026	0.26	5.0±0.2	0.074	0.74

[a)]Total differential absorption at t = 0, λ = 450 nm, normalized for the absorption of the pyrene chromophore at λ = 355 nm. [b)]Triplet decay rate constant. [c)]Differential triplet absorption at t = 0, λ = 450 nm, normalized for the absorption of the pyrene chromophore at λ = 355 nm. [d)]Fractional contribution of the triplet state to the transient absorption intensity at 450 nm. [e)]Rate constant of the radical cation decay. [f)]Differential radical cation absorption at t = 0, λ = 450 nm, normalized for the absorption of the pyrene chromophore at λ = 355 nm. [g)]Fractional contribution of the radical cation to the transient absorption intensity at 450 nm.

The overall transient absorptions ($\Delta A_{tot}/A$) of **A2P8** and **P2A8** are reduced with respect to that of **P2**, because of the more efficient quenching of the pyrene excited singlet state due to the azulene acceptor. However, the fraction related to the radical cation is slightly higher in these peptides than in the reference compound **P2**, showing that a photoinduced electron transfer process is indeed taking place. Moreover, the presence of signals of radical species also in the octapeptide **P2**, which lacks the electron acceptor azulene, indicates the occurrence of an electron transfer process from pyrene to the peptide backbone. However, the possibility of resonance energy transfer from pyrene to azulene has to be taken into account, since the Förster radius R_0 for pyrene and azulene, *i.e.* the characteristic distance at which the energy transfer efficiency is 50%, calculated from the emission and absorption spectra of the two chromophores (14.1 Å) is larger than the approximate distance of 12 Å between the azulene and pyrene moieties calculated for the 3_{10}-helix of the system under study.

In summary, both steady-state and time-resolved fluorescence quenching experiments did show a noticeable difference in the behavior of these two peptides, which differ in the position of the chromophore. The results indicate that the electric field generated by the peptide helix has a significant effect on the electron transfer rate. When the electron transfer takes place in the direction that is opposite to the direction of dipole moment, the quenching efficiency becomes higher and the lifetime of the excited state decreases.

The difference in decay rates for the excited pyrene chromophore in the two peptides **A2P8** and **P2A8** (with a ratio of approximately 1.7) is smaller than that obtained for α-helical peptides, where a ratio of eight between the two electron transfer rates was observed[59]. Even if the two data sets are not strictly comparable because of differences in the peptide sequence, the present results suggest that the 3_{10}-helical macrodipole has a lower effect than the α-helical dipole on the intramolecular electron transfer processes. The observed differences between the two helical conformations are very likely due to the imperfect alignment of the H-bond dipoles along the axis of 3_{10}-helix, leading to a lower overall electric field.

Taking together, the results allow to make the following conclusions:

- **Two octapeptides, based entirely on C^{α}-tetrasubstituted α-amino acids, containing pendant azulene and pyrene chromophores, were synthesized. The peptides differ in the relative position of the chromophores.**

- **FT-IR absorption and CD spectra strongly confirmed the 3_{10}-helical structure of the peptides.**

- **A detailed steady-state and time-resolved photophysical study revealed a marked difference in the rates of the intramolecular electron transfer reactions. The electron transfer is 1.7 time faster in the direction opposite to that of the helical macrodipole.**

CHAPTER 3

3_{10}-HELICAL PEPTIDES AS SPACERS FOR CD SPECTROSCOPIC STUDIES

An important issue in studying the overall conformation of large biopolymers is the development of new tools for the determination of the fine structure and the relative spatial disposition of specific probes. CD spectroscopy based on exciton coupling is a sensitive technique for the assessment of absolute stereochemistry of organic molecules in solution based on the interactions of chromophores which are preexisting in the substrate and/or introduced through derivatisations of the molecule of interest[62]. When the original substrate already contains a chromophore, the newly introduced chromophore may be selected so that its absorption maximum would be close to that of the preexisting chromophore[63]. However, in many cases overlap between the substrate and introduced chromophores complicate analyses of the CD curves. In order to avoid such interactions, the concept of "red-shifted" chromophores was developed[64, 65].

When two chromophores are chirally oriented and close enough to one another in space, their excited states couple and become non-degenerate. This phenomenon, called exciton coupling, produces a typical bisignate CD curve with two extrema (split Cotton effect). The signs and intensity of the CD bands are determined by the absolute skewness and distance between the interacting chromophores. The amplitudes of split Cotton effects are inversely proportional to the square of interchromophoric distance[66] and proportional to the square of extinction coefficients[67] of the coupled chromophores. Therefore, exciton coupling over a long distance can be achieved only with strongly absorbing chromophores. So far, the long distance effects have been examined with rigid homosteroid[68] and norsteroid[69] derivatives where the interacting transition moments of *para*-substituted benzoates attached to rings A and D with a C-C distance of 18 Å showed CD amplitudes or *A* values (distance between extrema of couplets in $\Delta\varepsilon$) up to ca. 20. While a distance of 18 Å practically covers all common natural products, the moderate *A* value of ca. 20 observed for benzoate chromophores is insufficient when dealing with samples available only in tiny amounts, or samples in

which the distance between stereogenic centers is much longer. Consequently, chromophores with more intense absorptions are needed for increased sensitivities.

Although the exciton coupled CD method has proved to be a sensitive tool in elucidating the absolute configuration and detection of even small conformational changes, its applicability in structural studies of biopolymers, such as proteins or nucleic acids, with covalently attached reporter chromophores has not been explored sufficiently. One drawback is the strong interfering absorption of the biopolymers themselves below *ca.* 300 nm, which therefore required suitable CD chromophores with an absorption above 350 nm. More importantly, the distances encountered in biopolymers need a CD chromophore which can couple over a long distance, namely, a chromophore with a very high extinction coefficient. The cyanine dye chromophores exhibit intense, red-shifted absorptions around 520 nm with narrow halfband widths of 1520 cm^{-1}; however, chemical instability makes them unsuited for practical applications [64].

Porphyrin derivatives, such as 5-(4-carboxy)-5,10,15,20-tetraphenylporphyrin, characterized by an extremely intense ($\varepsilon \sim 350\,000$) and sharp Soret band, should provide powerful CD chromophores for configurational and conformational analysis of natural products with remote stereogenic centers and for conformational studies of biopolymers. This porphyrin derivative readily acylates both hydroxyl and amino groups, produces a couplet at ca. 415 nm, and enhances the sensitivity over *p*-dimethylaminobenzoate (or benzamide)[70], one of the most sensitive chromophores, by 7 to 9-fold.

Porphyrins *per se* are achiral, but they become chiral upon stepwise symmetry breaking, which may either be due to a "chiral" environment (supramolecular chirogenesis) or to chiral substituents[71]. As a result, porphyrinoid systems become chiral if they are threaded in either clockwise or a counterclockwise twist[72].

The B (Soret) band in the UV-vis absorption spectra of a porphyrin core consists of two perpendicularly polarized transitions, B_x and B_y[63, 73] (**Fig. 25**). The directions labeled B_x and B_y are directed along the N-H/N-H and the N/N axes, respectively. However, because of the near degeneracy and approximate equivalence of these transitions, any linear combination of B_x and B_y can also be used, for example B_x' and B_y' or $B_{\parallel}$ and $B_{\perp}$. In symmetrically substituted metalloporphyrins, which have fourfold symmetry, these transitions are degenerate and have identical intensities.

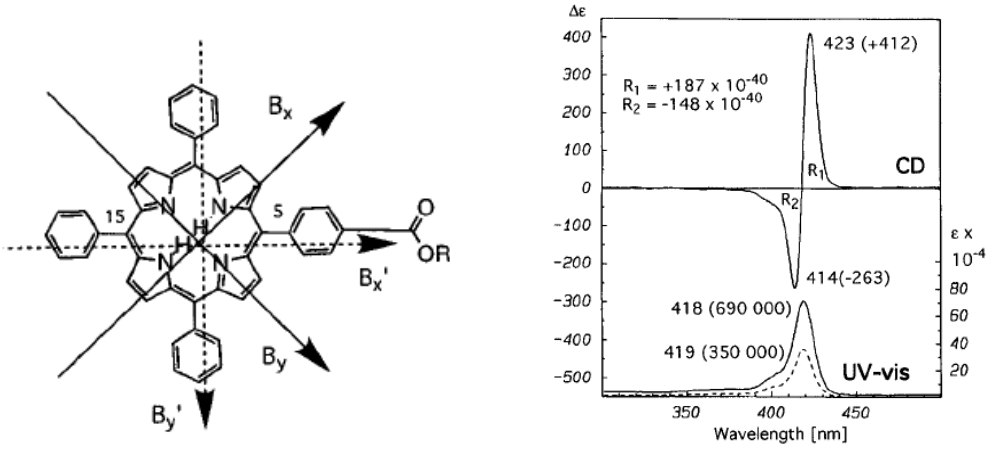

A **B**

Fig. 25. Two choices of transition moment directions for the porphyrin Soret transition (**A**). An example of bisignate CD curve formation due to exciton coupling in a *bis*-porphyrin conjugate (dotted line – 5-(4-carboxy)-5,10,15,20-tetraphenylporphyrin) (**B**).

In the free-base form of the porphyrin, with its lower symmetry, these transitions are not exactly degenerate and they will in general differ in intensity. However, most experimental and theoretical evidence argues against any sizable splitting or intensity difference in the components of the Soret band.

The excitonic coupling between the two pairs of the degenerate transitions $B_{\parallel}$ and $B_{\perp}$ gives rise to the split of Soret band (Davydov split) and such a phenomenon is often seen in UV-vis absorption spectra of *bis*-porphyrins in a linear structure where the two porphyrin rings are in an edge-to-edge spatial orientation. Static CD spectra of these systems contain two major bisignate Cotton effects. The positions of the first and second Cotton effects are closely matched to the maxima of the split Soret band which are well-resolved in UV-vis absorption spectra, and associated with the allowed $B_{\parallel}$ and $B_{\perp}$ electronic transitions, respectively. It is assumed that these transitions are the major contributors to the observed CD couplets. Although bi- or multichromophoric systems, if arranged in a chiral spatial orientation, are normally expected to exhibit bisigned CD couplets due to excitonic coupling between their electronic transitions, there are only a few examples of a good match between the CD split (which is determined by the

difference of the Cotton effect maxima) and Davydov split in the UV-vis absorption spectrum.

A distance dependency of the porphyrin coupling was investigated in the range between 10 and 50 Å[63]. Over short interchromophoric distances, significant changes in the conformational distribution introduced by the bulky porphyrin chromophores were observed. Over longer distances, the porphyrins show *ca.* 10-fold sensitivity increase over the commonly used chromophores. Porphyrins at the termini of dimeric steroids and brevetoxin B exhibit exciton coupling over interchromophoric distances up to 50 Å. This method was successfully applied for the conformational analysis of complex natural biomolecules such as gymnocin B[74]. The results confirm the fact that the porphyrins are promising reporter chromophores for extending the exciton coupled CD method to structural studies of biopolymers.

Recently porphyrinoids have been shown to be well-suited for studying the processes involved in supramolecular chirality induction owing to their spectral and physicochemical properties, easy handling, versatile modification, great biological importance, and wide applicability[75]. During the last few years, porphyrins and metalloporphyrins have attracted widespread attention as receptors for the determination of molecular chirality or chiral recognition[62, 76]. Various artificial receptors, that take advantage of their property to undergo intramolecular or intermolecular π-π stacking and host-guest complexation, have been synthesized[77].

Of the vast number of host-guest and self-associated systems, supramolecular assemblies based on porphyrin chromophores are of particular interest for investigation and potential application as tweezers, which are defined as a specially shaped type of 1:1 host-guest complexes arising from the insertion of a guest molecule between two binding sites of a molecular host through various noncovalent interactions[78]. The interaction of the chiral guest molecule with the achiral porphyrin tweezer takes place in stereocontrolled manner. CD spectra of the forming host-guest complexes are determined by the absolute stereochemistry of the guest and reflect the spacial orientation of the interacting electronic transition dipoles. In the case of the left-handed screw of *anti*-L formed by (*R*)-ligands the coupling $B_{\perp}$ transitions form a clockwise twist, while the coupling $B_{\square}$ transitions form an anticlockwise twist, which correspond to the positive first and negative second Cotton effects observed experimentally. The situation with the right-handed screw of *anti*-R induced by (*S*)-ligands is exactly

opposite to that with the left-handed screw of *anti*-L, giving negative first and positive second Cotton effects[79]. As shown in **Figure 26**, the substrate is sandwiched between the two porphyrin planes P-1 and P-2 forming either conformer **I** where the larger group (L) projects out and the smaller group (M) is situated in porphyrin binding pocket or conformer **II** where the situation is reversed. For steric reasons, conformer **I** associated with a positive CD couplet should be energetically favored, which was observed experimentally. It was shown also that temperature can serve as an effective tool for supramolecular chirality induction *via* the considerable low temperature enhancement of chiral ligand binding and the amplitude of the CD bands[80].

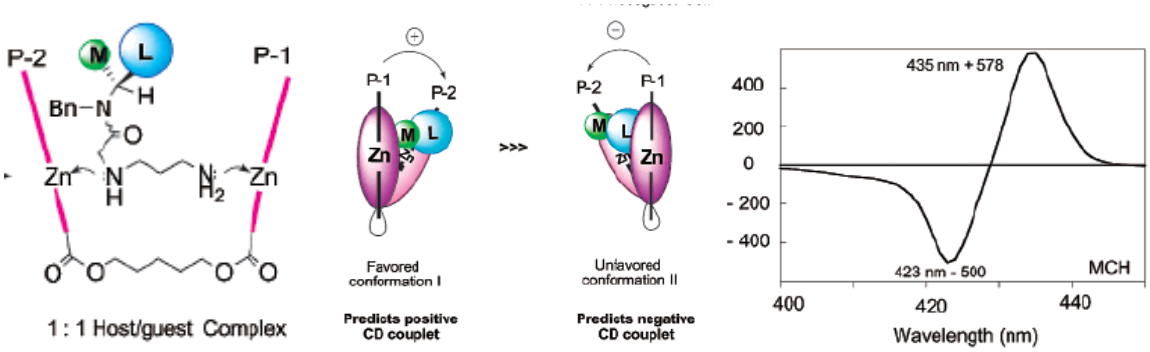

Fig. 26. Two possible ways of host-guest complex formation with opposite sense of twist[81].

Contrary to UV-vis absorption spectroscopy, CD spectroscopy can recognize individual optically active species or an excess of one of them in a mixture of antipodes. Thus, addition of the (*S*)-enantiomer to the initial mixture of *bis*(Zn porphyrin) and (*R*)-1-(1-naphthyl)ethylamine results in a gradual decrease of the induced Cotton effect intensities associated with formation of *anti*-L[82]. At the equimolar ratio of the mixture of (*R*)- and (*S*)-amines the whole supramolecular system becomes CD inactive (**Fig. 27**). Subsequent stepwise addition of (*S*)-1-(1-naphthyl)ethylamine results in a corresponding increase of new CD signals of opposite signs. The final CD spectrum obtained upon completion of the titration is an exact mirror image of that recorded for the initial mixture. These changes are the result of the equilibrium shift from the left-

handed *anti*-L to the right-handed *anti*-R conformer during addition of the (*S*)-amine. Since the directions of all of the coupling electronic transitions of *anti*-R are opposed to those of *anti*-L, the induced Cotton effects resulting from the supramolecular system obtained are expected to exhibit the opposite signs. It is also obvious that at the racemic point all of these coupling electronic transitions cancel each other, thus producing a CD inactive mixture.

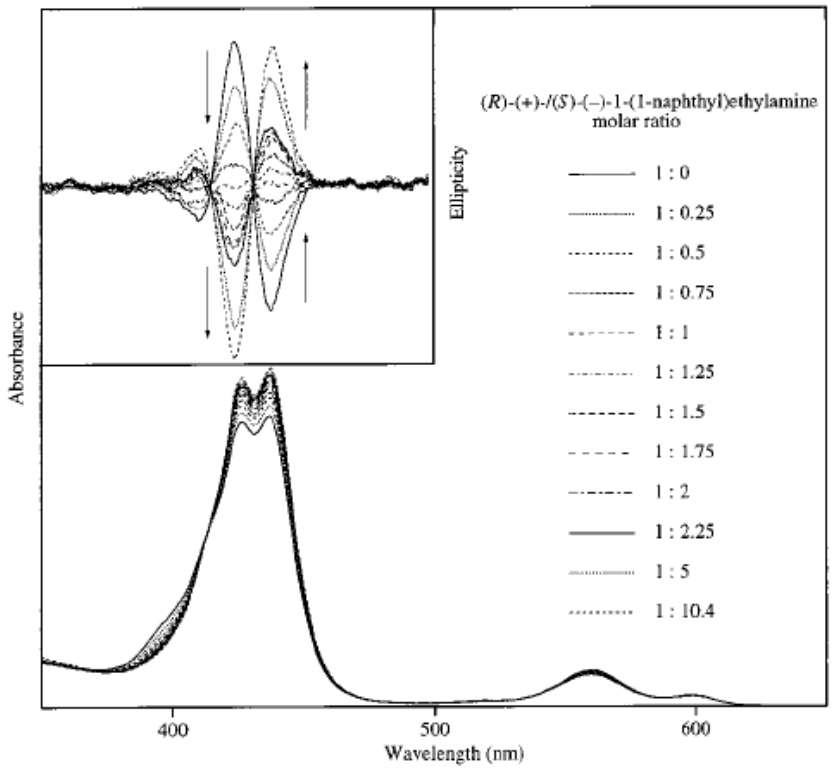

Fig. 27. A chirality inversion in the system consisting of *bis*(Zn porphyrin) and (*R*)-(+)-1-(1-naphthyl)ethylamine upon stepwise titration with (*S*)-(-)-1-(1-naphthyl)ethylamine[82].

The application of porphyrins for chiral recognition is favored by the intense and red-shifted Soret band in the spectral region where the majority of the prospective chiral guest molecules do not absorb, that allows CD monitoring with very high sensitivity. This approach has been extended to chiral diamines, amino acids, amino alcohols, primary amines and secondary alcohols for determining their absolute configuration[79, 83, 84]. In all these cases the complexes exibit exciton-coupled CD spectra, due to

stereodifferentiation leading to a preferred porphyrin helicity for a given absolute configuration[62, 85].

The CD exciton chirality method can be used not only for determining the absolute configuration and conformation of a variety of small organic molecules, but also for the assessment of the stereochemistry of more complicated systems, such as glycolipids, oligonucleotides and peptides, both in solution[86-88] and in the solid state [89].

The photophysical properties of porphyrins are not completely understood in spite of their fundamental significance for numerous applications. The study of the dependence of the excitation energy transfer on the distance between the donor and acceptor components, their mutual arrangement and the electronic and environmental factors is very important for the design of the supramolecular ensembles for molecular photonics and optoelectronics. Elaborate conjugated porphyrin assemblies, including heterobimetallic, π-overlapping polymers in which the communication between units arises through *face-to-face* π-overlap, have been prepared to afford "molecular wires" for a variety of potential applications[90, 91].

In naturally occurring photosynthetic light-harvesting complexes, biopolymer scaffolds hold pigments at intermolecular distances that optimize electronic coupling, photon capture, and energy transfer. Porphyrins, similar in structure to the naturally occurring (bacterio)chlorophyll pigments but more amenable to synthetic manipulations, have been used extensively in the design of artificial photosynthetic systems. Synthetic porphyrin model compounds can be very helpful in providing insight into the pigment molecular structure of porphyrin-based energy-transfer and electron-transfer processes in photosynthesis. Especially, porphyrins play an important role in the energy-transfer process in light-harvesting polypeptide complex of photosynthesis, where porphyrins such as bacteriochlorophylls are assembled according to cooperative interactions between the light-harvesting polypeptides and bacteriochlorophylls. Light-harvesting polypeptides organize the porphyrin complex so that an efficient energy transfer between porphyrins may occur. However, there has been little study of an artificial energy-transfer system involving light-harvesting polypeptides. In the work of Kashiwada *et al.*[92] it was investigated the process of the molecular assembly of *meso*-porphyrin dimers using LH-α and -β polypeptides from purple photosynthetic bacteria. It was demonstrated that the carboxyl group as well as the Zn or Ni atom in the *meso*-

porphyrin dimers is essential for the molecular assembly of the dimers with the LH polypeptides. A large split-CD signal at the red-shifted Soret band was observed due to the presence of the LH polypeptides especially when cooling from 25 to 4°C, implying that an edge-to-edge association of porphyrins induced by the LH polypeptides occurs.

Many covalently-linked peptide-bridged porphyrin dimers have been studied as models for charge separation and electron-transfer process and recombination that are involved in early photosynthetic events. However, artificial energy-transfer systems of porphyrin dimers using synthetic model polypeptides have been not well studied. To this aim, it is very important to control the structural properties of the assembly by manipulation of the spacing between the porphyrins along a peptide chain. Control of electronic interactions between the donor and acceptor porphyrins is also crucial for a rational design of efficient diporphyrin models. This is possible by tuning geometrical parameters, such as distance and orientation, as well as the electronic properties of the bridge. Studies of the orientation factor have, however, been rather limited so far. Investigations of heme-heme interactions in multi-heme proteins by CD are complicated by effects induced by amino acids surrounding each porphyrin chromophore. However, comparison of CD spectra of mono- and multi-heme proteins suggested heme-heme interactions. Calculations based on coordinates of isolated heme moieties taken from protein X-ray diffraction structures confirmed the possibility of long distance heme-heme interactions. The unique physical properties of the photosynthetic reaction center stimulated the synthesis of several model compounds, *i.e.* aryl- and alkylbridged porphyrin dimers. Shifts and/or splitting of the Soret band in the UV-vis absorption spectra of such achiral bridged porphyrin dimers have been attributed to exciton coupling strongly dependent on angle and distance.

Recently, it was reported the synthesis of directly *meso-meso* linked diporphyrins by one-electron oxidation of 5,15-diaryl Zn(II)-porphyrins with Ag(I)-salt or anodic oxidation[93, 94]. The close proximity of the two porphyrins in the array gives rise to a large exciton coupling, while each porphyrin retains the monomer-like properties due to their almost orthogonal disposition which minimizes electronic conjugation of the porphyrin π-systems[95]. Therefore, if the relative orientation of the two porphyrins in the *meso-meso* linked diporphyrin array can be changed in a systematic manner, it will constitute the basis for a good set of models for a study of the effect of dihedral angle on the electronic coupling. The magnitude of the electronic coupling will influence the

excitonic interactions and the rates of interporphyrin energy-transfer and electron-transfer reactions. In the work of N. Yoshida *et al.*[96] it was reported the synthesis of a series of *meso-meso* linked strapped diporphyrins (**Fig. 28**) with different dihedral angles between two porphyrin moieties. With decrease of the strap length, the absorption and fluorescence spectra and the one-electron oxidation potentials of $\mathbf{S}_n$ change in a systematic manner, suggesting a progressive increase in the electronic communication of the two porphyrins.

The absorption spectra of $\mathbf{S}_{10}$, $\mathbf{S}_8$, and $\mathbf{S}_6$ are close to that of non-strapped *meso-meso* coupled diporphyrin. Therefore, it can be supposed that relatively long straps have no significant influence on the dihedral angle between monomers. The absorption spectral changes at the Soret-band region with a change in the strap length are more prominent for S_4, $\mathbf{S}_3$, S_2, and S_1. These changes strongly indicate the increasingly enhanced electronic communication between the porphyrins.

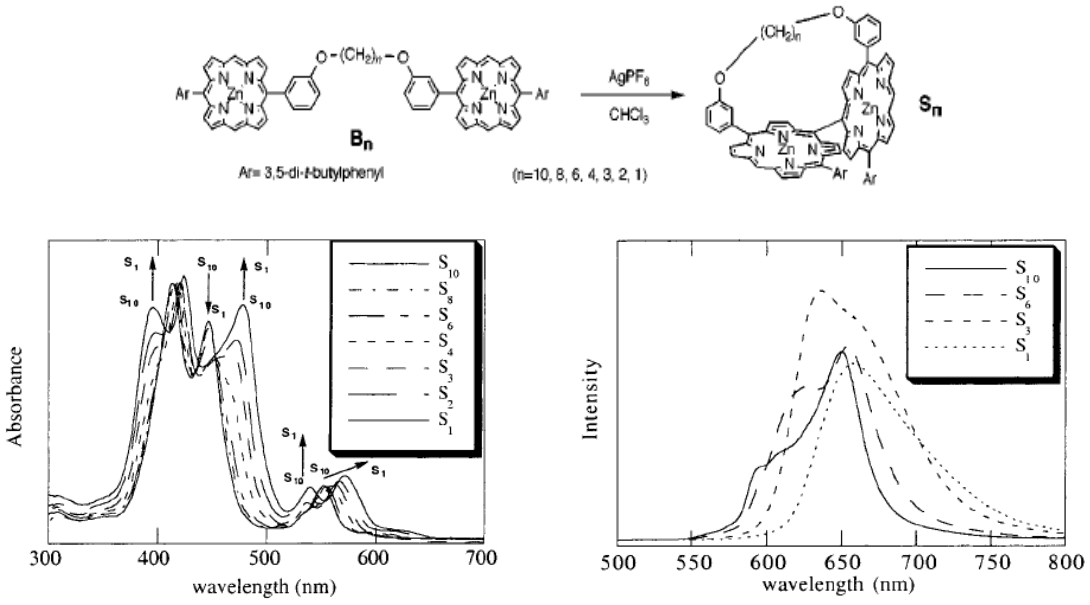

Fig. 28. A set of the *meso-meso* linked diporphyrins and their UV-vis absorption and fluorescence spectra [96].

The fluorescence spectra of selected $\mathbf{S}_n$ showed a steady red-shift with a loss of shoulders with the decrease of the strap length, roughly reflecting the red shift of the

respective absorption Q-bands. These changes also exhibit enhanced communication between the two porphyrin rings.

Photophysical properties of a series of polyisocyanides possessing porphyrin pendants (porphyrin polymers) (**Fig. 29**) were investigated by steady-state and time-resolved fluorescence spectroscopic methods[97]. These polyisocyanides exhibit a stable 4_1-helical structure when bulky substitutents are introduced. The absorption spectra, as well as fluorescence spectra, of the dimers are almost the same as those of the corresponding monomers, indicating quite small excitonic interaction between two porphyrin units (**Fig. 30**). This finding suggests that the porphyrin units in the dimer take a conformation where the excitonic interaction becomes minimal. In the cases of the polymers, the B (Soret) band shows splitting and substantial broadening with an increase in the number of repeating units. The shift to the higher energy side with an increase in relative intensity indicates that porphyrin units are stacked in a face-to-face conformation in which the transition dipole moments are aligned in a parallel form.

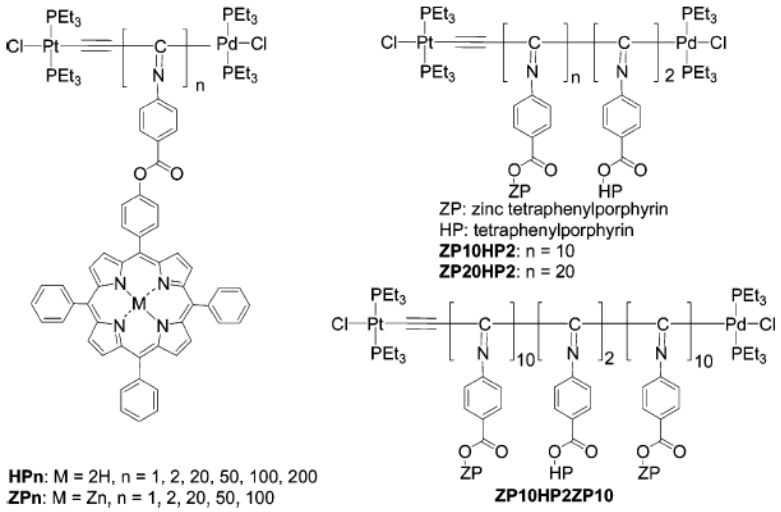

Fig. 29. Chemical structures of the porphyrin polymers studied in ref. [97].

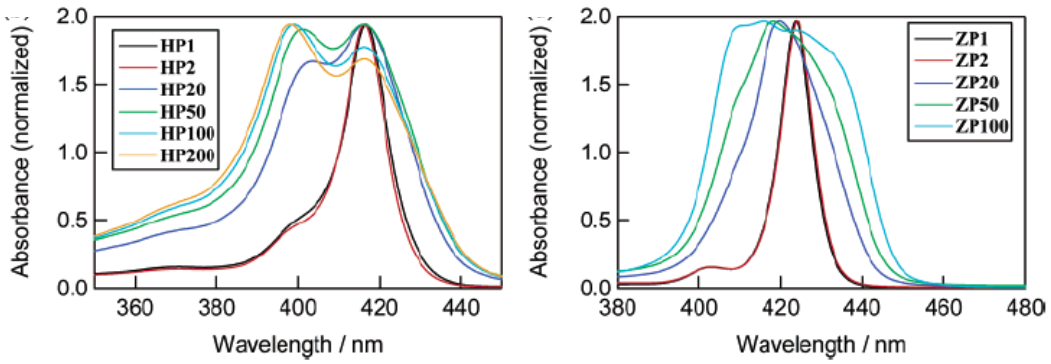

A

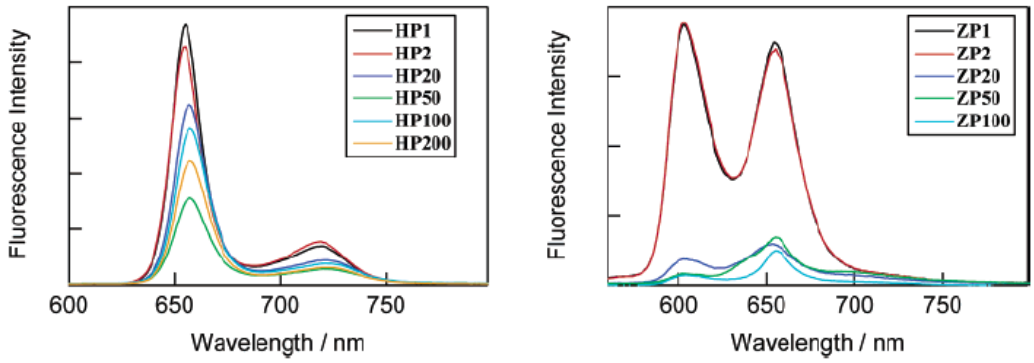

B

Fig. 30. Absorption (**A**) and fluorescence (**B**) spectra of the porphyrin polymers in tetrahydrofuran[97].

Time-resolved fluorescence measurements showed fast exciton-exciton annihilation rate accompanying the polymeric structural change after the fast exciton migration regardless of the length of polymer chain, indicating that the exciton migration in the polymer chain is quite fast.

The fast exciton migration was also found in porphyrin-functionalized α-helical Lys polypeptides[98] bearing spatially closed porphyrin pendants (**Fig. 31**). It was shown that the interaction between the porphyrins in these polypeptides is rather weak, suggesting that the distance between the porphyrin units is large even in the longest porphyrin polypeptide, **P8**.

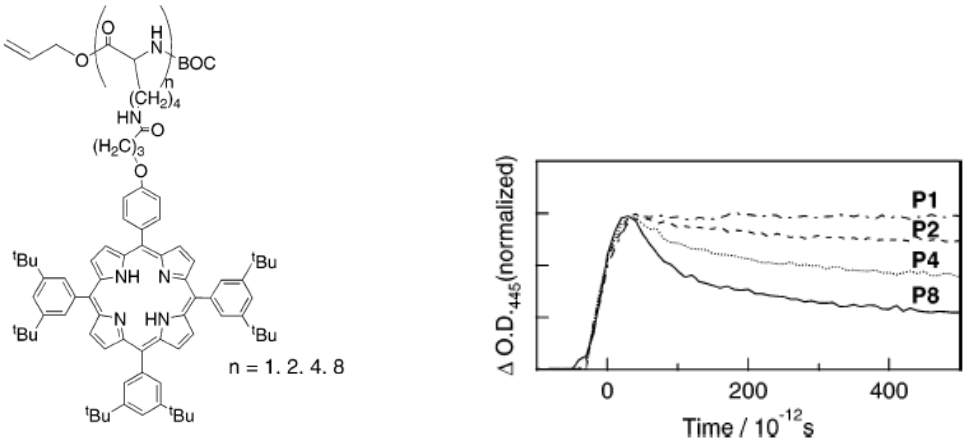

Fig. 31. Porphyrin polypeptides studied in ref. [98] and their time-resolved fluorescence spectra at 445 nm.

Peptides covalently linked to a porphyrin moiety represent models of natural photosynthetic light-harvesting complexes. Several laboratories have demonstrated self-assemblies of porphyrins using natural or synthetic polypeptides to organize an artificial hemoprotein models. In the work of Dunetz *et al.*[99] a short 10-mer peptide sequence Ac-Asn-Ala-Glu(TPP)-Ala-Ser-Ala-Glu(TPP)-Ser-Ala-Tyr-NH_2, consisting predominantly of the helix-promoting residues Ala and Glu, served as a scaffold for positioning two porphyrins on the same face of the α-helix. Self-assemblies in a "lego-like" fashion gave extended porphyrin arrays with properties that could be controlled by peptide concentration, temperature, and pH. The growth of the aggregate could be monitored over time (**Fig. 32**). A conservative, negative couplet develops in the 350-500 nm region of the CD spectrum, with a positive peak at 436 nm and a negative peak at 455 nm. The simplicity of the spectrum indicates the presence of one major species, and the signal strength and band shape are indicative of extensive electronic communication between a large number of porphyrin moieties[100].

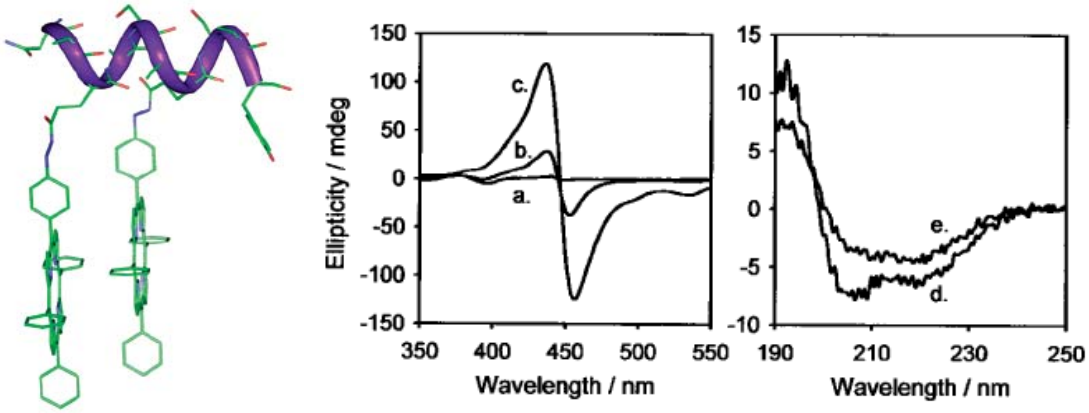

Fig. 32. (left) Representation of a computer model of the *bis*-porphyrin decapeptide. (right) CD spectra of a 15 μM solution of the peptide Ac-Asn-Ala-Glu(TPP)-Ala-Ser-Ala-Glu(TPP)-Ser-Ala-Tyr-NH_2 in TFE after storage at 4 °C and pH 7 for (**a**, **d**) 4 days, (**b**) 27 days, and (**c**, **e**) 101 days[99].

The region 190-250 nm of the CD spectrum of the peptide incubated at 4 °C (**Fig. 32d**), displayed features characteristic of the α-helical peptide structure. Changes in the peptide region occurred over time (**Figure 32e** shows that incubation of the peptide at 4°C over more than 100 days led to an overall reduction in intensity of the CD band and a loss in intensity of the 209 nm band with respect to the 222 nm band). The signal band shape is typical of that seen for moderately aggregated helical peptide spectra in which the spectral changes are consistent with light scattering effects brought about by aggregation[101].

In a study by Arai *et al.*[102] a tetraphenylporphyrin moiety was attached via a cysteine residue to a penta- or a heptapeptide sequence to furnish mono-porphyrin linked assemblies:

Ac-Cys(R_1)-Lys-Val-(Ser-Val)$_n$-Lys-Val-NH_2
5: n = 0, R_1 = H;
6: n = 1, R_1 = H;
7: n = 0, R_1 = CH_2CO-*p*-Por;
8: n = 0, R_1 = CH_2CO-*o*-Por;
9: n = 1, R_1 = CH_2CO-*p*-Por;
(*p*- or *o*-)Por: tri(*p*-tolyl)porphyrin-5-yl-C_6H_4-(*p*- or *o*-)NH

The CD spectra (**Fig. 33**) showed that the porphyrins linked at Cys induced β-structure formation, while the free peptides had random structure. Since the mono-porphyrins did not show exciton coupling, the strong exciton coupled Cotton effects in the CD spectra of the conjugates indicated that porphyrins were located nearby in the chiral orientation in the self-assembled structures, formed due to the stacking of the hydrophobic porphyrins in the aqueous system. The complex structure of the CD band of **7** is indicative of heterogeneity and several interactions of assembled porphyrins.

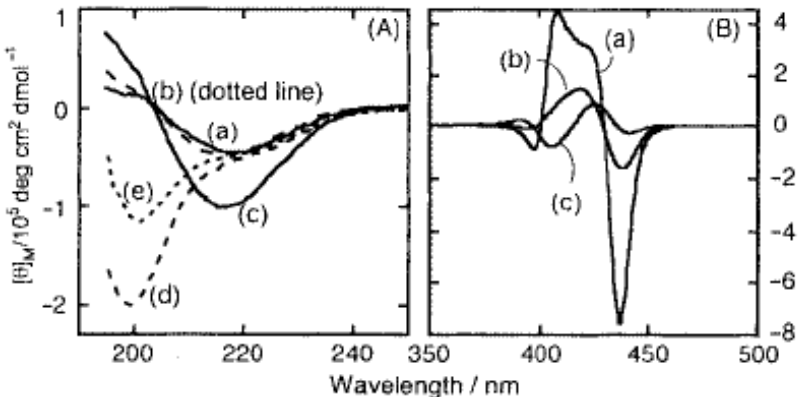

Fig. 33. CD spectra of **7** (**a**), **8** (**b**), **9** (**c**), **5** (**d**) and **6** (**e**) in pH 9 buffer-20% TFE [102].

Systems consisting of porphyrins covalently attached to peptidic scaffolds have been used to examine the distance and angle dependence on exciton coupling and energy transfer[103, 104]. The importance of the rigidity of a scaffold was clearly shown in the work of Arai *et al.*[105], where the rigid cyclic decapeptide gramicidin S (GS) and its analogues were used as templates for two porphyrin moieties (**Fig. 34**).

10b, **11b** and **12b** showed strong split Cotton effects due to the exciton coupling of the two porphyrins. The intensity of the corresponding CD bands were **10b** < **11b** > **12b**. The drastic difference between **11b** (Orn) and **12b** (Lys) may indicate that, on the contrary to Orn, the more flexible Lys side chains do not allow the close spatial orientation of the porphyrin rings. The Cotton effect for the porphyrins on GS is solvent dependent. The intensity of the Cotton effect is in the order toluene > MeOH > trimethylphosphate > TFE > CH_2Cl_2 > pyridine.

These observations may indicate that the two porphyrins in **11b(Zn_2)** are in close proximity in toluene and that the distance differed in the various solvents. The different assembling ability of porphyrins in these solvents might cause different CD, probably because of the different stabilization effect of the solvent for the π-π interaction. The details of the π-π interaction of the porphyrins are not clear yet; however, an electrostatic model may account for the tendency for porphyrin assembly in nonpolar solvents.

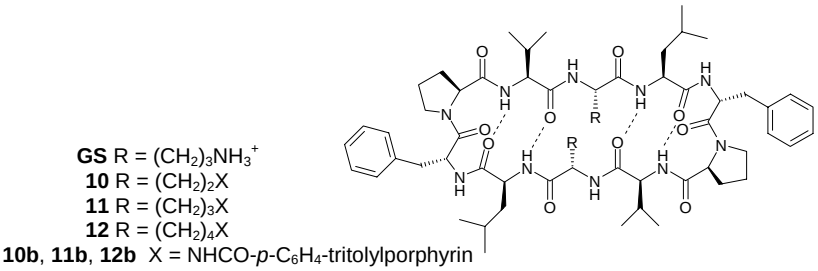

GS R = $(CH_2)_3NH_3^+$
10 R = $(CH_2)_2X$
11 R = $(CH_2)_3X$
12 R = $(CH_2)_4X$
10b, **11b**, **12b** X = NHCO-*p*-C_6H_4-tritolylporphyrin
11b(Zn_2) *bis*-zinc complex of **11b**

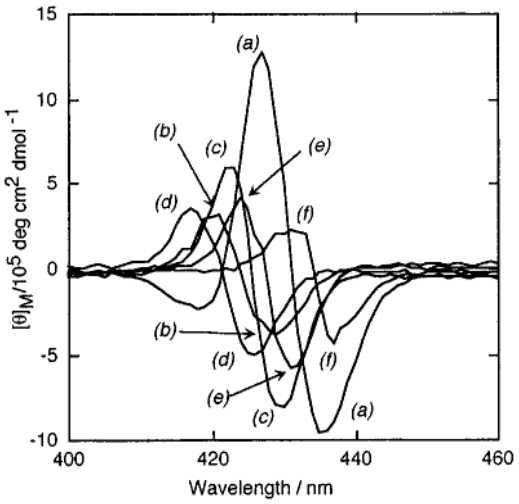

Fig. 34. CD spectra of **11b(Zn_2)** in (**a**) toluene, (**b**) CH_2Cl_2, (**c**) MeOH, (**d**) TFE, (**e**) trimethylphosphate and (**f**) pyridine[105].

Since the relative orientation and interchromophore distance determined by the dihedral angle between the two porphyrin units are key factors in controlling the interchromophoric interaction[106-108], it is relevant to investigate how the dihedral angle between the neighboring porphyrins influences the electronic nature of the porphyrin arrays. For this purpose it is very important to have in hand rigid, but conformationally

tunable spacers or templates with well defined geometry. Templates and spacers based on rigid 3_{10}-helical structures could be very promising for the control of the structure and electronic properties of the assembly by manipulation of the spacing between the porphyrins along a peptide chain.

We examined by the exciton coupled CD method the combined distance and angular dependencies generated by the seven conformationally restricted *β*-turn and 3_{10}-helical spacer peptides -L-Ala-[L-(αMe)Val]$_n$- (*n* = 1-7), [(αMe)Val, C^{α}-methylvaline], in a system formed by two intramolecularly interacting 5-carbamido-5,10,15,20-tetraphenylporphyrin (TPP) chromophores (**Fig. 35**).

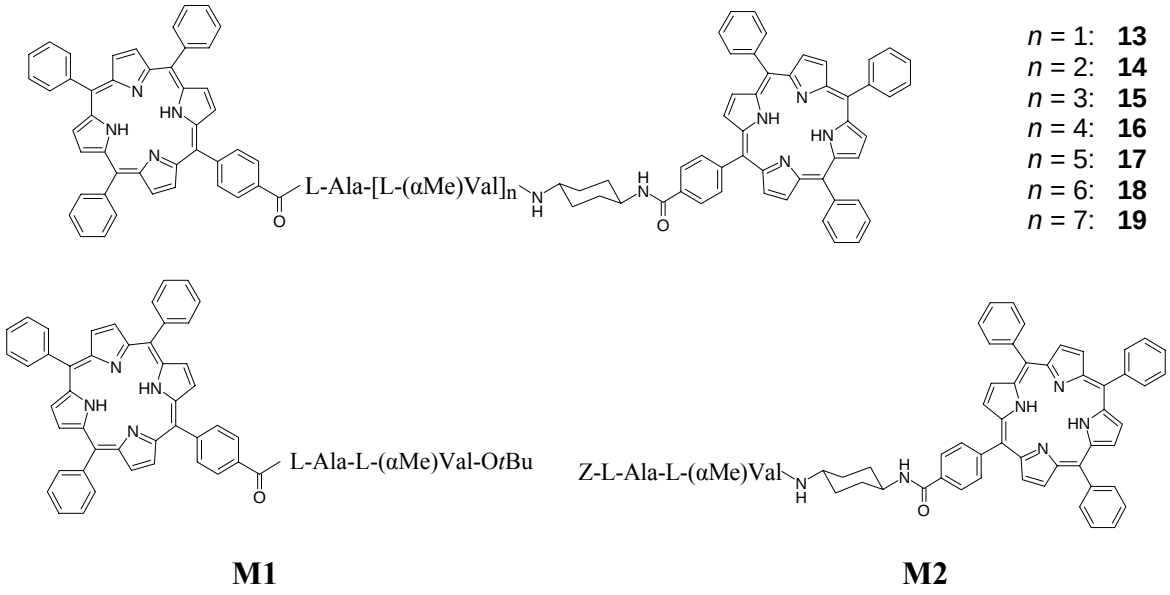

Fig. 35. The *bis*- and mono-porphyrin/peptide conjugates studied in this work.

To generate rigid structures for the spacers, we extensively used L-(αMe)Val residues which is known to possess a very strong propensity for *β*-turn and 3_{10}-helix formation, and the peptides of which exhibit a marked tendency to fold into right-handed secondary structures.

In a previous work a series of conjugates with complete amount of β-turns (*n* = 1, 3, 6) was prepared[109]. The shortest spacer [the N-acylated dipeptide amide -CO-L-Ala-L-(αMe)Val-NH- (compound **13**)] was long enough to form an intramolecular H-bonded *β*-turn conformation. The other two peptide spacers synthesized, -CO-L-Ala-[L-

(αMe)Val]$_4$- (compound **16**) and -CO-L-Ala-[L-(αMe)Val]$_7$- (compound **19**), differed by one and two additional turns of 3_{10}-helical structure, respectively. The achiral, *trans*-1,4-diaminocyclohexane, *semi*-rigid moiety at the C-terminus was incorporated to provide the system with identical chromophores (TPP-CO-NH-) at each terminus. Since the final coupling between two sterically demanding TPP-OH and H-[L-(αMe)Val]$_n$-NH-C_6H_{10}-NH-CO-TPP (n > 2) peptides failed, even with the acyl fluoride methodology, because of the extremely severe steric requirements of the two reagents, we were forced to add to the N-terminal L-(αMe)Val residue of our spacers a less bulky (but also less conformationally restricted) L-Ala residue, building up by that slightly less rigid spacers.

In this work we have extended our analysis to the preparation and spectroscopic investigation of all of the other members of the peptide spacer series (from **13** to **19**), -CO-L-Ala-[L-(αMe)Val]$_n$- (compounds **14**, **15**, **17**, and **18**). For spectroscopic comparison we also prepared the mono-porphyrin/peptide conjugates **M1** and **M2**.

First, the terminally protected peptides Z-L-Ala-[L-(αMe)Val]$_n$-O*t*Bu (Z, benzyloxycarbonyl; O*t*Bu, *tert*-butoxy; n = 1-7) were synthesized by solution methods. Coupling of Z-L-Ala-OH to the H-L-(αMe)Val derivative or peptides was achieved in excellent yield by the symmetrical anhydride method. Removal of the *tert*-butyl ester function from the N-terminally protected peptides was achieved by mild acidolysis (1:1 CH_2Cl_2/trifluoroacetic acid mixture). Coupling of the Z N-protected peptides with an excess of *trans*-1,4-diaminocyclohexane via the 5(4*H*)-oxazolone intermediates using EDC afforded the mono-acylated diamines, which were subsequently further acylated with TPP-COOH activated by the EDC/HOAt mixture. In the last step, the Z N-protection was removed by catalytic hydrogenation, followed by acylation of the liberated α-NH_2 function with TPP-COOH.

Schematic virtual conformations of these peptides (without energy minimization) give different values for the interchromophoric distances and angles (**Fig. 36**). To build up these representations, we took the literature data for the X-ray diffraction structure of 5,10,15,20-tetraphenylporphyrin[90, 110]. Also, we were forced to assume a few restrictions to the motion of the cyclohexane ring (preferably in the chair conformation) and the *trans* disposition of the peptide bonds, typical of the 3_{10}-helical backbone structure.

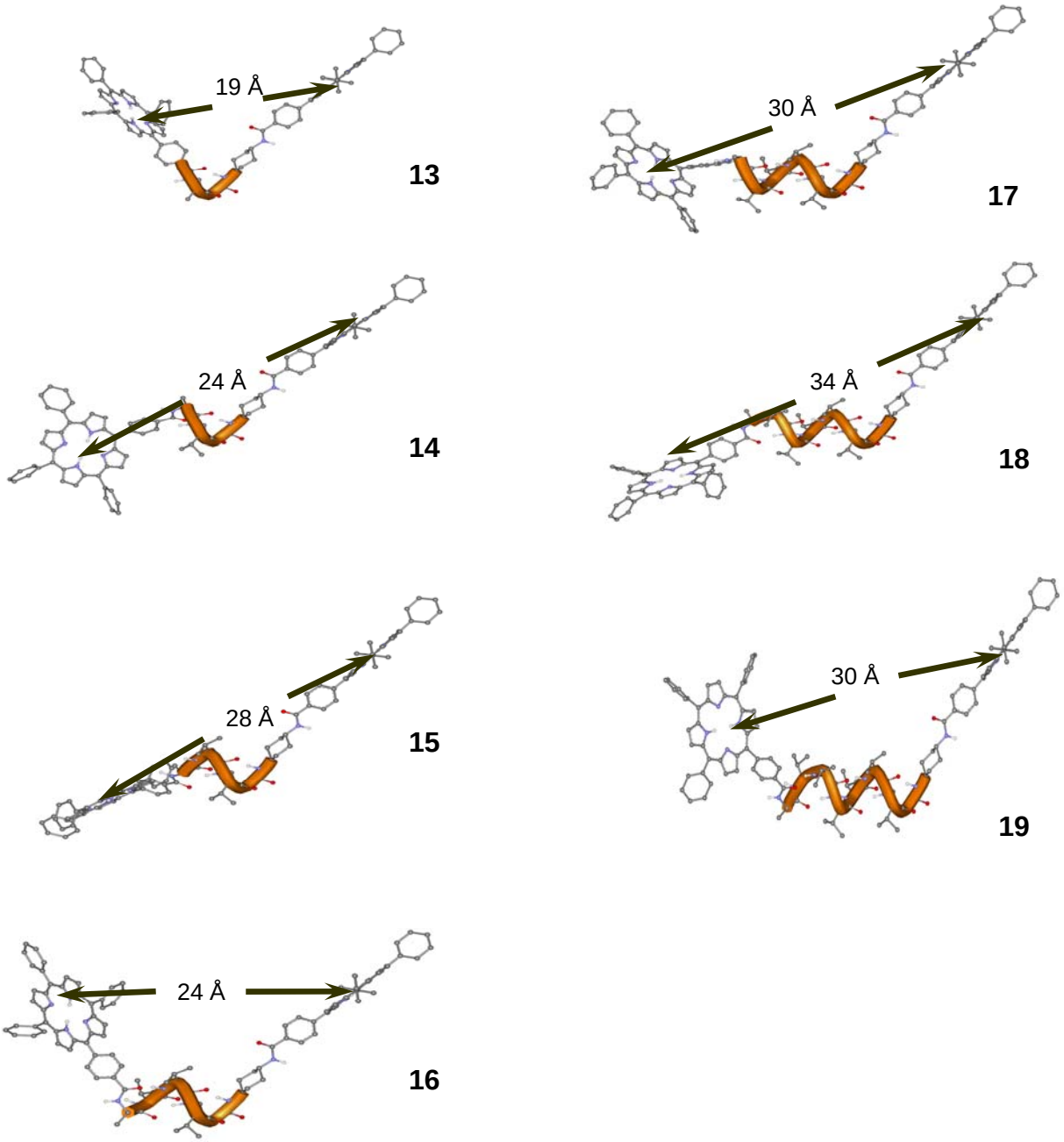

Fig. 36. Three-dimensional representations of the porphyrin/peptide conjugates studied in this work.

Formation of the 3_{10}-helix, stabilized by intramolecular C=O···H-N bonds, was confirmed by a FT-IR absorption analysis and NMR titrations. **Figure 37** summarizes the FT-IR absorption results in the conformationally informative N-H stretching region for all the members of the series. In the analysis of the spectra it should be taken into account that also the porphyrin N-H groups remarkably contribute to the absorption between 3340 and 3300 cm^{-1}. The relative intensity of the band associated with H-bonded peptide N-H groups (3360-3345 cm^{-1}) regularly increases compared with that assigned to free (solvated) peptide N-H groups (3445-3435 cm^{-1}) as a function of main-chain lengthening. These findings strictly parallel those reported for the β-turn and 3_{10}-helix forming [L-(αMe)Val]$_n$ (n = 2-8) homo-peptides[111]. The peptide concentration does not produce any remarkable effect on the spectra, at least in the range investigated (1×10^{-3} M to 0.1×10^{-3} M) (not shown). This latter result clearly indicates, although indirectly, that the observed C=O···H-N bonding is of the intramolecular type.

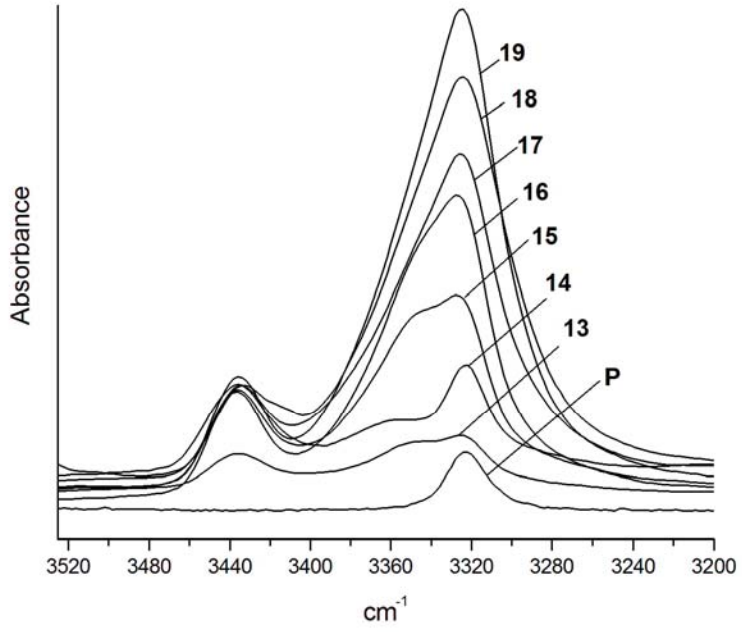

Fig. 37. FT-IR absorbtion spectra in the 3500-3200 cm^{-1} region of 5,10,15,20-tetraphenylporphyrin (**P**) and conjugates **13 – 19** ($CDCl_3$; concentration: 1×10^{-3}M).

The delineation of the inaccessible NH groups of the conjugate **16**, taken as a representative example, was carried out using the variation of the NH proton chemical shifts, by adding increasing amounts of the strong H-bonding acceptor solvent DMSO to the $CDCl_3$ solution (**Fig. 38**). Complete assignment of all NH protons was achieved from two-dimensional (2D)-ROESY and total correlation spectroscopy experiments.

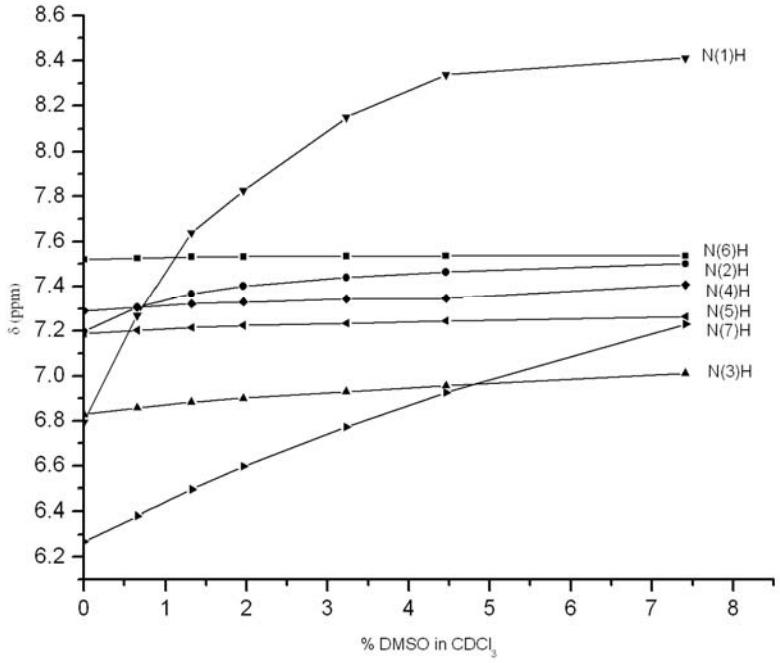

Fig. 38. Plot of NH proton chemical shifts in the ^{1}H NMR spectrum of conjugate **16** as a function of increasing percentages of DMSO (*v*/*v*) added to the $CDCl_3$ solution (concentration: 1×10^{-3}M).

The N(3)H-N(6)H protons of **16**, involved in the intramolecular H-bonds, show a behavior characteristic of shielded protons (a remarkable insensitivity of the chemical shift to the solvent composition). It is worth noting that the sensitivity of the N-terminal N(1)H and C-terminal N(7)H protons is remarkably high. The relatively poor sensitivity of the N(2)H proton to the addition of the polar DMSO is typical of L-(αMe)Val-rich oligopeptides as a result of its being positioned in a highly apolar cleft generated by the sterically demanding amino acid side chains.

The CD spectra of all mono- and *bis*-porphyrin conjugates synthesized were recorded in the same solvent ($CHCl_3$) which was used for the FT-IR absorption and ^1H NMR peptide conformational analyses. The CD curves of the mono-porphyrin/peptide conjugates **M1** and **M2** exhibit a relatively weak and positive Cotton effect in the Soret band region (at 418 ± 2 nm) (**Fig. 39**).

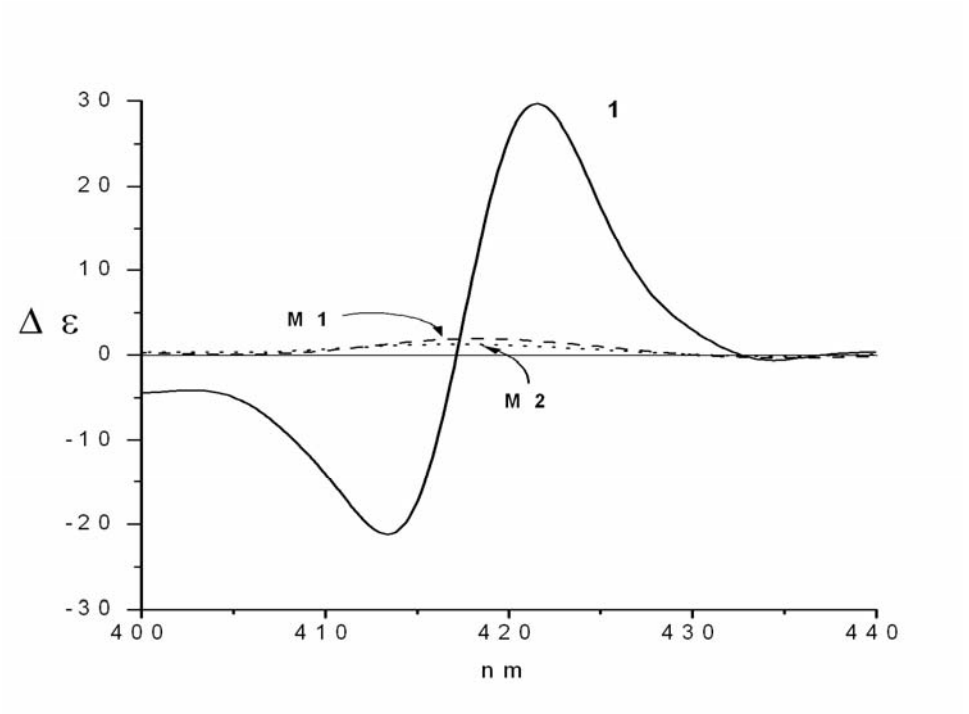

Fig. 39. CD spectra in the 400-440 nm region of conjugates **13** (**1**), **M1** and **M2** ($CHCl_3$, concentration: 1×10^{-6}M).

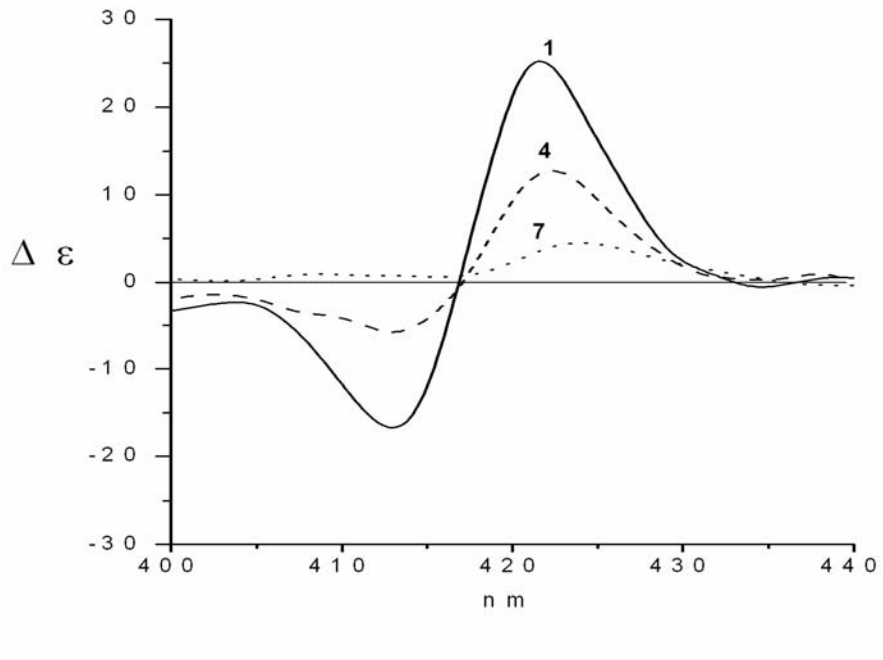

Fig. 40. CD spectra in the 400-440 nm region of conjugates **13** (**1**), **16** (**4**) and **19** (**7**) ($CHCl_3$, concentration: 1×10^{-6}M).

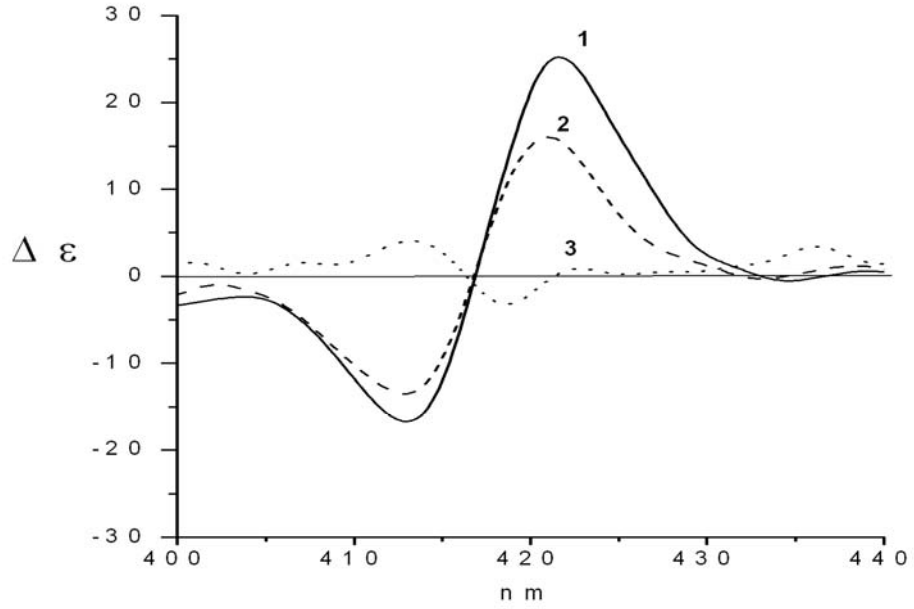

Fig. 41. CD spectra in the 400-440 nm region of conjugates **13** (**1**), **14** (**2**) and **15** (**3**) ($CHCl_3$, concentration: 1×10^{-6}M).

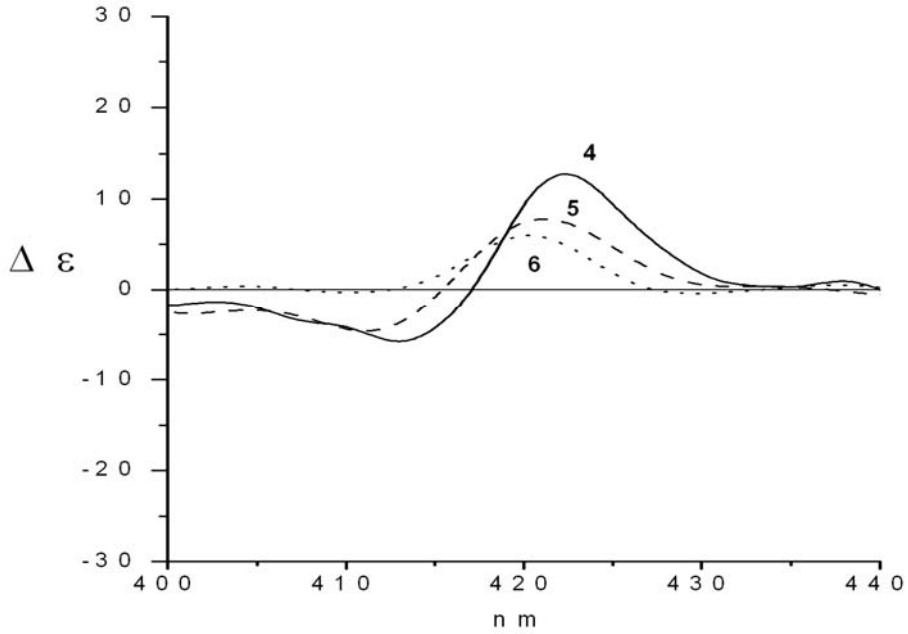

Fig. 42. CD spectra in the 400-440 nm region of conjugates **16** (**4**), **17** (**5**) and **18** (**6**) ($CHCl_3$; concentration: 1×10^{-6}M).

The intensity of the monosignate CD band is slightly higher in **M1** ($\Delta\varepsilon = 2.1$) than in **M2** ($\Delta\varepsilon = 1.2$). These findings are in good agreement with those reported by Nishino *et al.*[71, 112] on related systems and are in part associated with the longer distance separating the TPP-CO-NH- chromophore from the nearest amino acid chiral center in **M2** as compared with **M1**.

On the other hand, the CD spectrum of the *bis*-porphyrin/peptide conjugate **13**, with its conformationally restricted, *β*-turn forming, -L-Ala-L-(αMe)Val- bridge, shows a characteristic, intense, bisignate curve with a positive maximum at 422 nm ($\Delta\varepsilon = 28$), a negative maximum at 413 nm ($\Delta\varepsilon = -22$), and a cross-over point at 417 nm. (**Fig. 40-42**). The signs of CD couplet in the conjugate **13** parallel those exhibited by the related *bis*-(*p*-substituted benzoyl) peptides[70]. The observed non-conservativity of the CD band (the positive band is more intense than the negative band) supports the view that the Soret transitions are coupled to some extent with other transitions[63].

The distance dependency of the *bis*-porphyrin exciton coupled CD is clearly seen from the CD spectra in **Figures 41** and **42**. The intensity of the CD band decreases with

the length of the spacer. The Cotton effects of conjugates **16** and **17**, with their longer peptide spacers, characterized by one and more than one complete turn of 3_{10}-helix, respectively, are much less strong ($\Delta\varepsilon_{422}$ = 13, $\Delta\varepsilon_{413}$ = -6 for **16** and $\Delta\varepsilon_{421}$ = 8, $\Delta\varepsilon_{411}$ = -5 for **17**), than those of the single and double *β*-turn forming conjugates **13** and **14** ($\Delta\varepsilon_{421}$ = 17, $\Delta\varepsilon_{412}$ = -13), respectively. The signs (positive) of the CD couplet is the same in the four curves, thereby suggesting that the type of *β*-turn formed in the N^{α}-acylated dipeptide amide **13** is the same as that of the N-terminal *β*-turn of spacers **14**, **16**, and **17**. Furthermore, when the length of the peptide spacer is increased by one additional turn of 3_{10}-helix (from **16** to **19**), the corresponding CD curve is not exciton split, but rather it shows two relatively weak, positive Cotton effects ($\Delta\varepsilon \approx$ 1-5) with maxima at 410 and 424 nm. The CD results also indicate that the exciton coupling is quite strong over the interchromophoric distance of about 19 Å (conjugate **13**), and it is still clearly detectable over the longer distance of about 24 Å (conjugate **16**) but not at about 30Å (conjugate **19**).

The combined role of the distance and angular effects are quite evident from inspection of **Figures 41** and **42**. A particularly striking comparison is that between the curves of compounds **15** and **17**. In the curve of conjugate **15** the exciton coupled CD is missing, whereas in that of **17**, despite its slightly longer peptide spacer (28Å in **15** and 30Å in **17**), but with its more appropriate interchromophore orientation (roughly parallel in **15** and perpendicular in **17**), the intensity of the porphyrin…porphyrin interaction is still remarkable. This result highlightes the importance of the orientation factor between two chromophores for the exciton coupling. When the mutual orientation of the chromophores does not allow spatial proximity, despite a short separation, the phenomenon of CD exciton coupling does not take place.

The results obtained allow us to extract the following conclusions:

- **An exciton coupled CD phenomenon between two strong chromophores was observed over a full set of sterically hindered oligopeptide spacers (from di- to octapeptide) with an ordered secondary structure of progressively increasing length (evolving from a single β-turn to a completely developed 3_{10}-helix).**
- **A net decrease of the intensity of the CD bands with the length of the spacer between the two chromophores was seen.**

- **We highlighted a relevant role for the angular dependency between the directions of the effective transition moments of the two chromophores.**
- **Porphyrin derivatives proved to be extremely promising reporter groups for the conformational analysis of large peptide biopolymers.**

CHAPTER 4

3_{10}-HELICAL PEPTIDES FOR IR ABSORPTION SPECTROSCOPY STUDIES

Infrared absorption spectroscopy is widely used as a technique for determining the secondary structure and conformational changes of both short peptides and proteins[113, 114], which is based on the molecular vibration (and rotation) excited by the electromagnetic field in the region of infrared (IR) waves (with λ comprising the 780 nm – 2000 μm region). Characteristic bands found in the infrared spectra of proteins and peptides include the amide I and amide II:

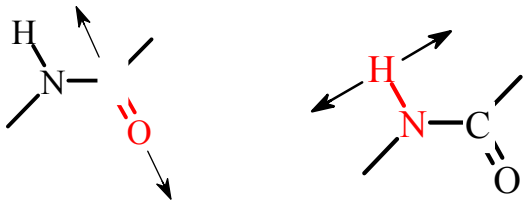

Amide I vibration Amide II vibration

These bands arise from the amide bonds that link the amino acids. The absorption associated with the amide I band is caused by stretching vibrations of the C=O bond of the amide, while overwhelmingly bending vibrations of the N-H bond lead to the absorption associated with the amide II band. Because both the C=O and the N-H bonds are involved in the H-bonding that takes place between the different elements of the peptide secondary structure, the locations of the amide I and amide II bands are sensitive to the conformation. Nevertheless, the amide II band is a less good reference for characterization of the secondary structure of peptides and proteins, since the shifts in this band are small compared to the width of the band and instead of a series of resolved peaks for each type of secondary structure, one broad peak is usually observed. Therefore, most studies have been focused on the amide I band, which occurs between 1700 and 1600 cm^{-1}. The properties of this band depend on the peptide secondary

structure, and different structural patterns, such as α-helices, β-pleated sheets, and random coils, can be distinguished based on differences in the frequency, splitting, bandwidth, and intensity of their amide I bands. This conformational dependence can be attributed to differences in intrapeptide H-bonding among the different secondary structures and transition dipole coupling between amide I modes of neighbor peptide moieties.

Typically, IR spectroscopy is a low-resolution technique for studying peptides and proteins. It is limited to the determination of the *overall* secondary structural content and does not allow the distinction between different structures at the *residue* level. Nevertheless, IR absorption spectroscopy can be made site specific by isotopic labelling of given residue carbonyls with ^{13}C. When site-specific ^{13}C labels are introduced into the peptide backbone, this modification, which causes the change of the reduced masses in the harmonic oscillators of the C=O bonds, decreases the amide I frequency (1700-1600 cm^{-1}) by approximately 40 cm^{-1}, according to the equation:

$$\tilde{\nu} = \frac{1}{2\pi \cdot c}\sqrt{\frac{k}{\mu}} \qquad \mu = \frac{m_1 m_2}{m_1 + m_2}$$

where c is vacuum velocity of light
k is force constant
μ is reduced mass

This phenomenon is observed as a well-resolvable shoulder to the main amide I band. Such an "isotope-edited" IR spectroscopy provides an opportunity to experimentally test the conformation of a specific, *local* segment of the peptides[115] or proteins[116] and to obtain direct information about residue coupling in a time-resolved manner and in a two-dimensional variant by introducing another isotope, such as ^{18}O[117].

The intensity of the ^{13}C amide I band depends on the amount of the labeled residues, as it was shown in the work of Barber-Armstrong *et al.*[118], who studied by the FT-IR spectroscopy method a series of model α-helical peptides labelled at different positions:

unlabeled	Ac-AAAAKAAAAKAAAAKAAAAKAAAAKY-NH_2
1L:	Ac-AAAAKAAAAKAAAAKAAAAKAAAAKY-NH_2
2L:	Ac-AAAAKAAAAKAAAAKAAAAKAAAAKY-NH_2
3L:	Ac-AAAAKAAAAKAAAAKAAAAKAAAAKY-NH_2
4L:	Ac-AAAAKAAAAKAAAAKAAAAKAAAAKY-NH_2
N4L:	Ac-AAAAKAAAAKAAAAKAAAAKAAAAKY-NH_2

2L2T: Ac-AAAAKAAAAKAAAKAAAAKAAAAKY-NH_2
2L1S: Ac-AAAAKAAAAKAAAKAAAAKAAAAKY-NH_2
2L2S: Ac-AAAAKAAAAKAAAKAAAAKAAAAKY-NH_2
2L3S: Ac-AAAAKAAAAKAAAKAAAAKAAAAKY-NH_2
2L4S: Ac-AAAAKAAAAKAAAKAAAAKAAAAKY-NH_2
2L5S: Ac-AAAAKAAAAKAAAAKAAAAKAAAAKY-NH_2
2L6S: Ac-AAAAKAAAAKAAAAAKAAAAKAAAAKY-NH_2

where A = ^{13}C-labelled Ala residues

The shoulder caused by ^{13}C=O is clearly detectable in the sequence having only one labeled residues (**1L**) (**Fig. 43**), while the IR spectrum of unlabeled peptide lacks this feature. Thus, even a single ^{13}C-labeled residue can be used as a local probe of peptide conformation. As the temperature increases and the peptide changes conformation from helix to random coil, the ^{13}C amide I band shifts to higher frequency and decreases in intensity, becoming a poorly resolved tail on the main ^{12}C band.

Some trends in spectral features as a function of the number and positioning of labelled residues were also observed, such as an effect of ^{13}C labels on the ^{12}C amide I band.

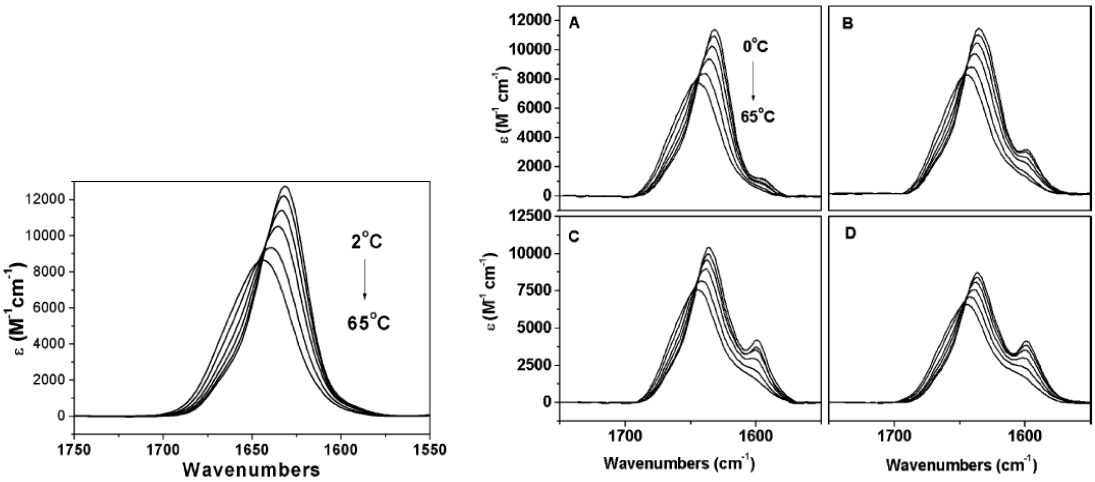

Fig. 43. FT-IR spectra of Ac-$(AAAAK)_5$-NH_2 (*left*) and the peptides **1L** (**A**), **2L** (**B**), **3L** (**C**), and **4L** (**D**) ^{13}C-labelled residues of Ala (*right*) ***118***.

While introduction of one ^{13}C-labeled residue into the center of the helix does not significantly perturb the frequency of the ^{12}C amide I band, a block of labelled residues can disrupt coupling between the ^{12}C amide I modes along the helix, inducing formation of two shorter unlabelled helices with a higher frequency amide I band. It was observed for the peptides **2L** through **4L**. At the same time, in a peptide labelled exclusively at N-terminus (**N4L**) the ^{12}C residues still form a single helical segment, and the resulting ^{13}C amide I band frequency is not shifted significantly from that of the unlabelled peptide.

The label position influenced the variations in the ^{13}C and ^{12}C amide I frequencies with a sinusoidal correlation according to the helical structure of the peptides. "Peaks" occurring for the **2L3S** and **2L6S** peptides (the labels separated by one turn and two turns, respectively) were observed in the curve reflecting the dependence of frequency on spacing between the labels (**Fig. 44**). Quantitatively, the trends observed in these spectra could be described in terms of dipole coupling between the two labelled ^{13}C amide I modes[119].

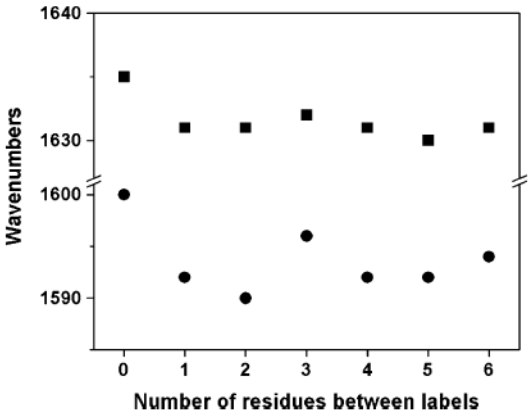

Fig. 44. Trends in ^{12}C (squares) and ^{13}C (circles) amide I frequencies as a function of spacing between two labelled residues in peptides **2L2T** through **2L6S**. Frequencies taken from spectra measured at 2°C[118].

In the works of Decatur and colleagues[120, 121] while studying FT-IR absorption of a series of labelled peptides in helical conformation (**Fig. 45**), a ^{13}C carbonyl stretching band was seen near 1600 cm^{-1}.

4A: AAAAKAAAAKAAAAKAAAAY-NH_2
4AL1: AAAAKAAAAKAAAAKAAAAY-NH_2
4AL2: AAAAKAAAAKAAAAKAAAAY-NH_2
4AL3: AAAAKAAAAKAAAAKAAAAY-NH_2
4AL4: AAAAKAAAAKAAAAKAAAAY-NH_2

A: ^{12}C, A: ^{13}C

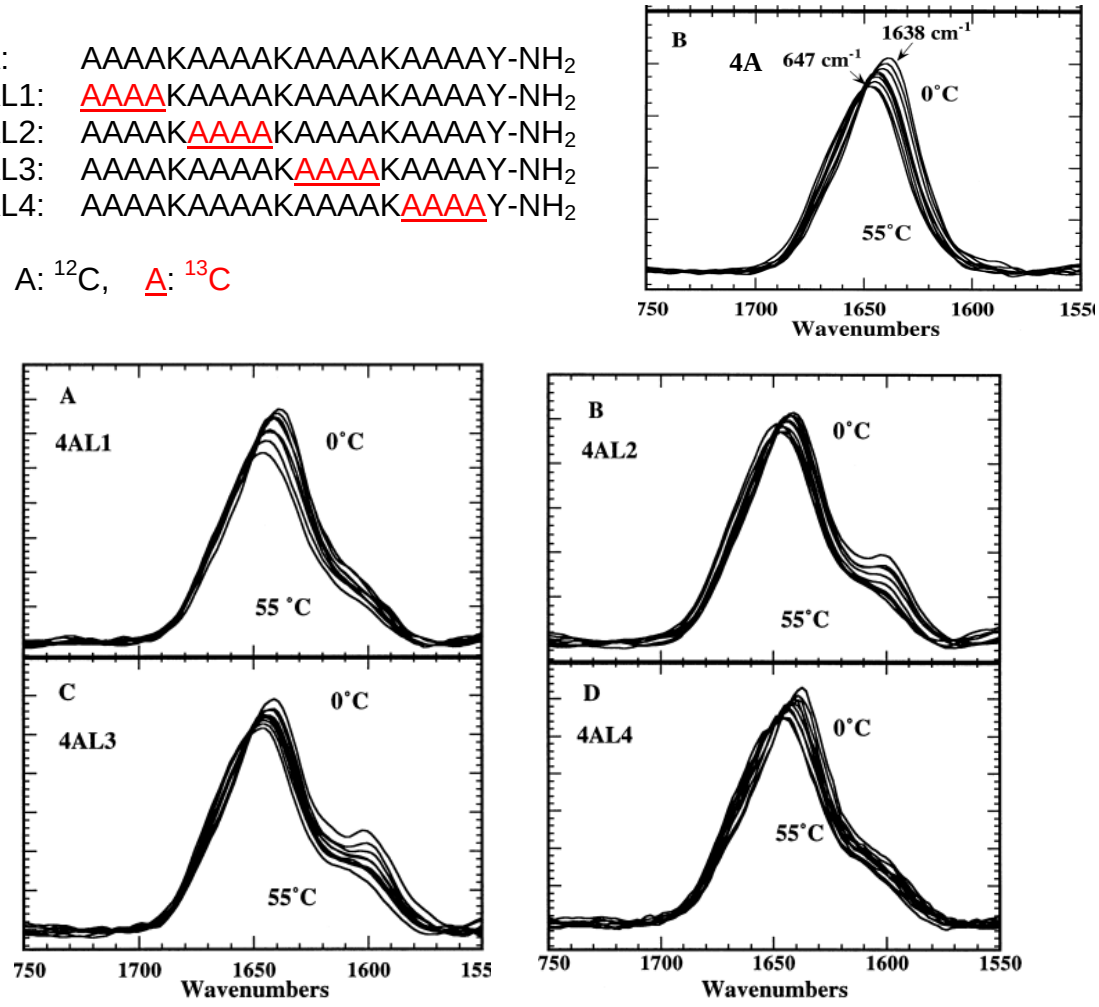

Fig. 45. Temperature dependence of IR absorption spectra of the peptides studied in ref. [120].

No significant absorbance was found near 1600 cm^{-1} for the unlabelled peptide. The intensity of this band related to the labelled residues is significantly lower for **4AL1** and **4AL4** than for **4AL2** and **4AL3**, suggesting N- and C-terminal fraying.

At low temperature (0 °C), the amide I band is sharp with a maximum at 1638 cm^{-1} and it decreases in intensity, broadens, and shifts to higher frequency till 1647 cm^{-1} as the temperature increases. The same behavior shows the band caused by C=O labelled bonds till it almost disappears. Helix-coil dynamics experiments showed that the folding of an α-helix proceeds more rapidly at the helical C-terminus than at the N-terminus,

probably because of reduced steric restrictions of the last C-terminal three residues which are characterized by non-H-bonded carbonyl groups.

Thus, by a systematic labelling of the amino acid residues, a remarkable amount of information has been obtained on α-helix and β-sheet[122, 123] stabilities and dynamics (*e.g.*, terminal fraying) at the residue level. However, no data are available so far on the peptide 3_{10}-helix using this methodology.

In collaboration with dr. S. M. Decatur (Department of Chemistry, Mount Holyoke College, South Hadley, MA) we decided to extend the isotope-edited IR absorption spectroscopic method to the 3_{10}-helix formed exclusively by C^{α}-tetrasubstituted α-amino acids [Aib, and L(or D)-(αMe)Val]. To this purpose, we synthesized six N^{α}-acetylated and C-terminally amidated hexapeptides (both in the labelled and in the unlabelled forms):

20 Ac-D-(αMe)Val-D-(αMe)Val-$(Aib)_4$-NH*i*Pr

21 Ac*-L-(αMe)Val*-L-(αMe)Val-$(Aib)_4$-NH*i*Pr (*bis*-labelled at the N-terminus)

22 Ac-$(Aib)_4$-D-(αMe)Val-D-(αMe)Val-NH*i*Pr

23 Ac-$(Aib)_4$-L-(αMe)Val*-L-(αMe)Val*-NH*i*Pr (*bis*-labelled at the C-terminus)

24 Ac-$(Aib)_2$-D-(αMe)Val-D-(αMe)Val-$(Aib)_2$-NH*i*Pr

25 Ac-$(Aib)_2$-L-(αMe)Val*-L-(αMe)Val*-$(Aib)_2$-NH*i*Pr (*bis*-labelled at consecutive central positions).

where asterisked Ac and (αMe)Val indicate $^{13}C{=}O$ labelled sites.

The choice of the L- or the D-configuration for the (αMe)Val residues was exclusively dictated by the availability of the starting, chirally pure, C^{α}-tetrasubstituted α-amino acid. The goal of this investigation was to detect N- and/or C-terminal fraying, if any, in 3_{10}-helical peptide structures.

The strategies of synthesis for peptides **20** (**21**), **22** (**23**) and **24**(**25**) are shown in **Figures 46-48**. For the difficult (αMe)Val-(αMe)Val, (αMe)Val-Aib, and Aib-(αMe)Val couplings between two sterically hindered residues we took advantage of the powerful acyl fluoride or EDC/HOAt C-activation method. In the segment condensation strategy Aib-Aib bond formation was easily achieved *via* 5(4*H*)-oxazolone activation.

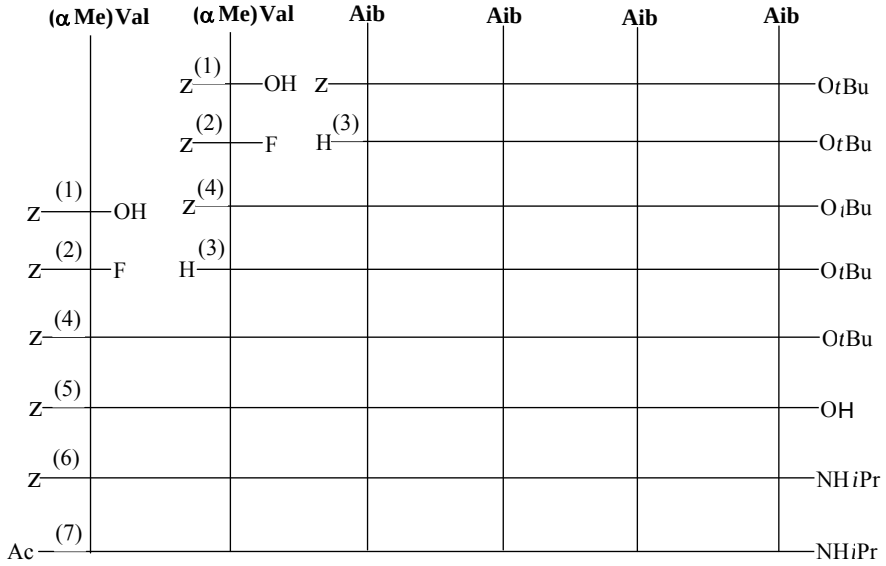

(1): Z-OSu/Et_3N in CH_3CN/H_2O; (2): cyanuric fluoride/pyridine/CH_2Cl_2; (3): H_2/Pd/MeOH; (4): NMM/CH_2Cl_2; (5): TFA/ CH_2Cl_2; (6): EDC/*i*PrNH$_2$; (7): H_2/Pd/Ac_2O.

Fig. 46. Scheme of synthesis for peptides **20** and **21**.

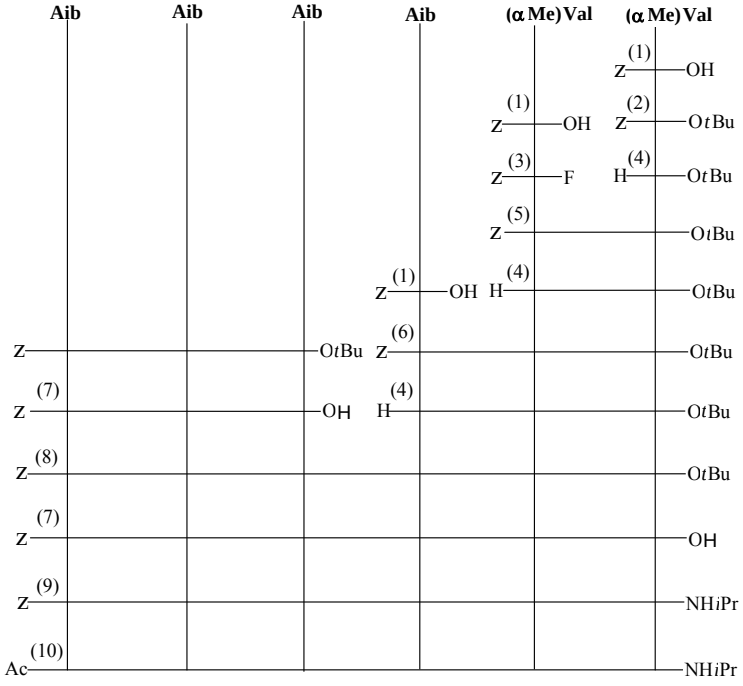

(1): Z-OSu/Et_3N in CH_3CN/H_2O; (2): isobutene/H_2SO_4; (3): cyanuric fluoride/pyridine/CH_2Cl_2; (4): H_2/Pd/MeOH; (5): NMM/CH_2Cl_2; (6): EDC/HOAt /NMM; (7): TFA/CH_2Cl_2; (8): EDC, acetonitrile, 80 ^oC; (9): EDC/*i*PrNH$_2$; (10): H_2/Pd/Ac_2O.

Fig. 47. Scheme of synthesis for peptides **22** and **23**.

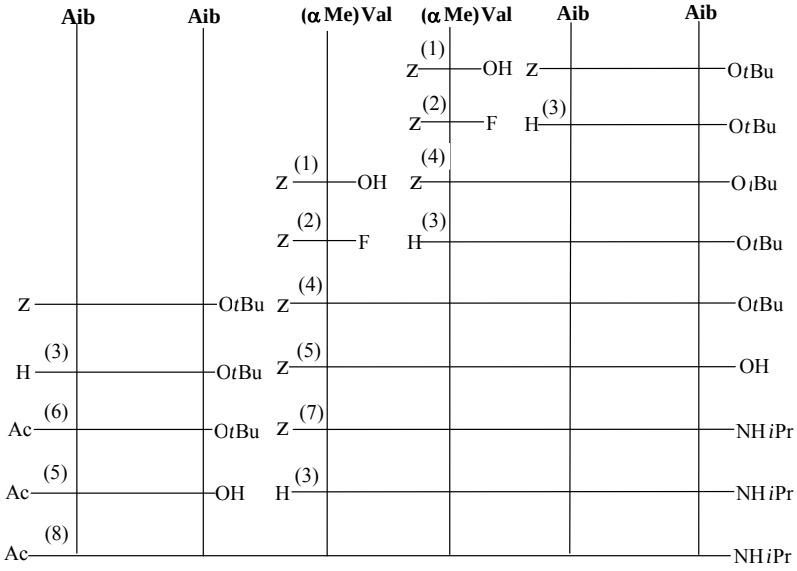

(1): Z-OSu/Et_3N in CH_3CN/H_2O; (2): cyanuric fluoride/pyridine/CH_2Cl_2; (3): H_2/Pd/MeOH; (4): NMM/CH_2Cl_2; (5): TFA/CH_2Cl_2; (6): Ac_2O/CH_2Cl_2; (7): EDC/*i*$PrNH_2$; (8): EDC, acetonitrile, 80°C.

Fig. 48. Scheme of synthesis for peptides **24** and **25**.

C-Terminal amidation was obtained by treatment of the Z N^{α}-protected hexamer (or tetramer in the case of peptides **24** and **25**) free acid with an excess of *iso*propylamine in the presence of EDC in acetonitrile under reflux overnight [either Aib or (αMe)Val was the C-terminal residue]. The yields were rather low (30-35%) in the presence of an N-terminal Aib [not of an (αMe)Val] due to significant formation of an N-terminal hydantoin peptide (presumably derived from loss of the benzyloxy moiety from the Z group, followed by cyclization with the amine). N^{α}-Acetylation was carried out in the last step of the syntheses on the N^{α}-deprotected hexapeptides by use of acetic anhydride in methylene chloride [either Aib or (αMe)Val was the N-terminal residue].

The results of the conformational investigation using FT-IR absorption at different concentrations, ^{1}H NMR titration with the strongly perturbing agent DMSO, and CD support the view that in the structurally benign solvent $CDCl_3$ the hexapeptides largely prefer the 3_{10}-helical conformation, extensively stabilized by intramolecular C=O···H-N H-bonds (**Fig. 49-51**).

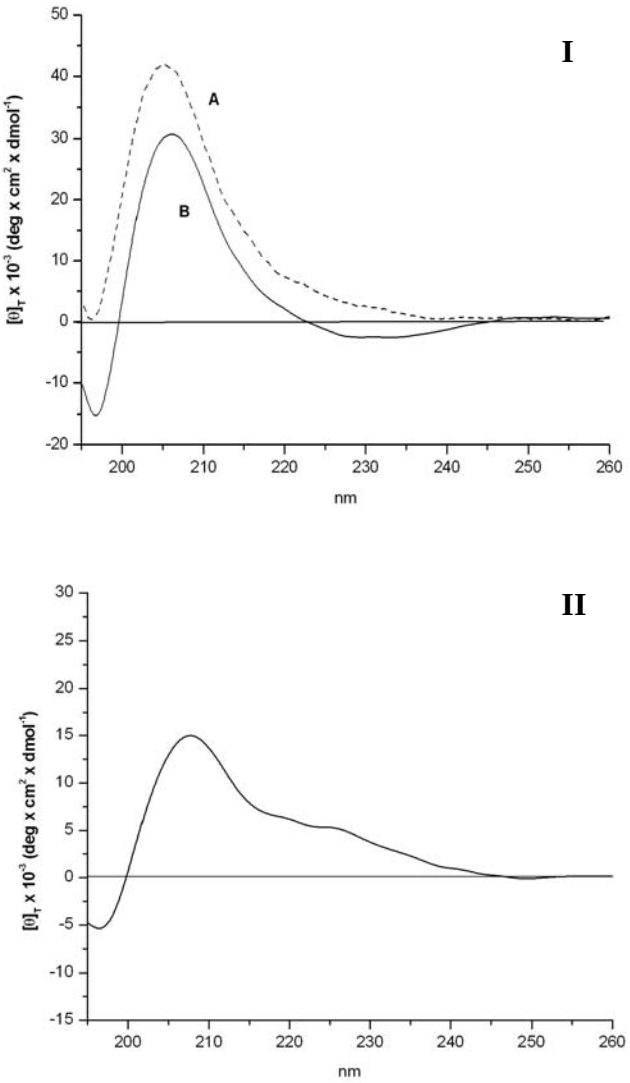

Fig. 49. Far-UV CD spectra of the unlabelled peptides **22** (**A**), **20** (**B**) (**I**) and **24** (**II**) in MeOH solution. Peptide concentration: 1×10^{-3} M.

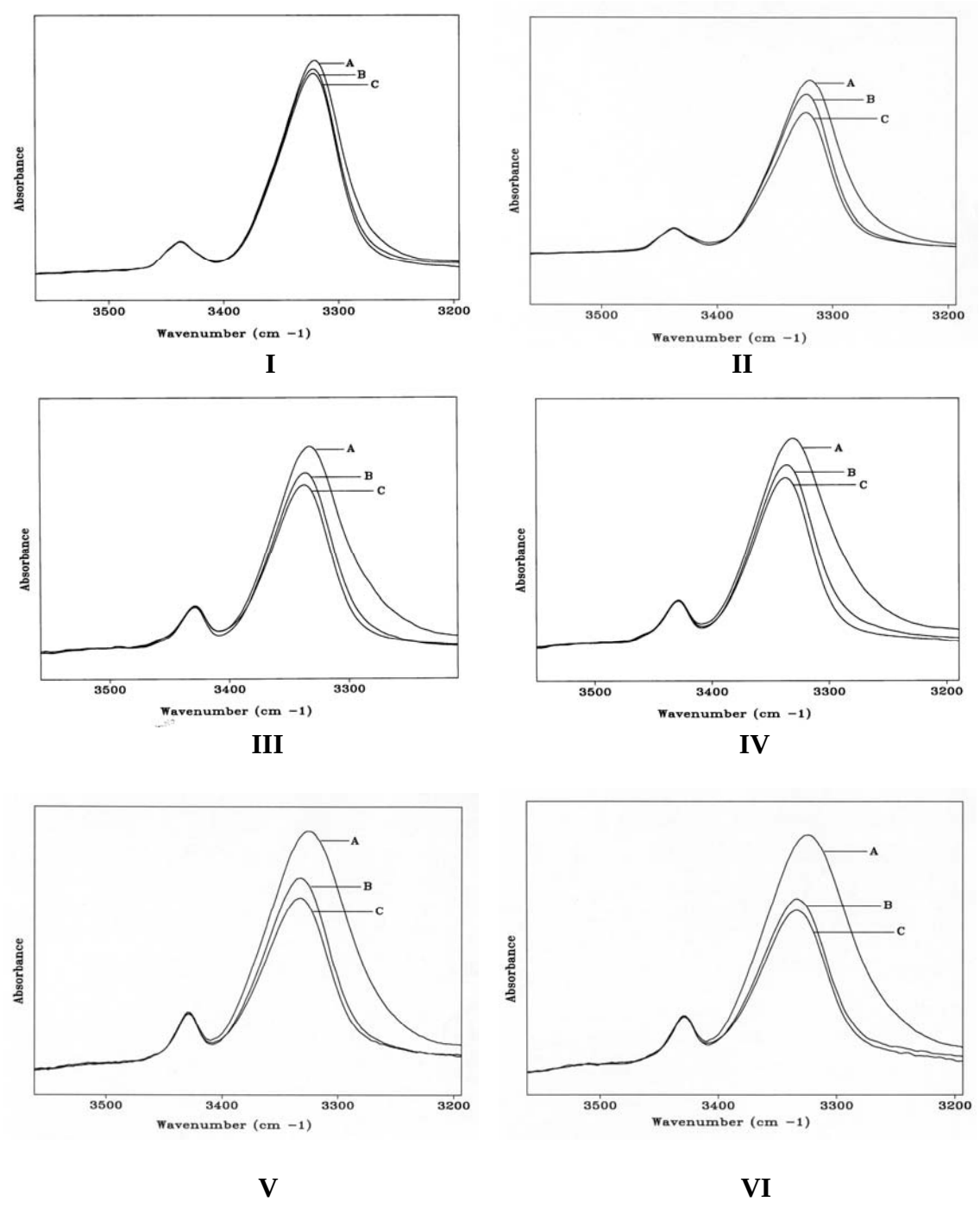

Fig. 50. FT-IR absorption spectra in the 3500-3200 cm^{-1} region of the unlabelled and labeled peptides **20** (**I**), **21** (**II**), **22** (**III**), **23** (**IV**), **24** (**V**), and **25** (**VI**) in $CDCl_3$ solution. Peptide concentrations: 1×10^{-2} M (**A**), 1×10^{-3} M (**B**), and 1×10^{-4} M (**C**).

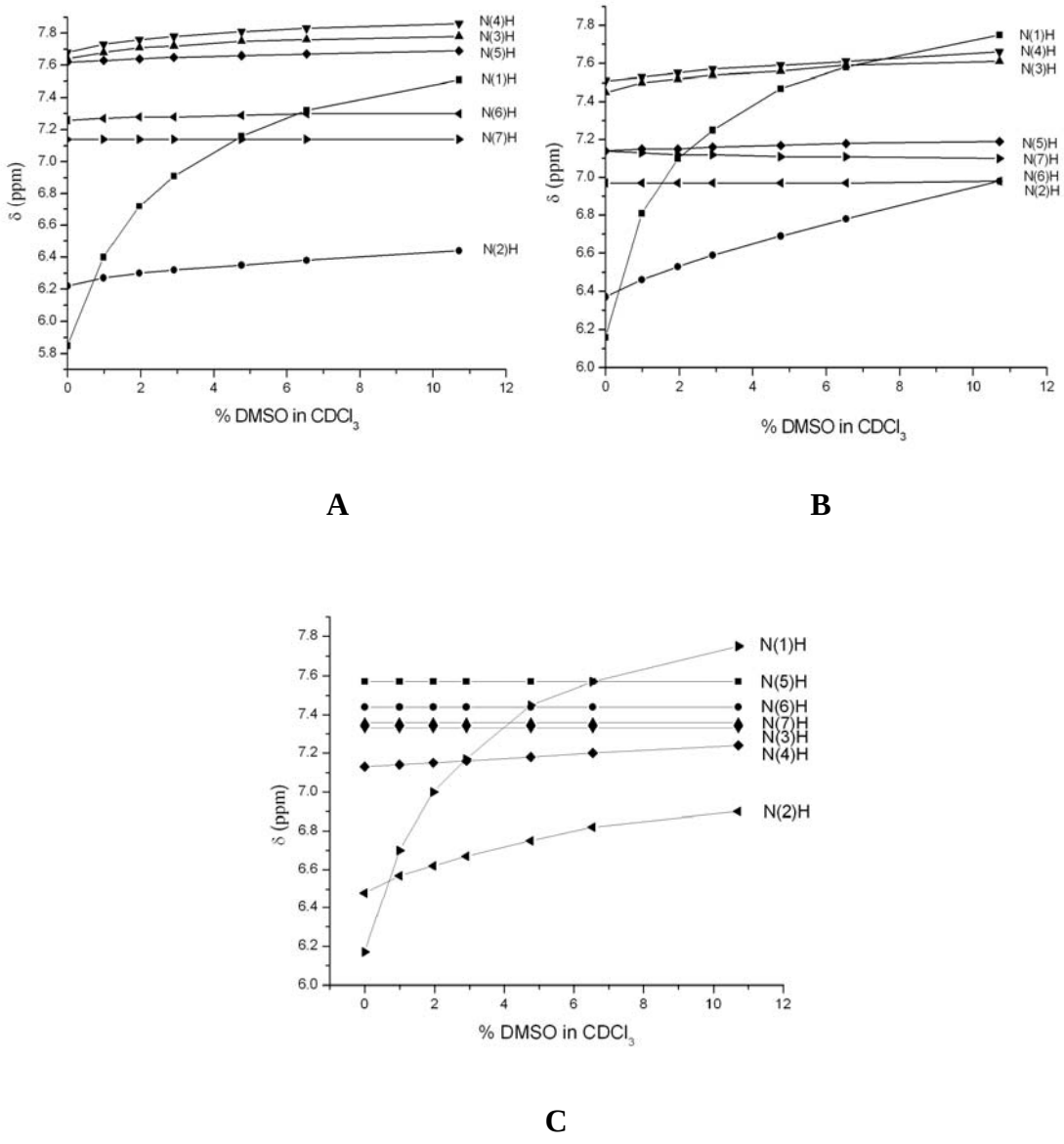

Fig. 51. Plots of NH proton chemical shifts in the ^{1}H NMR spectra of the unlabelled peptides **20** (**A**), **22** (**B**) and **24** (**C**) as a function of the increasing percentages of DMSO (*v*/*v*) added to the $CDCl_3$ solution. Peptide concentration: 1×10^{-3} M. Note that the D-(αMe)Val residue at position 2 of the peptide in plot **A** is less accessible to the perturbing agent than the corresponding Aib residues of the peptides in plots **B** and **C**.

As expected, the helix screw sense is left-handed for the D-(αMe)Val peptides.

We were able to solve the X-ray diffraction structure of the hexapeptide amide **22**, Ac-(Aib)$_4$-D-(αMe)Val-D-(αMe)Val-NH*i*Pr (**Fig. 52**). Both independent molecules (**A** and **B**) in the asymmetric unit are folded in regular, left-handed, 3_{10}-helices, stabilized by five C=O···H-N intramolecular H-bonds.

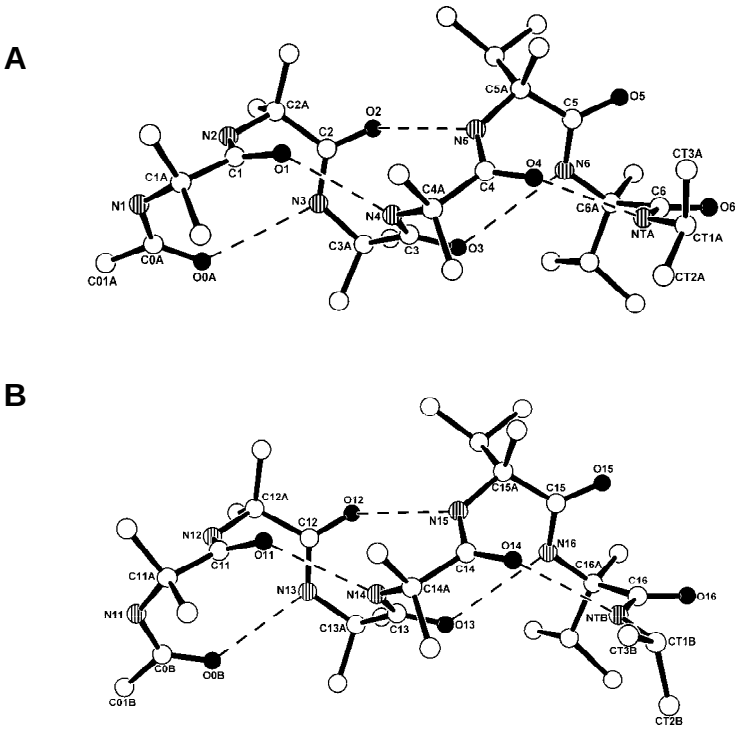

Fig. 52. X-Ray diffraction structures of the two independent molecules (**A** and **B**) in the asymmetric unit of the hexapeptide amide **22**. The five C=O···H-N intramolecular H-bonds are indicated by dashed lines.

A detailed FT-IR absorption study showed the appearance of two amide I bands in the spectra of peptides **21**, **23**, and **25**, arising from the presence of the ^{13}C labeled residues (**Fig. 53**), while the unlabelled peptides have very similar IR spectra with only one amide I maximum at ~1668 cm^{-1}. The frequency of the second band of the ^{13}C=O stretching mode in the labelled peptides is not the same. This finding reflects the differences in local environments at the three different positions (**Table 6**). In particular, the carbonyls at the N-terminus give rise to amide I bands at higher frequency than that of the bonds of the residues at the C-terminus and in the middle of the peptide sequence.

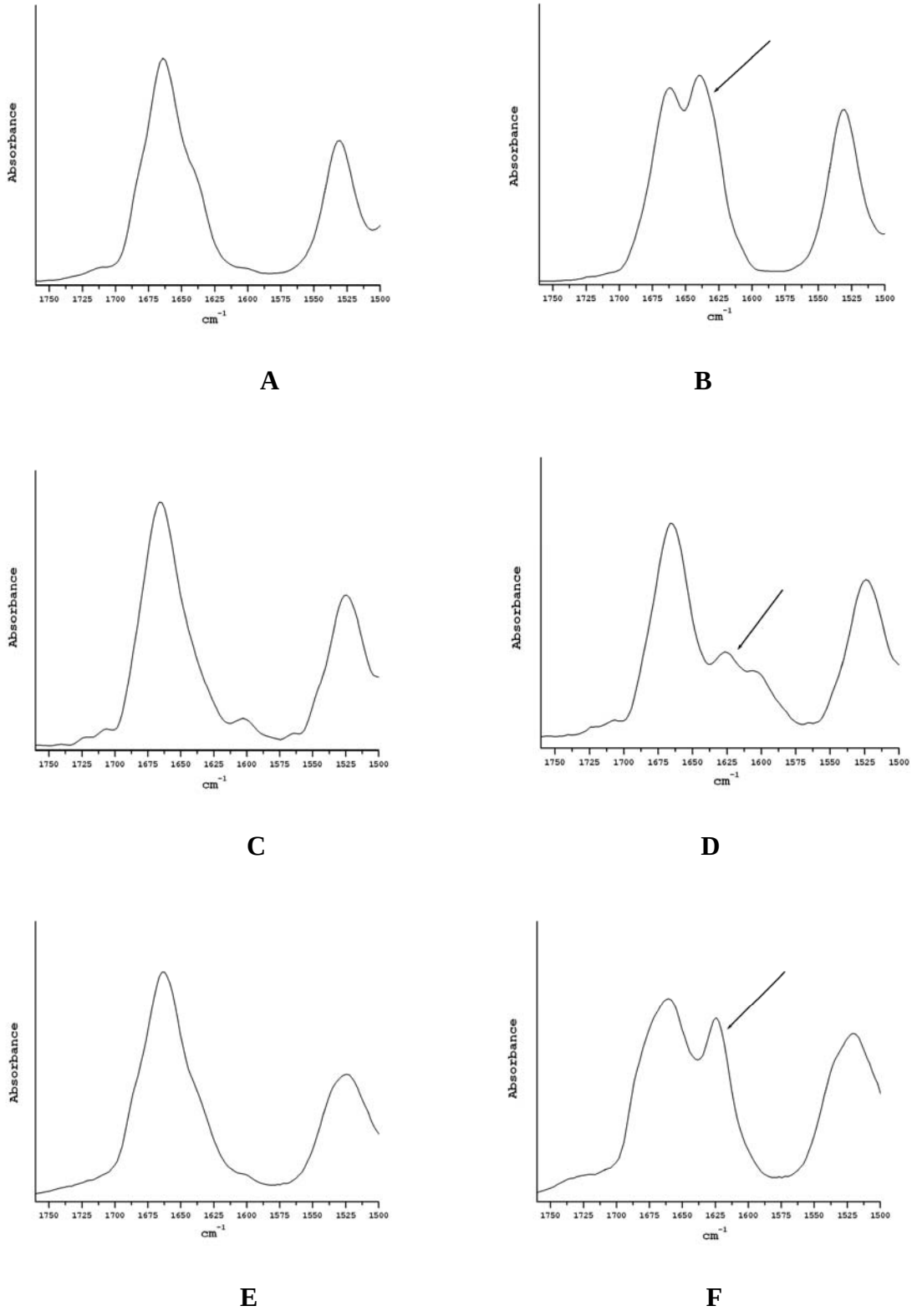

Fig. 53. FT-IR absorption spectra of the peptides **20-25** (**A-F**, respectively) in the 1750-1500 cm^{-1} region (peptide concentration: 1×10^{-3} M). The arrows indicate amide I bands of the labelled residues.

Table 6. Summary of the IR data for the labelled peptides.

Peptide	^{12}C amide I band maximum	^{13}C amide I band maximum
All unlabelled peptides	1668 cm^{-1}	-
N-terminal labelled	1667 cm^{-1}	1640 cm^{-1}
Middle labelled	1680 and 1665 cm^{-1}	1627 cm^{-1}
C-terminal labelled	1667 cm^{-1}	1627 cm^{-1}

This result was quite surprising, since, based on the 3_{10}-helical structure of the peptides, it is reasonable to expect that the C-terminal carbonyls would have the most unique environment, since they are the only carbonyls *not* engaged in intrahelical H-bonds (**Fig. 54**). These results suggest that other factors, besides intrahelical H-bonding, are playing a dominant role in determining the amide I frequency.

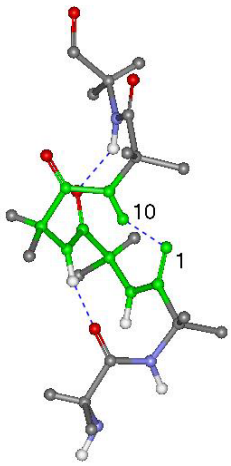

Fig. 54. Scheme of intramolecular H-bonding for the 3_{10}-helical peptide structure.

The results obtained in this study allow to make the following conclusions:

- **A series of hexapeptides, both unlabelled and containing two ^{13}C labels at vicinal carbonyl groups, was synthesized. The labels were incorporated at the N-terminus, at the C-terminus, and at central positions.**
- **Our ^{1}H NMR titration, FT-IR absorption, and CD analyses, as well as an X-ray diffraction study, strongly confirm the predicted 3_{10}-helical conformation for these peptides.**
- **Results of the FT-IR absorption analysis show that the amide I band of the ^{13}C carbonyl groups of the labelled residues is well separated from the main amide I band of the unlabelled residues.**
- **Apparently not only intrahelical H-bonding influences the position of the amide I band.**

CHAPTER 5

3_{10}-HELICAL PEPTIDES AS TEMPLATES FOR ORGANIC SYNTHESIS (INTRAMOLECULAR RING-CLOSING METATHESIS)

Peptides are flexible biopolymers and exhibit numerous conformations in solution and even in the solid state. Their structure and conformation are strongly influenced by the nature of constituent amino acids and also the biophysical environment in which they exist. However, this high conformational flexibility presents a potential problem in generating therapeutics and biological probes since a peptide must attain a certain conformation in order to bind to its biological target. Therefore, the pre-organization of peptide shape, via the introduction of a structural motif that imparts conformational restriction, can enhance binding and hence therapeutic potential[124].

Recent developments in the domain of drug-discovery have focused attention on the synthesis of small-constrained mimics of bioactive conformations of potent therapeutic molecules[125, 126]. It is very important for a peptide molecule to hold its conformational features *in vivo* to bind strongly to the target. The elements of local or global constraint in a molecule can lock it into a particular conformation, which may mimic the exact bioactive conformation[127-129]. Local constraints in terms of side-chain modifications in the amino acids, incorporation of protein secondary structures like turns, helices, etc., into the molecule, and cyclization[130] as part of global constraints are commonly practiced.

Cyclic peptides and their derivatives[131] attract much attention of synthetic chemists and biologists[132]. Apart from the occurrence of a variety of naturally occurring bioactive molecules, cyclic peptides are often more stable *in vivo* than their linear counterparts and therefore often represent promising drug candidates. Another feature that contributes to the appeal of cyclic peptides is their reduced conformational mobility which allows them to be used in the study and mimicry of protein folding and to present diverse functionality in a defined and predictable orientation[133].

In view of the importance of constrained conformations, there have been many attempts to lock peptides into turn and helical configurations and to synthesize molecules that might mimic normal peptides[134]. Reduction of the flexibility by intramolecular bridges, such as salt bridges[135], metal ligation between natural[136] and unnatural amino acids[137], disulfide bridges[138, 139], or more complicated acetylenic or oxyethylenic bridges[140], which act as a "molecular stapler", is the well-known way to control the three dimensional structure. Cyclic alkenes resulting from ring-closing metathesis reaction can be considered as a stable alternative of such bonds. Ring-closing metathesis (RCM), catalyzed by transition metal carbenes, has recently become a popular mild method for the formation of the new C-C bonds and is utilized in many organic transformations. RCM is a part of a vast class of reactions which is known as olefin metathesis[141], a unique carbon skeleton redistribution in which unsaturated carbon-carbon bonds are rearranged in the presence of metal carbene complexes. With the discovery of the efficient catalysts, this reaction has emerged as a powerful tool for the formation of C-C bonds in chemistry. The number of applications of this reaction has dramatically increased in the past few years.

Olefin metathesis can be utilized in several closely related types of reactions[142] (**Fig. 55**).

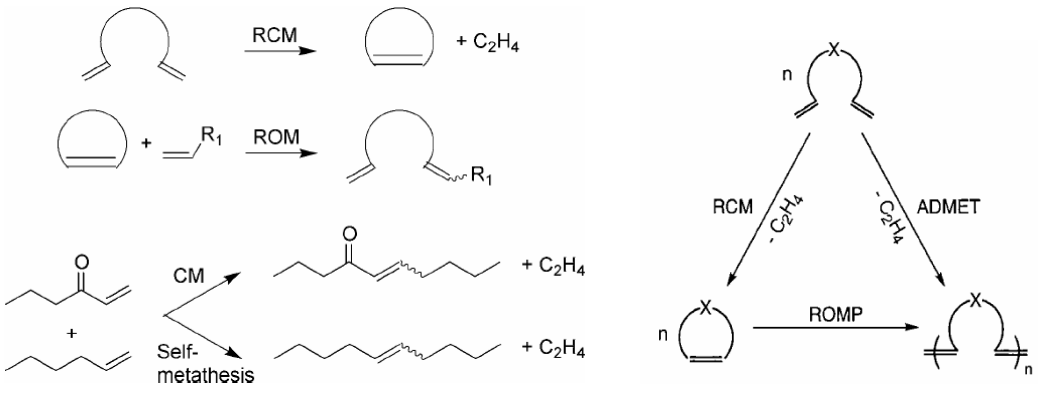

A **B**

Fig. 55. Olefin metathesis reactions for synthetic organic chemistry (**A**) and olefin metathesis polymerization modes (**B**).

Ring-closing metathesis (RCM) is the unimolecular condensation reaction of a diene to form a cyclic olefin and a small condensate olefin as a byproduct, and is being used extensively in critical ring-closure steps in the synthesis of complex organic molecules[143, 144]. Acyclic dienes may also be polymerized and whether a polymer or a cyclic compound is formed from any given diene is most often determined by thermodynamic rather than kinetic factors.

Ring-opening metathesis (ROM) is the reverse reaction of RCM, in which a cyclic olefin is reacted with an acyclic olefin to produce a new acyclic diene. ROM polymerization (ROMP) is thermodynamically favoured for strained ring systems such as 3- and 4-membered compounds. In many cases, ROMP of strained cyclic olefins initiated by metal carbene complexes shows the characteristic features of a living polymerization and therefore block copolymers can be prepared by sequential addition of different monomers.

Cross metathesis (CM) is the reaction of two acyclic olefins to form two new olefins[145]. Of critical importance to CM is the selectivity of the reaction, because it can happen the preference of the products of self metathesis, which is the metathesis of two identical molecules, over the forming so-called cross-product. ADMET is a condensation polymerization, and is essentially the self metathesis of a diene, usually a terminal diene, which forms a high polymer.

The number of catalyst systems that initiate olefin metathesis is very large. But only in recent years well-defined single component metal carbene complexes have been prepared and utilized. Although a number of titanium[146] and tungsten[147] organometallic catalysts have been developed for metathesis and related reactions, molybdenum and ruthenium compounds have found the most applications[148] (**Fig. 56**). Complexes of other metals (such as rhenium and osmium) appear to promote olefin metathesis, but these exhibit lower stability and/or reactivity, and have not been as extensively investigated. Critical drawbacks of the Mo-based highly active Schrock's catalyst **A** are its moderate to poor functional group tolerance, high sensitivity to air, moisture or even to trace impurities present in solvents, thermal instability on storage and expense of preparation. On the contrary, Ru-carbene systems, discovered by R. H. Grubbs, exhibit high reactivity in a variety of ROMP, RCM and CM reactions under mild conditions, but also have remarkable tolerance toward many different organic functional groups.

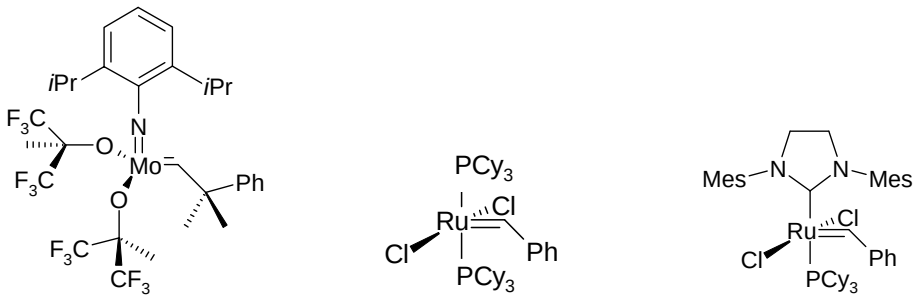

A **B** **C**

Fig. 56. Most commonly used olefin metathesis catalysts: Schrock's catalyst (**A**), Grubbs' 1st generation catalyst (**B**), Grubbs' 2nd generation catalyst (**C**) (Cy = cyclohexyl, Mes = mesityl).

Catalytic activity of such compounds is not reduced significantly in the presence of air and moisture and they can be stored even in the air atmosphere without severe decomposition for several weeks[142]. These reagents turned out to be very efficient catalysts for all kinds of metathesis reactions and have therefore found numerous applications in the synthesis of complex target molecules and the preparation of different polymers[149, 150].

The Mo=C or Ru=C double bonds serve as points of contact between the catalyst and olefins. The metal centers are crucial to the properties of these catalysts. It is now generally accepted that the mechanism of both cyclic and acyclic olefin metatheses proceeds through a series of metallacyclobutanes and carbene complexes. Although the relative stability of the carbenes and metallacyclobutanes can change with reaction conditions, catalyst composition and alkene substitutions, the mechanism of olefin metathesis appears to be the same for all catalysts.

Overall, the catalytic cycle (**Fig. 57**) consists of an initiation phase (generation of the active complex) and a propagation phase (the active complex promotes additional cycles)[151]. Catalysis commences by a cross metathesis between an active carbene or alkylidene (M=C) and one of the two olefins of the substrate (**i**) to generate a metallacyclobutane (**ii**). The metallacyclobutane might revert to **i** and M=C (pathway **a**) or the other two bonds of the ring might be ruptured, furnishing **iii**, where the metal (M) is within the substrate (pathway **b**).

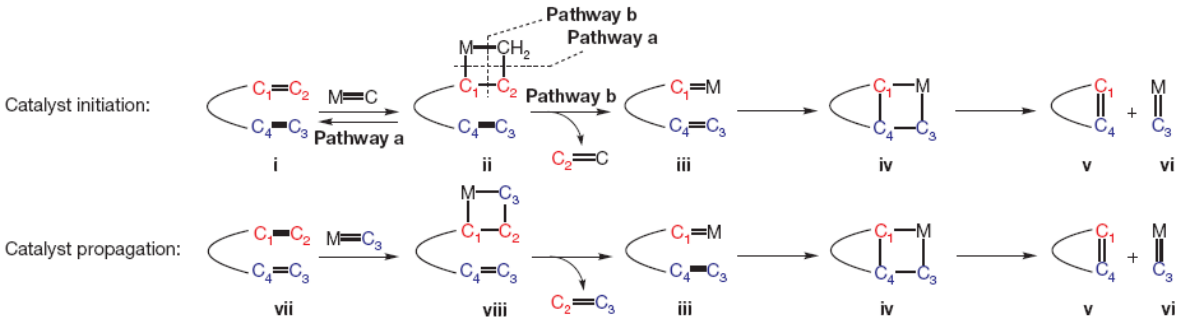

Fig. 57. The general mechanism for ring-closing olefin metathesis[151].

Formation of another metallacyclobutane (**iv**) and its disintegration furnishes cyclic product **v** and M=C_3 (**vi**), which is the metal-bearing agent serving as the catalyst. What typically drives reactions is that the cyclic product (**v**) does not easily react with the active catalyst (M=C_3) to cause ring-opening metathesis. The identity of the intermediates in the catalytic cycle is well understood[152]; it is, however, often unclear whether it is catalyst–substrate association (**i** and **vii** first chelate with the metal centre of M=C before conversion to **ii** or **viii**), formation of the metallacyclobutane or its cleavage that is the irreversible, product- or rate-determining step.

Efficient synthesis of the large ring depends on striking a balance among cross metathesis, a process that delivers the undesired coupling of two substrate molecules, ring-closing metathesis, a reaction that affords the desired product, and a ring-opening metathesis pathway that would destroy the desired cyclic compound.

Ring closing metathesis has emerged as a powerful tool for the synthesis of different ring systems from five-membered rings to macrocycles. However, the product distribution of monomer and oligomers is often a problem in the formation of medium to large rings. It was found that the product distribution is affected not only by the reaction concentration, but can be improved also by adjustment of the reaction temperature. Typically, metathesis reactions are carried out in degassed solvents (dichloromethane or benzene) in the presence of 5–10% ruthenium catalyst at concentrations ranging from 0.004 to 0.05 M. High dilution concentrations are employed to minimize the formation of dimer, resulting from cross-metathesis when the reaction rates are slow. The yields of monomer can be significantly enhanced relative to

runs at lower temperature. This observation could be explained by the difference of entropy in activation energy leading to each product. If the formation of the monomer is entropically favored over that of the dimer, the kinetic ratio of the two products should shift toward the monomer at higher temperature. In particular, the ratio of the products obtained after short time of macrocyclization reaction of a series of dienes studied in the work[153] appeared to be a kinetic ratio, since runs with longer reaction times resulted in the formation of more dimer. This result indicates that the monomer might eventually revert to the thermodynamically favored dimers.

It was also reported a noticeable improvement of ring-closing metathesis reaction under solvent-free conditions and by microwave activation under green chemistry conditions[154].

In the field of designing of stable peptide β-turn and helix mimics, the combination of unsaturated amino acids and RCM appeared extremely useful. The synthesis of sterically hindered rigid amino acids which could considerably enhance conformational stability of peptides plays an important role in the design of new medicines. The most efficient approach to conformationally rigid peptides is based on introduction of medium-size cyclic α-amino acids (usually, 5-7-membered) into strategic positions of peptide chains[155]. As a rule, this leads to significant improvement of pharmacological parameters of potential peptide medicines. Such cyclic amino acids and their derivatives and analogs can be easily made by intramolecular ring-closing metathesis of dienes and enynes[156-159].

Though cyclizations to large rings are performed usually in diluted solutions to suppress competing acyclic diene metathesis (ADMET), RCM is also applicable to polymer-supported substrates. Experiments were reported on the dimerization of peptides on solid-phase using a ruthenium catalyst after N-terminal acylation with different ω-alkenoic acids[160]. It was shown that the size of the peptide (from one to four amino acid residues) did not influence the reaction, meaning that the required length allowing cross linking is already reached with the smallest peptide (one amino acid) and pentenoic acid. On the other hand, two or more methylene groups are required between the double bond and the carbonyl group for metathesis to proceed smoothly. The complete failure to obtain the dimeric product with 3-butenoic acid derived peptoids is not due to the inability to reach a second alkene on solid support, since the longer peptides should compensate for the shortness of the butenoic acid.

The cyclisation/cleavage from solid support has also proven to be very effective for the synthesis of macrocycles[161]. According to the concept of Pernerstorfer *et al.* [162] (**Fig. 58**), the catalyst is expected to selectively attack a terminal double bond for steric reasons.

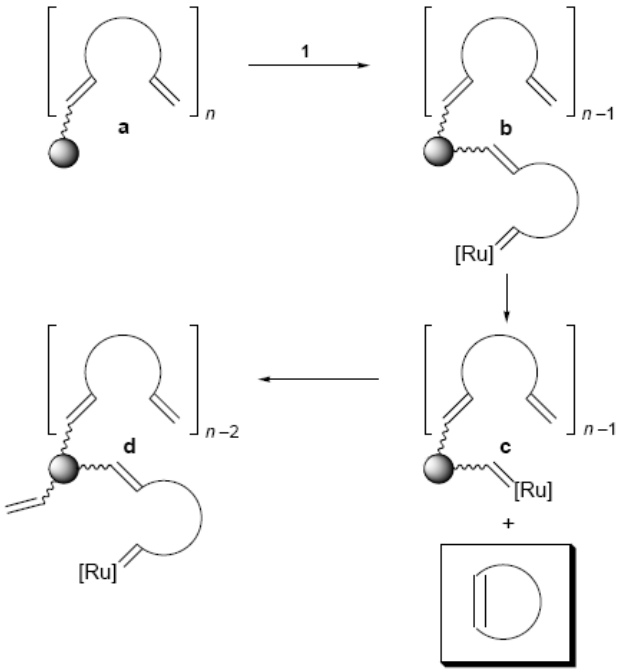

Fig. 58. Scheme of the solid-phase synthesis of peptide macrocycles[162].

This initial step (**a→b**) is followed by a RCM resulting in the liberation of one equivalent of the macrocycle and in the formation of the polymer-bound metal-carbene complex **c**. Assuming sufficient flexibility, a transfer of the metal complex on the polymer surface (**c→d**) should take place, thus enabling further catalytic cleavage cycles. Byproducts resulting from quasi-intermolecular crossed metatheses of terminal double bonds remain bound to the resin during the entire process. Using such a strategy a series of the cyclic tetrapeptides was successfully synthesized. The extent of cyclisation/cleavage was shown to depend strongly on the length of spacer, which separates the peptide chain from the polymer surface, and, thus, on the mobility of the polymer-supported intermediates. It appeared also that the relative cyclisation/cleavage rates of different precursor dienes correlated with their probability to form β-turn-like

structures and, therefore, depended on the proximity of double bonds. Polymer-bound substrates cyclized rapidly when exhibiting favourable conformations.

The importance of the disposition of double bonds taking part in the ring-closing metathesis was clearly shown in the work of Sastry *et al.*[163] In this work an α-, β-didehydrophenylalanine (ΔPhe) as a structure-supporting residue was used. This phenylalanine analogue is very interesting because of its turn-inducing as well as helix-forming propensity. The sp^2-C_α in the ΔPhe residue results in specific backbone φ and ψ torsion angles which facilitate β-turn formation of the sequence. It was also observed that the ΔPhe residue, when present as part of a peptide, enhances stability towards proteolytic degradation. The authors have shown that the pre-organization into a β-turn in the molecule can bring the terminal olefin bonds in sufficiently close proximity to undergo a facile RCM cyclization. For this purpose three tripeptides having two terminal olefinic bonds at the C- and N-termini (**Fig. 59**), both with and without a ΔPhe residue, were synthesized. The ^{1}H NMR study clearly supported the presence of two consecutive β-turns, which suggests that the acyclic peptide **26** is organized as a 3_{10}-helical structure. When the tripeptide **26** was subjected to Ru-carbene catalyzed RCM reactions, it underwent a smooth cyclization to afford the corresponding cyclic peptide **27** as an *E*-isomer in good yields. The solution ^{1}H NMR study on the cyclic peptide **27** revealed that after cyclization the 3_{10}-helical structure in peptide **26** has been transformed into a single cyclic β-turn mimic **27**. An almost equal abundance of both *cis* and *trans* isomers were observed in DMSO-d_6 solution. On the contrary, tripeptides **28** and **29**, having L-Phe and D-Phe, respectively, did not show any well defined structure. When subjected to RCM conditions, peptide **28** did not undergo any cyclization. Also, peptide **29** was cyclized, but in a very poor yield (5–10%). These results clearly indicate that the close proximity of the terminal olefins, missed in peptides **28** and **29**, is a prerequisite for RCM cyclization. Furthermore, absence of the β-turn in **28** and **29** also supported the role of the ΔPhe residue induced β-turn pre-organization of 2**6** leading to the proximity of terminal alkenes for a successful RCM reaction.

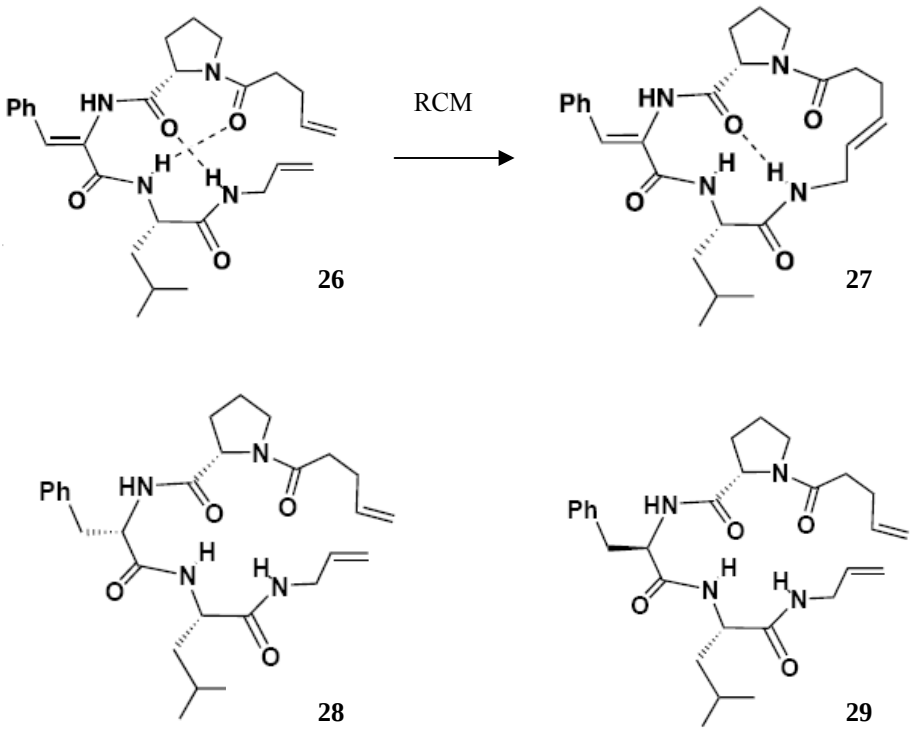

Fig. 59. Tripeptides studied in ref. [163].

The replacement of a H-bond between the *i* and *i* + 4 residues at the N-terminus of a short peptide with a carbon-carbon bond results in a highly stable, constrained α-helix, as it was shown by Chapman *et al.*[164] (**Fig. 60**). The advantage of this strategy is that it allows access to short α-helices with strict preservation of solvent-exposed molecular recognition surfaces required for biomolecular interactions and it does not remove the important side-chain functionalities. It also can nucleate the helical structure, as it was shown that the energetically demanding organization of three consecutive amino acids into this structure is a slow step in helix formation[165].

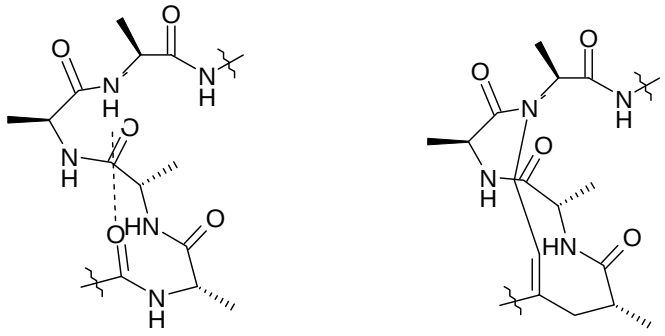

α-helix **artificial α-helix**

Fig. 60. Strategy of stabilization of an α-helix by replacement of a C=O···H-N bond by covalent bonds.

To test the stabilization properties of the metathesis-derived internal crosslink, octapeptide **31** bearing a crosslink at the *N*-terminus *via* RCM reaction from the precursore peptide **30** was synthesized (**Fig. 61**).

The CD spectrum of **31** displayed two negative maxima at 202 and 222 nm, characteristic of an α-helix. This peptide did not show any increase in helicity upon addition of the α-helix inducing solvent 2-,2-,2-trifluoroethanol (TFE).

The unconstrained peptide Ac-GEAAAAEA-OMe did not display any α-helicity in aqueous buffer (**Figure 61a**) and 0-100% TFE solutions (data not shown). The cyclized peptide **31** remained fully helical when heated from 5 to 95 °C, and at the guanidinium chloride (GnHCl) concentration up to 4 M, indicating that the peptide helical structure is very stable (**Figure 61b**).

Methodology for the RCM of peptides without need for modification of the side chains has been also demonstrated by Reichwein *et al.*[166] (**Fig. 62**). The introduced "loops" connect two amide nitrogens, leaving the rest of the amino acid sequence unaffected. Importantly, these macrocycles may be formed by connecting any two amide nitrogens, so long as the length of the alkene substituents is adjusted appropriately.

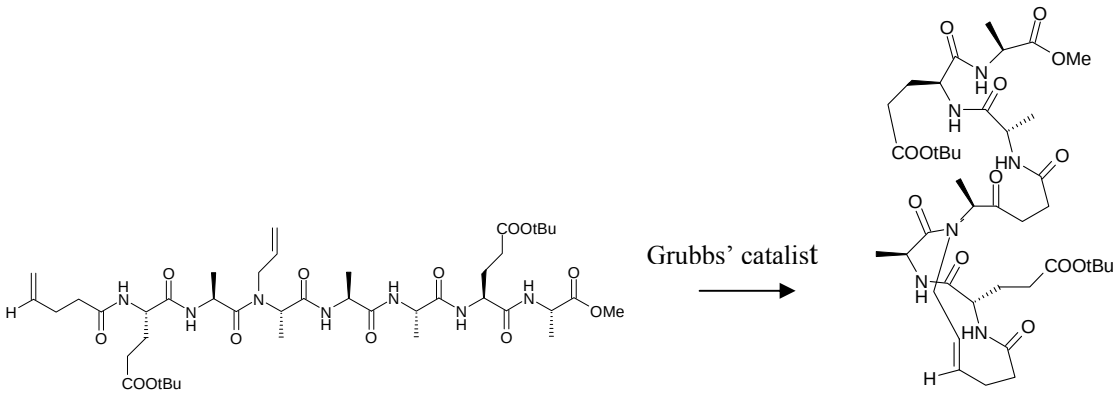

30 **31**

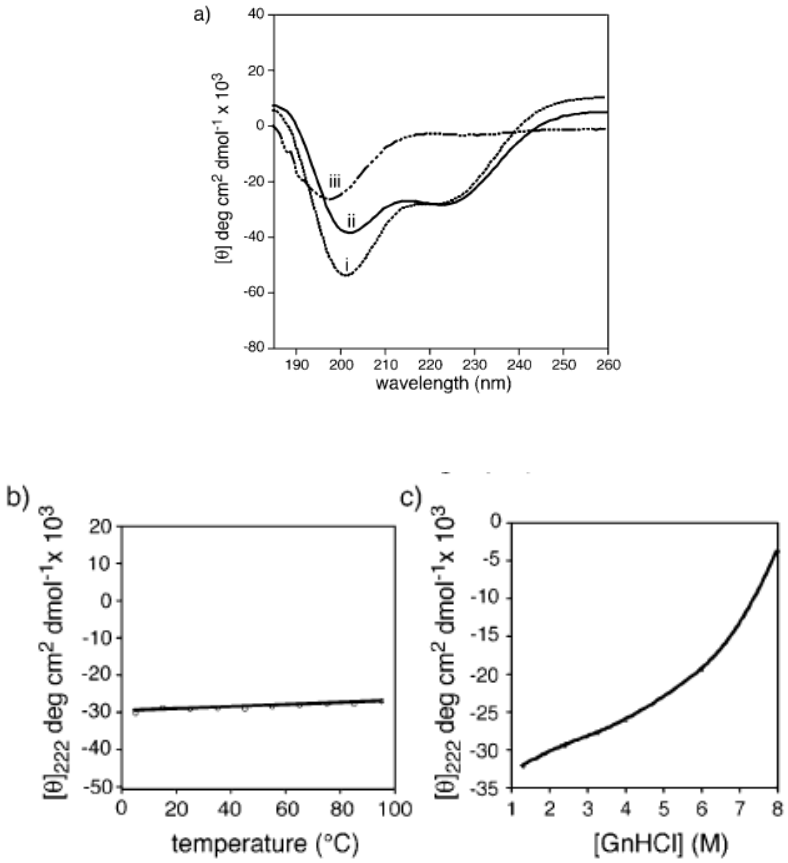

Fig. 61. (**a**) Circular dichroism spectra of **31** in 30 mM phosphate buffer (pH 7.0) (**i**) and 20% TFE/phosphate buffer (**ii**). Spectrum of unconstrained peptide (Ac-GEAAAAEA-OMe) in phosphate buffer (**iii**). Effect of (**b**) temperature and (**c**) GnHCl on the stability of α-helical structure of **31**[165].

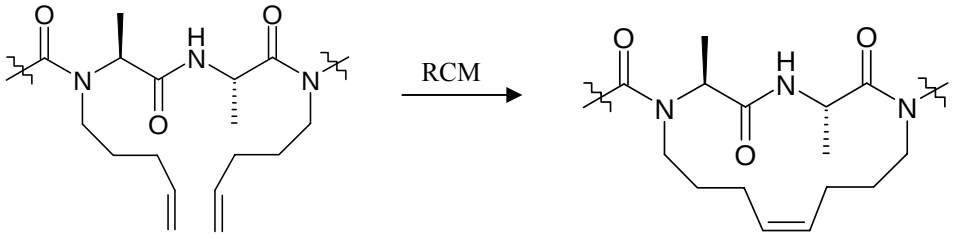

Fig. 62. The action of the "molecular stapler" for the peptide secondary structure stabilization by connecting two amide nitrogens[166].

It was established during the course of this work that RCM can be conducted using *N*-allylamides for a loop bridging two amides, *N*-pentenylamides for a loop spanning three amides, and *N*-homoallylamides when four or more amides are involved in the ring.

The metabolic stability of C–C bonds makes olefin RCM a particularly attractive method for the synthesis of constrained cyclic peptide structures[167]. The Grubbs' group have reported a facile procedure wherein RCM is used to introduce a link between the *i* and *i* + 4 amino acid side chains[168]. L-Serine and L-homoserine residues were derivatised as *O*-allyl ethers, then treated with ruthenium complex to yield olefinic macrocycles, which subsequently could be reduced by catalytic hydrogenation. Linkers bridging the *i, i* + 4 or *i, i* + 7 positions delivers substantial stabilization of α-helical motifs and places the tethered side chains on the same side of the helix (**Fig. 63**).

Apparently, in the same way it is possible to fix 3_{10}-helical conformation. Earlier work from our group suggested that it is feasible to synthesize 3_{10}-helical peptides containing a RCM crosslink between amino acids separated by two residues (*i* and *i*+3), if each side chain contains at least five atoms[169]. We decided to continue the study of the 3_{10}-helix formation during RCM and the effect of placing the RCM constraint between the *i* and *i*+3 amino acid residues.

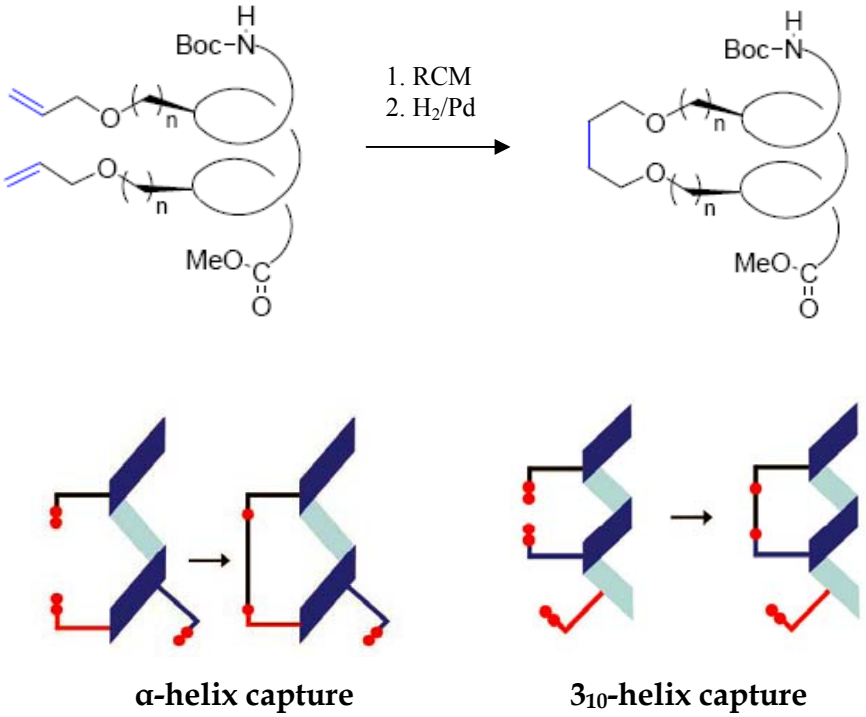

Fig. 63. The action of the "molecular stapler" for the helical structure stabilization by RCM.

We began our work by performing a circular dichroism (CD) analysis of the linear octapeptide Boc-(Aib)$_3$-L-Ser(Al)-(Aib)$_2$-L-Ser(Al)-Aib-OMe (Al, allyl) (**32**), as well as the product of its RCM cyclization (**33**) and the cyclized hydrogenated peptide (**34**) (**Fig. 64**), all synthesized in the group headed by Dr. D. J. O'Leary (Pomona College, Claremont, USA). It is worth stressing the point that the two Ser(Al) residues bear five atoms in their side chain and are incorporated at relative positions *i*, *i*+3.

For all three compounds in MeOH solution we have recorded CD patterns resembling those of the 3_{10}-helical conformation [a strong negative maximum near 205 nm and a much weaker (60-75% less intense) negative maximum at 222-232 nm] and, apparently, of a mixed 3_{10}-/α-helix in TFE solution (the $\theta_{222\text{-}232}/\theta_{205}$ ratio is about 0.5) (**Figs. 65** and **66**). ^{1}H NMR solvent perturbation experiments, carried out by adding increasing amounts of the strong H-bonding acceptor solvent DMSO to the $CDCl_3$ solution, are in agreement with the conclusion of the type of helical structure (mostly 3_{10}) adopted by the peptides in solvents of low and moderate polarities (**Fig. 67**).

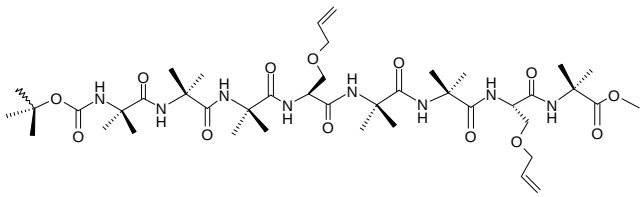

32

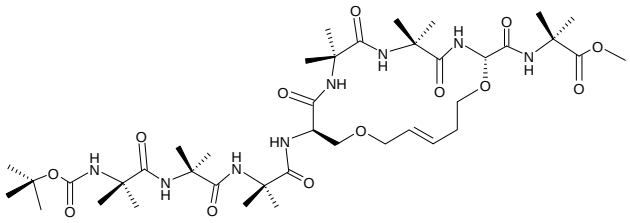

33

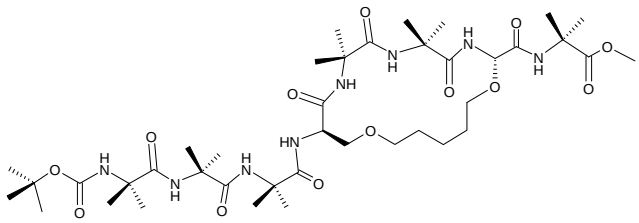

34

Fig. 64. The chemical structures of the octapeptides studied in this work: the linear peptide (**32**), the RCM cyclized peptide (**33**) and the cyclized hydrogenated peptide (**34**).

Complete assignment of all NH protons was achieved by two-dimensional (2D)-ROESY and total correlation spectroscopy experiments. It is worth noting that the sensitivity of the N-terminal N(1)H and N(2)H protons, outside the macrocycle and not engaged in the intramolecular H-bonding scheme, is remarkably high.

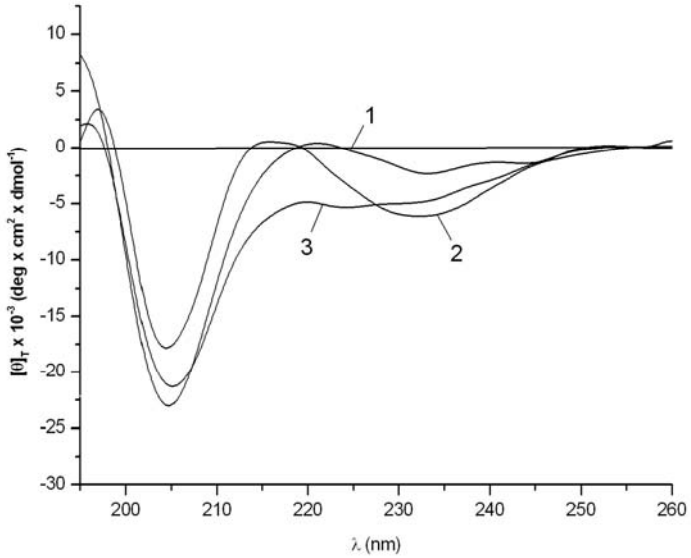

Fig. 65. Far-UV CD spectra of octapeptides **32** (**1**), **33** (**2**) and **34** (**3**) in MeOH solution. Peptide concentration: 1×10^{-3} M.

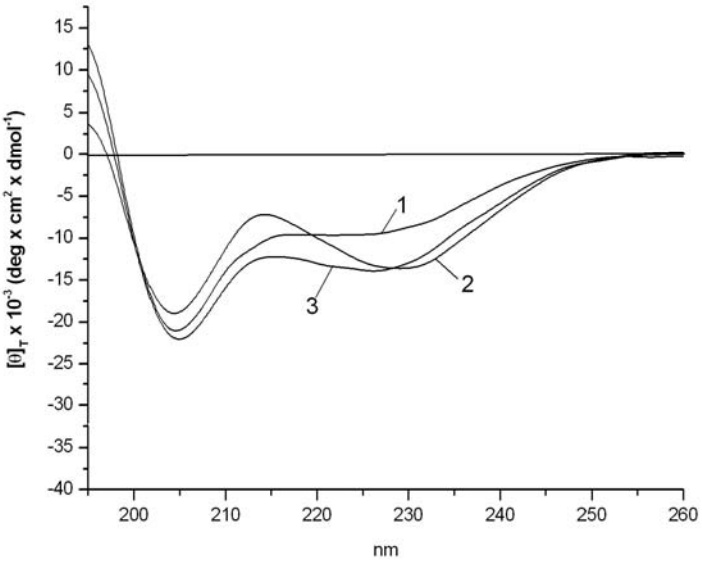

Fig. 66. Far-UV CD spectra of octapeptides **32** (**1**), **33** (**2**) and **34** (**3**) in TFE solution. Peptide concentration: 1×10^{-3} M.

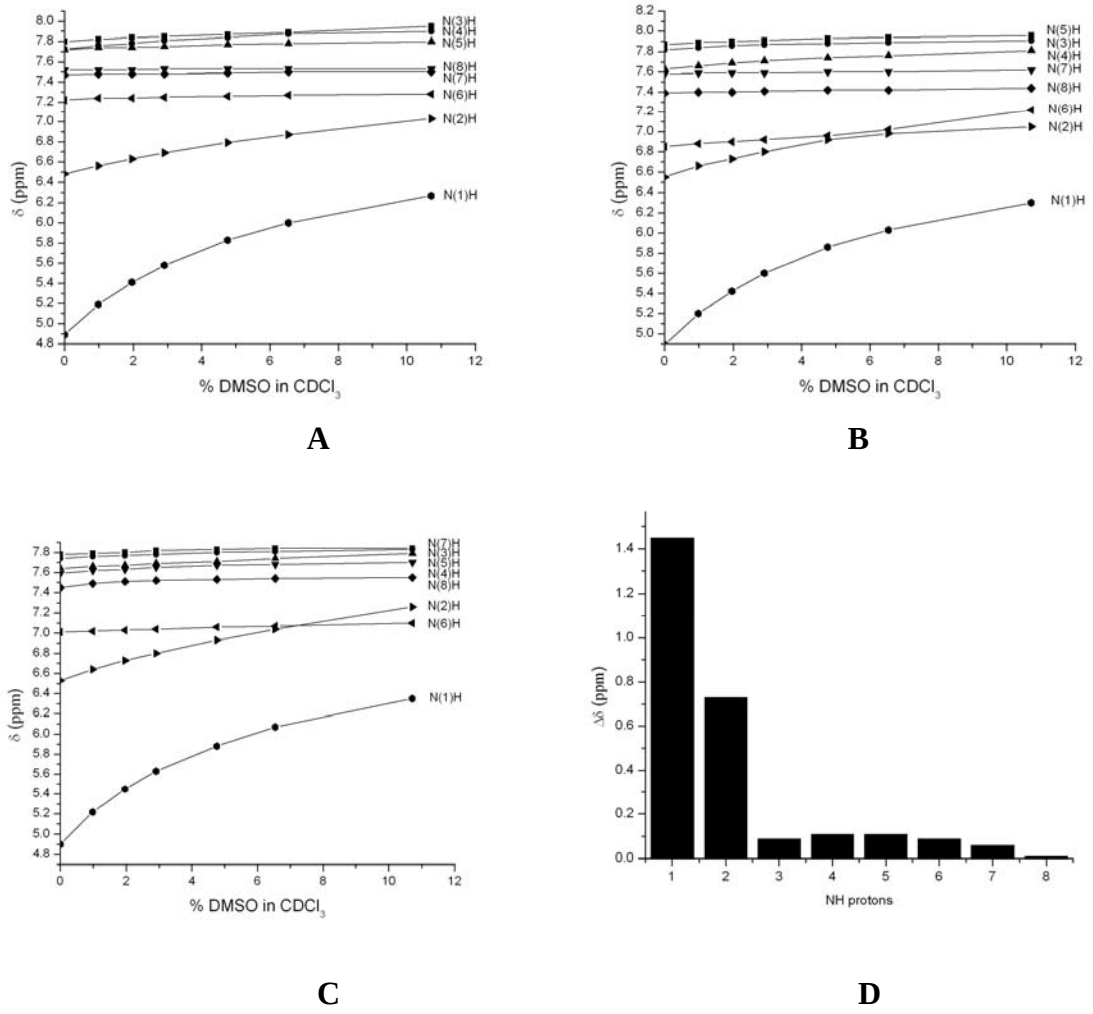

Fig. 67. Plot of NH proton chemical shifts in the ^{1}H NMR spectra of **32** (**A**), **33** (**B**) and **34** (**C**) as a function of increasing percentages of DMSO-d_6 (v/v) added to the $CDCl_3$ solution (concentration: 1×10^{-3}M). Histogram showing the variations of the NH proton chemical shifts for **34** (**D**).

An X-ray diffraction analysis (**Fig. 68**) of peptides **32-34** provided a structural comparison at each stage of the modification. To the best of our knowledge, this is the first case where the RCM reaction and the subsequent chemical modification of the RCM product were 3D-structurally examined at the atomic resolution level. Each of the three peptides adopts a well-developed right-handed 3_{10}-helical structure.

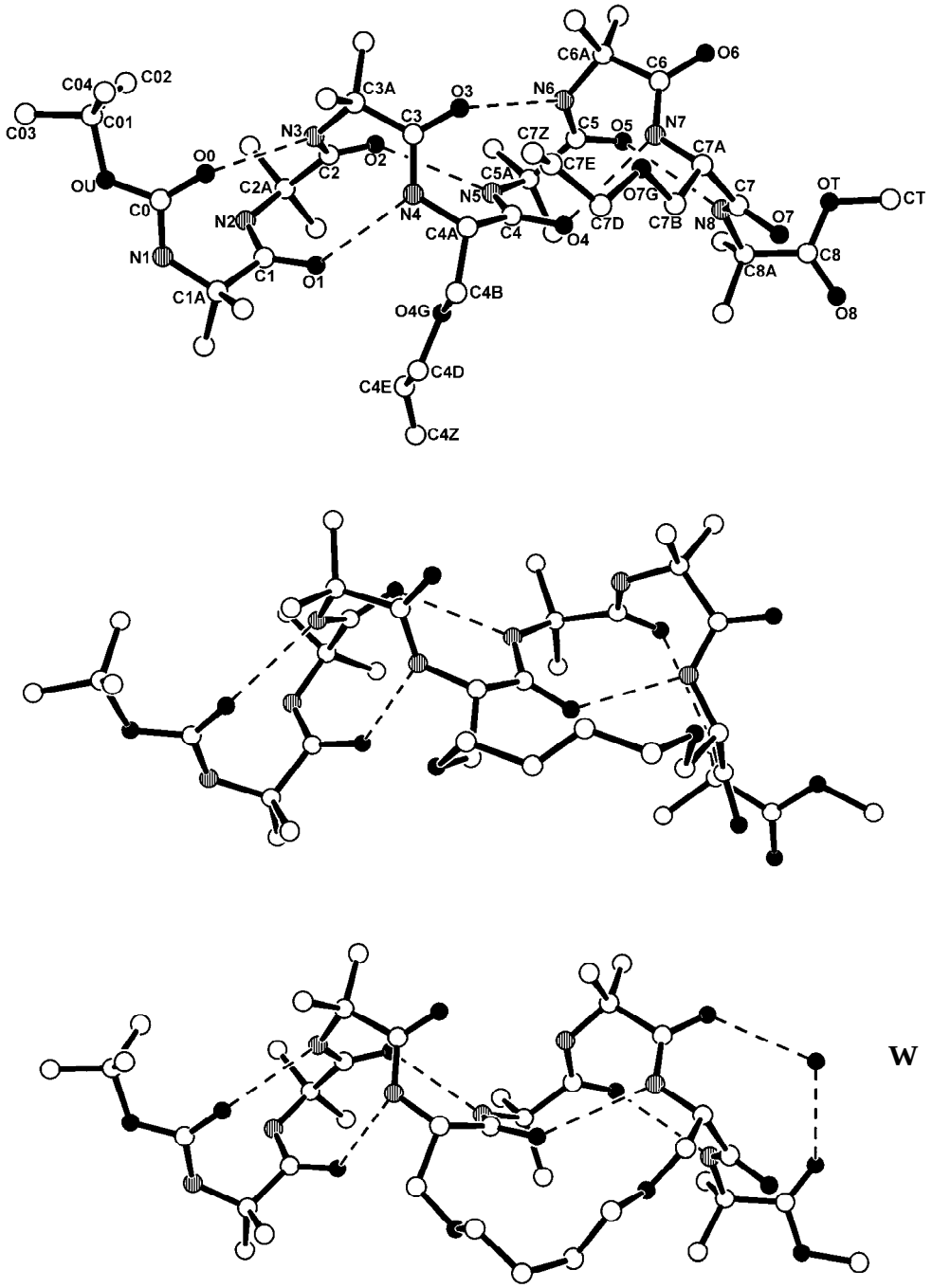

Fig. 68. X-Ray diffraction structures of the linear peptide **32** (top), the same peptide after RCM cyclization (*trans* C=C bond) **33** (middle) and the same peptide after RCM cyclization and hydrogenation **34** (bottom). Dashed lines represent intramolecular C=O···H-N H-bonds. In **34**, the co-crystallized water molecule (W) is also shown.

Peptide **32** is 3_{10}-helical through residues 1-6 and contains a type-I β-turn at the C-terminal residues 6 and 7 (a 3_{10}-helix consists of repeat type-III β-turns). This C-terminal turn behavior is also seen in peptides **33** and **34**, where the regularity of the helix is slightly disturbed at residues 4 and 5, with a deviation greater for unsaturated peptide **33** than for the saturated macrocycle **34**. Despite these small differences, the structures are quite similar to one another with small deviations for backbone atoms. All internal Aib residues exhibit φ and ψ torsion angles typical of 3_{10}-helical residues[6]. In peptide **34**, the 3_{10}-helical H-bonding pattern is interrupted by the lack of the intramolecular H-bond between N6 and O3, as each of these two atoms is intermolecularly H-bonded to a co-crystallized solvent (water) molecule. With the exception of the C-terminal residue 8, which is helical in **32** and **33** while *semi*-extended in **34**, most of the backbone φ and ψ torsion angle values of corresponding residues in **33** and **34** do not differ by more than 10° if compared to **32**. In conclusion, a comparison of our X-ray diffraction structures of peptides **32-34** has confirmed that the initial 3_{10}-helical backbone structure is maintained after macrocyclization.

In the framework of our RCM study on 3_{10}-helical peptides, we have synthesized the following series of pentapeptides:

Boc-L-hhMag-L-Ala-L-Ala-L-hhMag-L-Ala-OMe	**35**
Boc-L-hhMag-Aib-Aib-L-hhMag-Aib-OMe	**36**
Boc-L-hhMag-Aib-L-hhMag-Aib-Aib-OMe	**37**

hhMag = 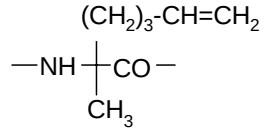

where hhMag (C^{α}-methyl, C^{α}-homo-homo-allylglycine), as Ser(Al), does contains five atoms in its longest side chain. All of the peptides were obtained by the classical methods of synthesis in solution, according to the strategies shown in **Figures 69-71**.

The C^{α}-tetrasubstituted α-amino acid hhMag, instead of Ser(Al), could additionally stabilize the 3_{10}-helical conformation of the peptides.

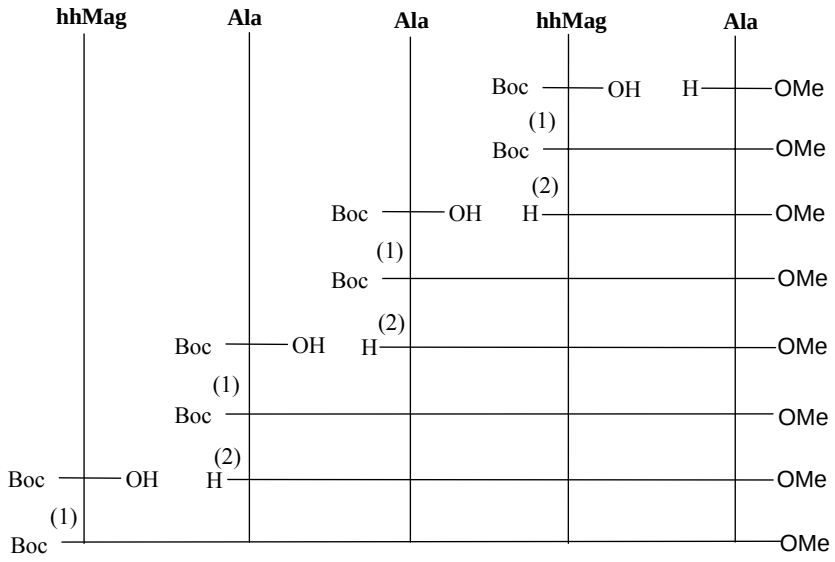

(1): EDC/HOAt; (2): TFA/CH_2Cl_2.

Figure 69. Scheme of synthesis for peptide **35**.

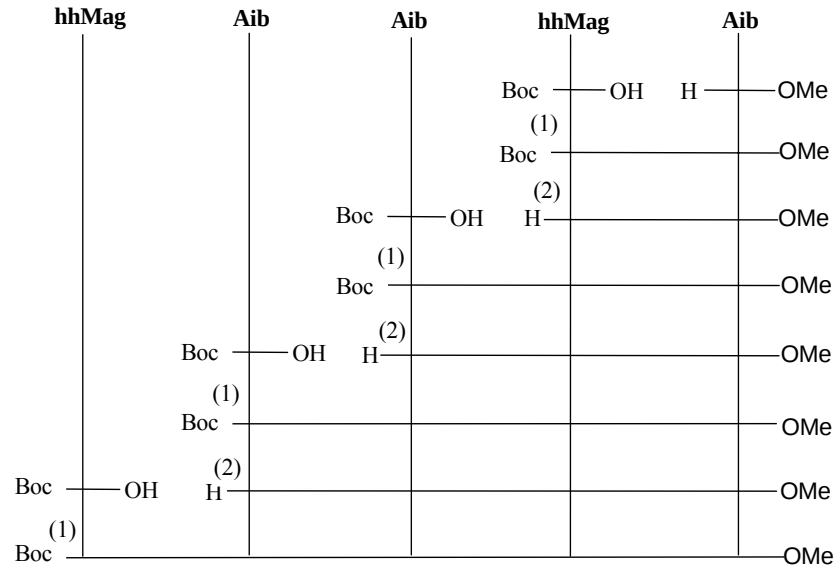

(1): EDC/HOAt; (2): TFA/CH_2Cl_2.

Figure 70. Scheme of synthesis for peptide **36**.

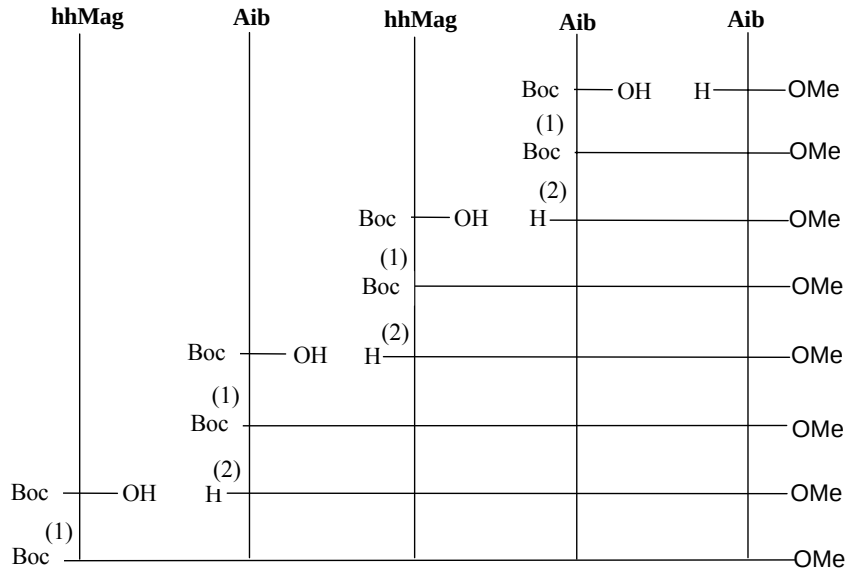

(1): EDC/HOAt; (2): TFA/CH_2Cl_2.

Figure 71. Scheme of synthesis for peptide **37**.

Though RCM offers the substantial benefit that the cyclisation is apparently sequence-independent, and because the introduced loop may in principle span any number of peptide bonds, it is important to deal with double bonds reactive in RCM spatially oriented in a favorable manner. Peptides **35** and **36** contain two residues of hhMag at relative positions *i*, *i*+3, allowing them to form a 3_{10}-helix after RCM cyclization (**Fig. 72**).

35 **36** **37**

Fig. 72. Relative spatial disposition of C=C bonds in the peptides **35-37**.

The presence in peptide **37** of only one Aib residue between the two hhMag residues prevents the ideal sterical proximity of the two reactive allyl double bonds, thus making the RCM cyclization reaction difficult.

The results obtained in the laboratory of Dr. D. J. O'Leary apparently confirmed such an hypothesis (**Table 7**). All of the peptides were subjected to RCM by refluxing in CH_2Cl_2 them in the presence of the Grubbs' catalyst (**Fig. 56C**). Peptide **37** was not as reactive as the other two peptides toward RCM. Even after three hours most of the starting peptide remained in the reaction mixture. After 24 hours the major product was a dimer. On the contrary, peptides **35** and **36** formed a main cyclized monomeric product as the major component in 0.5 – 1 hour.

Table 7. Products of the RCM reaction for peptides **35-37**.

Peptide	Time of reaction	Main fraction	Main product of the fraction
35	1 hour (5 mol% of catalyst)	74%	monocyclized peptide (*cis*/*trans*)
36	0.5 hour (5 mol% of catalyst)	33%	monocyclized peptide (*cis*/*trans*)
37	24 hours (20 mol% of catalyst)	59%	dimeric peptide

The results obtained in the RCM reaction of the 3_{10}-helix forming peptides can be summarized as follows:

- **Our ^{1}H NMR titrations and CD analyses, as well as the results of an X-ray diffraction study on octapeptides, strongly confirm that the 3_{10}-helical structure is maintained after peptide macrocyclization.**

- **Set of three pentapeptides, based on the protein amino acid Ala or containing only C^{α}-tetrasubstituted α-amino acids with a different disposition of the two hhMag residues was synthesized.**
- **The relative spatial disposition of the two allyl bonds reactive toward RCM significantly influences the type of product obtained.**
- **We conclude that 3_{10}-helical peptides are suitable candidates as templates for organic macrocyclization reactions.**

EXPERIMENTAL PART

1 Reagents and solvents

Acros-Janssen (Geel, Belgium):

α-amino isobutyric acid, N-benzyloxycarbonyloxysuccinimide, deuterochloroform, deuterated dimethylsulphoxyde, methanol for spectroscopy, N-ethyl-N'-(3-dimethylamino)propyl-carbodiimide chlorohydrate, acetic anhydride, N,N-diisopropylethylamine, *tert*-butylamine, trifluoroacetic acid.

Carlo Erba (Milan, Italy):

ethyl acetate, acetone, acetic acid, sodium bicarbonate, potassium bisulphate, 1-butanol, chloroform, dichloromethane, ethanol, methanol, diethyl ether, petroleum ether, sodium hydroxyde, sodium hypochlorite, methanol, triethylamine, anhydrous sodium sulphate.

Fluka (Buchs, Switzerland):

trifluoroacetic acid, acetonitrile, 10% Pd/C catalist, N-methylmorpholine, ninhydrin, 1-hydroxy-7-aza-1,2,3-benzotriazol.

Merck (Darmstadt, Germany):

silica gel for *flash* chromatography.

Prolabo (Paris, France):

sodium chloride, sodium hydroxide.

DSM Research (Geleen, The Netherlands):

C^{α}-methyl-, C^{α}-homo-homo-allylglycine, C^{α}-methylvaline, C^{α}-methylnorvaline.

2 Instruments and methods

Thin layer chromatography

The reactions were followed by thin layer chromatography using plates of silica gel 60 F_{254} (Merck). The retention coefficients were measured using the following solvent mixtures:

$CHCl_3$/EtOH 9:1	Rf_1
1-butanol/AcOH/H_2O 3:1:1	Rf_2
toluene/EtOH 7:1	Rf_3

For the determination of the products on the plates, a UV lamp, iodine vapours, the reagent TDM[170] for amide groups, and a ninhydrin reagent[171] for the primary amino groups were used.

Melting points determination

Melting points were measured on the Leitz apparatus model Laborlux 12.

Circular dichroism

CD spectra were recorded on the dichrograph Jasco model J-715, using quartz cells (Hellma) (pathlenghts 0.02 cm or 0.01 cm).

Flash chromatography

For the *flash* chromatography silica gel 60 Merck (40-63 μm) was used. In various purifications the product dissolved in a selected eluant was directly loaded on top of the column.

Fluorescence measurements

Steady-state fluorescence spectra were recorded on a SPEX Fluoromax spectrofluorimeter, operating in the single photon counting mode. All experiments were performed using a thermostat at 298 K. The solutions

were contained in quartz cuvettes (absorbance at excitation wavelength ≅ 0.03; optical pathlength 1 cm). Quantum yields were determined by using a fluorescent standard the quantum yield of which was known and the emission spectral properties of which closely matched those of the compound under investigation. The quantum yield of the sample is then operationally defined as:

$$\varphi_s = \varphi_r (A_r/A_s) (F_s/F_r)(n_s/n_r)^2$$

where φ is the quantum yield, *A* is the absorbance at the excitation wavelength, *F* is the integrated emission area across the band, *n* the refractive index of the solvent, and the subscripts *s* and *r* refer to the sample and the reference, respectively. The reference used was anthracene in ethanol (φ_0=0.27 ± 0.03). The experimental errors were ± 15%. Fluorescence decay were measured using a CD900 single photon counting apparatus from Edinburgh Analytical Instruments. The excitation source was a gas discharge lamp (model nF 900) filled with ultrapure hydrogen for excitation in the UV range. Under the experimental conditions (300 mm Hg gas pressure, 40 kHz repetition rate) used the full width half maximum of the excitation profile was 1.2 ns. Decay curves were fitted by a non linear least-squares analysis to exponential functions by an iterative deconvolution method. All experiments were carried out in quartz cells using solutions previously bubbled for 20 minutes with ultrapure nitrogen.

Nanosecond transient absorption experiments were performed with an LKS 60 apparatus (Applied Photophysics) using a Brilliant B Nd YAG Q-switched laser (Quantel) equipped with a third harmonic generator module to obtain a 355 nm excitation light with a pulse duration of 4 ns (full width half maximum) and an energy of about 20 mJ. Monochromatic probe light was obtained by filtering the output of a 150 W pulsed Xenon lamp through two consecutive monochromators, positioned one in front of and the other behind the sample (bandpass 3 and 3 mm).

HPLC

HPLC analyses and purifications were carried out with a chromatograph Pharmacia LKB-LCC 2252. UV detection was set at 226 nm (Uvicord SD). *Semi*-preparative (250 × 10 mm) and analytical (250 × 4.6 mm) reverse phase columns C_4 Vydec were used. As an eluant, the following solvent mixtures were used:

A: H_2O/CH_3CN 9:1 + TFA 0.05%

B: CH_3CN/H_2O 9:1 + TFA 0.05%

Polarimetric measurements

Polarimetric measurements were carried out on a Perkin-Elmer model 241 polarimeter with an Haake model D8 thermostat, using a cell with an optical pathlength of 10 cm.

Mass spectrometry

Mass spectra were recorded on mass spectrometer Mariner model ESI-TOF (Perseptive Biosystems). The positive and negative ions were accelerated at 10, 15, 20 or 30 keV.

IR absorption spectroscopy

IR absorption measurements in solution were performed on a Perkin Elmer model 1720 X FT-IR spectrophotometer, nitrogen flushed, equipped with a sample-shuttle device, at 2 cm^{-1} nominal resolution, averaging 100 scans. Solvent (baseline) spectra were obtained under the same conditions. Cells with pathlengths of 0.1, 1 and 10 mm (with CaF_2 windows) were used.

UV-Vis absorption spectroscopy

UV-*Vis* absorption experiments were carried out at room temperature on solutions contained in quartz cells (optical pathlength 1 cm) with a Cary 100 scan and UV- 250 1 PC Shimadzu spectrophotometers.

NMR spectroscopy

^{1}H-NMR and 2D-NMR spectra were recorded on Bruker AM 400 and Brucker AM 200 spectrometers. As a reference tetramethylsilane was used. For the elaboration of the spectra the programs XwinNMR e MestRe-C2.3 were applied.

3 Peptide syntheses

3.1 Synthesis of the azulene- and pyrene-bearing peptide

For this synthesis a previously obtained in the laboratory heptapeptide Z-Api(Boc)-(αMe)Nva-Aib-[(αMe)Nva]$_2$-Aib-Api(Pyr)-NH*t*Bu was used.

Z-Aib-Api(Boc)-(αMe)Nva-Aib-[(αMe)Nva]$_2$-Aib-Api(Pyr)-NH*t*Bu

To a solution of Z-Aib-OH (31 mg, 0.13 mmol), HOAt (18 mg, 0.13 mmol) and EDC·HCl (25 mg, 0.13 mmol) in anhydrous CH_2Cl_2 cooled to 0°C, H-Api(Boc)-(αMe)Nva-Aib-[(αMe)Nva]$_2$-Aib-Api(Pyr)-NH*t*Bu [obtained by catalytic hydrogenation with Pd/C of the corresponding Z-derivative (114 mg, 0.09 mol) in MeOH] and NMM (15 µl, 0.13 mmol) were added. The reaction mixture was stirred 25 days at rt. During this period another 6 equivalents of the mixture of Z-Aib-OH, HOAt and EDC·HCl followed by NMM were added. Then the solvent was evaporated and the product was purified by *flash* chromatography by eluting with the mixture of EtOAc/PE (v/v 9:1). Oil. Yield: 60%.

Rf$_1$: 0.60; **Rf$_2$:** 0.95; **Rf$_3$:** 0.35.

$[\alpha]_D^{20} = +2.8^o$ (c = 0.5, MeOH).

IR (film): ν_{max} 3305, 1782, 1706, 1657, 1532 cm^{-1}.

^{1}H NMR (400 MHz, $CDCl_3$): δ 8.25 – 7.95 (m, 9H, CH pyrene); 7.65 (s, 1H, NH); 7.52 (s, 1H, NH); 7.34 (m, 8H, 5H Z-CH phenyl, 3H NH); 6.55 (s, 1H, NH); 5.89 (s, 1H, NH); 5.48 (s, 1H, NH); 5.08 (m, 2H, Z-CH_2); 4.89 (s, 1H, NH); 3.95 – 3.70 (m, 1H, CH_2 Api); 3.31 – 2.78 (m, 7H, CH_2 Api); 1.71 – 1.22 (m, 59H, 9H α-CH_3 (αMe)Nva,

18H CH_3 Aib, 9H O*t*Bu-CH_3, 9H NH*t*Bu-CH_3, 8H CH_2 Api, 6H β-CH_2 (αMe)Nva); 1.01 – 0.83 (m, 9H, γ-CH_3 (αMe)Nva.

Z-Aib-Api(Azu)-(αMe)Nva-Aib-[(αMe)Nva]$_2$-Aib-Api(Pyr)-NH*t*Bu

To a solution of Azu-COOH (15 mg, 0.09 mmol), HOAt (12 mg, 0.09 mmol) and EDC·HCl (17 mg, 0.09 mmol) in acetonitrile cooled to 0°C, Z-Api-(αMe)Nva-Aib-[(αMe)Nva]$_2$-Aib-Api(Pyr)-NH*t*Bu [obtained by the Boc-deprotection of Z-Api(Boc)-(αMe)Nva-Aib-[(αMe)Nva]$_2$-Aib-Api(Pyr)-NH*t*Bu (60 mg, 0.04 mmol) by a 3.3 N solution of HCl in EtOAc] and NMM (10 µl, 0.09 mmol) were added. After 3 days the solvent was evaporated and the product was purified by *flash* chromatography by eluting with the mixture of EtOAc/PE (v/v 9:1). Yield: 82%.

Rf_1: 0.55; **Rf_2:** 0.95; **Rf_3:** 0.15.

$[\alpha]_{436}^{20}$ = -24.5° (c = 0.5, MeOH).

IR (in a film): ν_{max} 3307, 1657, 1531 cm^{-1}.

^{1}H NMR (400 MHz, $CDCl_3$): δ 8.58 (m, 1H, CH Azu); 8.42 (m, 1H, CH Azu); 8.25 – 7.95 (m, 9H, CH pyrene); 7.89 (m, 1H, CH Azu); 7.75 – 7.51 (m, 5H, 4H CH Azu, 1H NH); 7.39 (m, 2H, NH); 7.32 (m, 7H, 5H Z-CH phenyl, 2H NH); 7.10 (s, 1H, NH); 6.97 (m, 1H, NH); 6.34 (s, 1H, NH); 5.07 (m, 2H, Z-CH_2); 4.65 (m, 1H, NH); 3.95 – 3.70 (m, 1H, CH_2 Api); 3.39 – 2.92 (m, 7H, CH_2 Api); 1.45 – 1.10 (m, 50H, 9H α-CH_3 (αMe)Nva, 18H CH_3 Aib, 9H NH*t*Bu-CH_3, 8H CH_2 Api, 6H β-CH_2 (αMe)Nva); 1.01 – 0.83 (m, 9H, γ-CH_3 (αMe)Nva.

Mass spectrometry (ESI-TOF): $[M+H]^+_{calc}$ = 1436.80; $[M+H]^+_{exp}$ = 1436.79.

3.2 Synthesis of porphyrin conjugates

For this synthesis the peptides Z-[(αMe)Val]$_n$-O*t*Bu (*n* = 2, 3, 5, 6) previously obtained in our laboratory were used.

(Z-Ala)$_2$O

To a solution of Z-Ala-OH (3 g, 0.0134 mol) in acetonitrile, cooled to 0°C, EDC·HCl (1.29 g, 0.0067 mmol) was added. The reaction mixture was stirred 20 min under cooling and 2 hours at the rt. Then the solvent was evaporated, the oily residue was dissolved in EtOAc and the organic solution washed with 10% $KHSO_4$, H_2O, 5% $NaHCO_3$, and H_2O. The organic layer was dried over anhydrous Na_2SO_4 and evaporated to dryness.

M. p.: 105-107ºC.

3.2.1 Synthesis of TPP-CO-Ala-[(αMe)Val]$_2$-NH-C$_6$H$_{10}$-NH-CO-TPP

Z-Ala-[(αMe)Val]$_2$-O*t*Bu

(Z-Ala)$_2$O (151 mg, 0.3528 mmol) and H-[(αMe)Val]$_2$-O*t*Bu [obtained by catalytic hydrogenation with Pd/C of the corresponding Z-derivative (108 mg, 0.2485 mmol) in MeOH] were dissolved in CH_2Cl_2. NMM was added (40 µl, 0.3528 mmol) and the reaction mixture was stirred 24 hours at rt. Then the solvent was evaporated and the oily residue was purified by "flash chromatography" by eluting with PE/EtOAc (4/1; 3/1). Oil. Yield: 76%.

Rf_1: 0.85; Rf_2: 0.95; Rf_3: 0.35.

$[\alpha]_D^{20}$ = -6.2; $[\alpha]_{578}^{20}$ = -4.8 (c = 0.5, MeOH).

IR (in a film): ν_{max} 3309, 1714, 1675, 1519 cm^{-1}.

^{1}H NMR (400 MHz, $CDCl_3$): δ 7.34 (s, 6H, 5H Z-CH phenyl, 1H NH); 6.57 (s, 1H, NH); 5.38 (s, 1H, NH); 5.15 – 5.05 (m, 2H, Z-CH_2); 4.20 (m, 1H, CH Ala); 2.55 – 2.45 (m, 1H, β-CH); 2.28 – 2.15 (m, 1H, β-CH); 1.50 – 1.42 [m, 15H, 6H α-CH_3 (αMe)Val, 9H *t*Bu-CH_3); 1.37 (d, 3H, CH_3 Ala); 1.03 – 0.85 (m, 12H, γ-CH_3 (αMe)Val).

Z-Ala-[(αMe)Val]$_2$-OH

To a solution of Z-Ala-[(αMe)Val]$_2$-O*t*Bu (60 mg, 0.1187 mmol) in 3 ml of anhydrous CH_2Cl_2, cooled to 0°C, 3 ml of TFA were added under stirring. After one hour the

solvent was evaporated and the remaining traces of TFA removed by repetitive evaporations with Et_2O. Oil. Yield: 86%.

Rf_1: 0.30; Rf_2: 0.90; Rf_3: 0.15.

$[\alpha]_D^{20}$ = -4.4; $[\alpha]_{578}^{20}$ = -4.8 (c = 0.5, MeOH).

IR (in a film): ν_{max} 3310, 1704, 1664, 1520 cm^{-1}.

^1H NMR (200 MHz, $CDCl_3$): δ 7.32 (s, 6H, 5H Z-CH phenyl, 1H NH); 6.90 (s, 1H, NH); 5.79 (s, 1H, NH); 5.08 (m, 2H, Z-CH_2); 4.25 – 4.09 (m, 1H, CH Ala); 2.55 – 2.35 (m, 1H, β-CH); 2.23 – 2.10 (m, 1H, β-CH); 1.37 – 1.15 [m, 9H, 6H α-CH_3 (αMe)Val, 3H CH_3 Ala); 1.03 – 0.81 (m, 12H, γ-CH_3 (αMe)Val).

Z-Ala-[(αMe)Val]$_2$-NH-C_6H_{10}-NH_2

A solution of Z-Ala-[(αMe)Val]$_2$-OH (42 mg, 0.0934 mmol) and EDC·HCl (27 mg, 0.1401 mmol) in acetonitrile was stirred 3 hours. Than NH_2-C_6H_{10}-NH_2 (64 mg, 0.5604 mmol) was added. After two days the solvent was evaporated to dryness, and the solid was redissolved in $CHCl_3$. The organic solution was washed with 5% $NaHCO_3$ and H_2O. The organic solution was dried over anhydrous Na_2SO_4 and the solvent was evaporated. Oil. Yield: 91%.

Rf_2: 0.70.

$[\alpha]_D^{20}$ = 7.0; $[\alpha]_{578}^{20}$ = 9.4 (c = 0.5, MeOH).

IR (film): ν_{max} 3319, 1704, 1670, 1533 cm^{-1}.

^1H NMR (200 MHz, $CDCl_3$): δ 7.33 (s, 5H, Z-CH phenyl); 7.18 (s, 1H, NH); 7.01 (s, 1H, NH); 6.53 (s, 1H, NH); 6.34 (s, 1H, NH); 5.18 – 4.97 (m, 2H, Z-CH_2); 4.12 – 4.00 (m, 1H, CH Ala); 3.75 – 3.55 (m, 1H, CH cyclohexane ring); 3.05 – 2.80 (m, 1H, CH cyclohexane ring); 2.05 – 1.75 (m, 10H, 2H β-CH, 8H CH_2 cyclohexane ring); 1.48 – 1.28 [m, 9H, 6H α-CH_3 (αMe)Val, 3H CH_3 Ala); 0.95 – 0.75 (m, 12H, γ-CH_3 (αMe)Val).

Z-Ala-[(αMe)Val]$_2$-NH-C_6H_{10}-NH-CO-TPP

To a solution of TPP-COOH (61 mg, 0.0924 mmol) and HATU (35 mg, 0.0924 mmol) in anhydrous CH_2Cl_2 cooled to 0°C, Z-Ala-[(αMe)Val]$_2$-NH-C_6H_{10}-NH_2 (42 mg, 0.0770

mmol) and NMM (10 µl, 0.0924 mmol) were added. The reaction mixture was stirred 24 hours. Then the solvent was evaporated to dryness and the product was purified by "flash chromatography" by eluting with CH_2Cl_2/EtOH (10/0; 10/0.2; 10/0.3; 10/0.4; 10/0.5) and recrystallized from EtOAc. Yield: 68%.

M. p.: 252-254ºC.

Rf_1: 0.75; Rf_2: 0.95; Rf_3: 0.40.

IR (KBr): ν_{max} 3317, 1709, 1671, 1523 cm^{-1}.

^1H NMR (200 MHz, $CDCl_3$): δ 8.90 – 8.72 (m, 8H, CH pyrrole); 8.30 – 8.12 (m, 10H, 8H *o*-CH phenyl, 2H *m*-CH phenyl); 7.80 – 7.72 (m, 9H, 3H *p*-CH phenyl, 6H *m*-CH phenyl); 7.67 (s, 1H, NH); 7.36 (s, 5H, Z-CH phenyl); 6.69 (s, 1H, NH); 6.43 (s, 1H, NH); 6.37 (d, 1H, NH); 5.37 (d, 1H, NH); 5.25 – 5.03 (m, 2H, Z-CH_2); 4.27 – 4.05 (m, 1H, CH Ala); 3.95 – 3.75 (m, 1H, CH cyclohexane ring); 3.70 – 3.52 (m, 1H, CH cyclohexane ring); 2.35 – 2.05 (m, 6H, 2H β-CH, 4H CH_2 cyclohexane ring); 1.65 – 1.55 (m, 4H, CH_2 cyclohexane ring); 1.52 – 1.35 [m, 9H, 6H α-CH_3 (αMe)Val, 3H CH_3 Ala); 0.95 – 0.80 (m, 12H, γ-CH_3 (αMe)Val); -2.78 (s, 2H, NH pyrrole).

TPP-CO-Ala-[(αMe)Val]$_2$-NH-C_6H_{10}-NH-CO-TPP

To a solution of TPP-COOH (11 mg, 0.0172 mmol) and HATU (7 mg, 0.0172 mmol) in anhydrous CH_2Cl_2 cooled to 0°C, (H-Ala-[(αMe)Val]$_2$-NH-C_6H_{10}-NH-CO-TPP [obtained by catalytic hydrogenation with Pd/C of the corresponding Z-derivative (15 mg, 0.0126 mmol) in a mixture CH_2Cl_2/MeOH] were dissolved in CH_2Cl_2. NMM was added (2 µl, 0.0172 mmol) and the reaction mixture was stirred 24 hours at rt. Then the solvent was evaporated to dryness and the residue was purified by "flash chromatography" by eluting with CH_2Cl_2/EtOH (10/0; 10/0.1; 10/0.2; 10/0.3). Oil. Yield: 92%.

Rf_1: 0.90; Rf_2: 0.95; Rf_3: 0.45.

IR (film): ν_{max} 3424, 3324, 1653, 1631, 1528 cm^{-1}.

^1H NMR (200 MHz, $CDCl_3$): δ 8.93 – 8.71 (m, 16H, CH pyrrole); 8.42 – 8.03 (m, 20H, 16H *o*-CH phenyl, 4H *m*-CH phenyl); 7.81 – 7.65 (m, 19H, 6H *p*-CH phenyl, 12H *m*-CH phenyl, 1H NH); 7.36 (s, 1H, NH); 6.90 (s, 1H, NH); 6.55 (s, 1H, NH); 6.27 (d, 1H, NH); 4.80 (m, 1H, CH Ala); 4.00 – 3.75 (m, 1H, CH cyclohexane ring); 3.70 – 3.52 (m, 1H, CH cyclohexane ring); 2.35 – 2.05 (m, 6H, 2H β-CH, 4H CH_2 cyclohexane ring);

1.65 – 1.40 (m, 13H, 4H CH_2 cyclohexane ring, 6H α-CH_3 (αMe)Val, 3H CH_3 Ala); 1.15 – 0.95 (m, 12H, γ-CH_3 (αMe)Val); -2.79 (s, 4H, NH pyrrole).

3.2.2 Synthesis of TPP-CO-Ala-[(αMe)Val]$_3$-NH-C_6H_{10}-NH-CO-TPP

Z-Ala-[(αMe)Val]$_3$-O*t*Bu

To a solution of Z-Ala-OH (0.58 g, 0.0026 mol), and HATU (1 g, 0.0026 mol) in anhydrous CH_2Cl_2 cooled to 0°C, H-[(αMe)Val]$_3$-O*t*Bu [obtained by catalytic hydrogenation with Pd/C of the corresponding Z-derivative (0.71 g, 0.0013 mol) in MeOH] and NMM (286 µl, 0.0026 mol) were added. The reaction mixture was stirred 2 days at rt. Then the solvent was evaporated, the oily residue was dissolved in EtOAc and the organic solution washed with 10% $KHSO_4$, H_2O, 5% $NaHCO_3$, and H_2O. The organic layer was dried over anhydrous Na_2SO_4 and evaporated to dryness. The product was purified by "flash chromatography" by eluting with PE/EtOAc (4/1; 3/1) and recrystallized from EtOAc/PE. Yield: 85%.

M. p.: 134-136ºC.

Rf_1: 0.85; Rf_2: 0.95; Rf_3: 0.30.

$[\alpha]_D^{20}$ = -4.7; $[\alpha]_{578}^{20}$ = -3.1 (c = 0.5, MeOH).

IR (KBr): ν_{max} 3439, 3320, 1725, 1703, 1666, 1523 cm^{-1}.

^{1}H NMR (200 MHz, $CDCl_3$): δ 7.34 (s, 6H, 5H Z-CH phenyl, 1H NH); 7.10 (s, 1H, NH); 6.56 (s, 1H, NH); 5.60 (s, 1H, NH); 5.11 (m, 2H, Z-CH_2); 4.27 – 4.08 (m, 1H, CH Ala); 2.43 – 2.08 (m, 3H, β-CH); 1.54 – 1.30 [m, 21H, 9H α-CH_3 (αMe)Val, 9H *t*Bu-CH_3, 3H CH_3 Ala); 1.03 – 0.80 (m, 18H, γ-CH_3 (αMe)Val).

Z-Ala-[(αMe)Val]$_3$-OH

To a solution of Z-Ala-[(αMe)Val]$_3$-O*t*Bu (124 mg, 0.2004 mmol) in 3 ml of CH_2Cl_2, cooled to 0 °C, 3 ml of TFA were added under stirring. After one hour the solvent was evaporated and the remaining traces of TFA removed by repetitive evaporations with Et_2O. Oil. Yield: 95%.

Rf_1: 0.35; Rf_2: 0.90; Rf_3: 0.20.

$[\alpha]_D^{20}$ = 11.6; $[\alpha]_{578}^{20}$ = 12.4 (c = 0.5, MeOH).

IR (film): ν_{max} 3317, 1729, 1704, 1665, 1521 cm^{-1}.

^1H NMR (200 MHz, $CDCl_3$): δ 7.34 (s, 6H, 5H Z-CH phenyl, 1H, NH); 6.99 (s, 1H, NH); 6.94 (s, 1H, NH); 6.06 (d, 1H, NH); 5.18 – 5.00 (m, 3H, 2H Z-CH_2, 1H, NH); 4.05 – 3.90 (m, 1H, CH Ala); 2.35 – 2.15 (m, 1H, β-CH); 2.10 – 1.76 (m, 2H, β-CH); 1.50 – 1.35 [m, 12H, 9H α-CH_3 (αMe)Val, 3H CH_3 Ala); 1.15 – 0.76 (m, 18H, γ-CH_3 (αMe)Val).

Z-Ala-[(αMe)Val]$_3$-NH-C_6H_{10}-NH_2

A solution of Z-Ala-[(αMe)Val]$_3$-OH (104 mg, 0.1848 mmol) and EDC·HCl (53 mg, 0.2772 mmol) in acetonitrile was stirred 3 hours after that NH_2-C_6H_{10}-NH_2 (127 mg, 1.1088 mmol) was added. After two days the solvent was evaporated to dryness, and the solid was redissolved in $CHCl_3$. The organic solution was washed with 5% $NaHCO_3$ and H_2O. The organic solution was dried over anhydrous Na_2SO_4 and the solvent was evaporated. Yield: 96%.

M. p.: 113-114ºC.

Rf_2: 0.75.

$[\alpha]_D^{20}$ = 6.9; $[\alpha]_{578}^{20}$ = 6.2 (c = 0.5, MeOH).

IR (KBr): ν_{max} 3326, 1704, 1665, 1522 cm^{-1}.

^1H NMR (200 MHz, $CDCl_3$): δ 7.34 (s, 6H, 5H Z-CH phenyl, 1H, NH); 6.95 (s, 1H, NH); 6.83 (s, 1H, NH); 6.75 (s, 1H, NH); 6.41 (s, 1H, NH); 5.22 – 5.00 (m, 2H, Z-CH_2); 4.12 – 3.95 (m, 2H, 1H CH Ala, 1H CH cyclohexane ring); 3.25 – 3.10 (m, 1H, CH cyclohexane ring); 2.10 – 1.75 (m, 7H, 3H β-CH, 4H CH_2 cyclohexane ring); 1.51 – 1.32 [m, 13H, 9H α-CH_3 (αMe)Val, 4H CH_2 cyclohexane ring); 1.31 – 1.25 (d, 3H CH_3 Ala); 1.05 – 0.75 (m, 18H, γ-CH_3 (αMe)Val).

Z-Ala-[(αMe)Val]$_3$-NH-C_6H_{10}-NH-CO-TPP

To a solution of TPP-COOH (114 mg, 0.1730 mmol) and HATU (66 mg, 0.1730 mmol) in anhydrous CH_2Cl_2 cooled to 0°C, Z-Ala-[(αMe)Val]$_3$-NH-C_6H_{10}-NH_2 (114 mg, 0.1730 mmol) and NMM (20 µl, 0.1815 mmol) were added. The reaction mixture was stirred 24 hours. Then the solvent was evaporated to dryness and the product was

purified by "flash chromatography" by eluting with CH_2Cl_2/EtOH (10/0; 10/0.2; 10/0.3; 10/0.4; 10/0.5) and recrystallized from EtOAc. Yield: 86%.

M. p.: 223-224ºC.

Rf_1: 0.75; Rf_2: 0.95; Rf_3: 0.40.

IR (KBr): ν_{max} 3320, 1704, 1667, 1521 cm^{-1}.

^1H NMR (200 MHz, $CDCl_3$): δ 8.95 – 8.72 (m, 8H, CH pyrrole); 8.35 – 8.12 (m, 10H, 8H *o*-CH phenyl, 2H *m*-CH phenyl); 7.91 – 7.62 (m, 10H, 3H *p*-CH phenyl, 6H *m*-CH phenyl, 1H NH); 7.38 (s, 5H, Z-CH phenyl); 6.87 (s, 1H, NH); 6.71 (s, 1H, NH); 6.60 (s, 1H, NH); 6.29 (d, 1H, NH); 5.25 – 5.01 (m, 3H, 2H Z-CH_2, 1H NH); 4.27 – 4.05 (m, 2H, 1H CH Ala, 1H CH cyclohexane ring); 3.95 – 3.71 (m, 1H, CH cyclohexane ring); 2.35 – 1.83 (m, 7H, 3H β-CH, 4H CH_2 cyclohexane ring); 1.70 – 1.45 (m, 16H, 4H CH_2 cyclohexane ring, 3H CH_3 Ala, 9H α-CH_3 (αMe)Val); 1.07 – 0.81 (m, 18H, γ-CH_3 (αMe)Val); -2.78 (s, 2H, NH pyrrole).

TPP-CO-Ala-[(αMe)Val]$_3$-NH-C_6H_{10}-NH-CO-TPP

To a solution of TPP-COOH (47 mg, 0.0713 mmol) and HATU (27 mg, 0.0713 mmol) in anhydrous CH_2Cl_2 cooled to 0°C, (H-Ala-[(αMe)Val]$_3$-NH-C_6H_{10}-NH-CO-TPP [obtained by catalytic hydrogenation with Pd/C of the corresponding Z-derivative (70 mg, 0.0539 mmol) in a mixture CH_2Cl_2/MeOH] were dissolved in CH_2Cl_2. NMM was added (8 µl, 0.0713 mmol) and the reaction mixture was stirred 24 hours at rt. Then the solvent was evaporated to dryness and the residue was purified by "flash chromatography" by eluting with CH_2Cl_2/EtOH (10/0; 10/0.1; 10/0.2; 10/0.3). Yield: 89%.

M. p.: 259-261ºC.

Rf_1: 0.85; Rf_2: 0.95; Rf_3: 0.45.

IR (KBr): ν_{max} 3427, 3318, 1653, 1516 cm^{-1}.

^1H NMR (200 MHz, $CDCl_3$): δ 8.95 – 8.74 (m, 16H, CH pyrrol); 8.39 – 8.15 (m, 20H, 16H *o*-CH phenyl, 4H *m*-CH phenyl); 7.77 (m, 18H, 6H *p*-CH phenyl, 12H *m*-CH phenyl); 7.51 (d, 1H, NH); 7.18 (s, 1H, NH); 7.05 (s, 1H, NH); 7.00 (d, 1H, NH); 6.90 (s, 1H, NH); 6.31 (d, 1H, NH); 4.73 (m, 1H, CH Ala); 4.28 – 4.15 (m, 1H, CH cyclohexane ring); 3.95 – 3.78 (m, 1H, CH cyclohexane ring); 2.40 – 1.95 (m, 7H, 3H β-CH, 4H CH_2 cyclohexane ring); 1.70 – 1.55 (m, 16H, 4H CH_2 cyclohexane ring, 9H

α-CH_3 (αMe)Val, 3H CH_3 Ala); 1.20 – 1.05 (m, 18H, γ-CH_3 (αMe)Val); -2.78 (s, 4H, NH pyrrole).

3.2.3 Synthesis of TPP-CO-Ala-[(αMe)Val]$_5$-NH-C_6H_{10}-NH-CO-TPP

Z-Ala-[(αMe)Val]$_5$-O*t*Bu

$(Z\text{-Ala})_2O$ (176 mg, 0.4108 mmol) and H-[(αMe)Val]$_5$-O*t*Bu [obtained by catalytic hydrogenation with Pd/C of the corresponding Z-derivative (159 mg, 0.2054 mmol) in MeOH] were dissolved in CH_2Cl_2. NMM was added (45 µl, 0.4108 mmol) and the reaction mixture was stirred 24 hours at rt. Then the solvent was evaporated, the oily residue was dissolved in EtOAc and the organic solution washed with 10% $KHSO_4$, H_2O, 5% $NaHCO_3$, and H_2O. The organic layer was dried over anhydrous Na_2SO_4 and evaporated to dryness. The product was purified by "flash chromatography" by eluting with PE/EtOAc (2/1; 1.5/1) and recrystallized from EtOAc/ PE. Yield: 80%.

M. p.: 185-186ºC.

Rf_1: 0.85; Rf_2: 0.95; Rf_3: 0.30.

$[\alpha]_D^{20}$ = 5.7; $[\alpha]_{578}^{20}$ = 8.6 (c = 0.5, MeOH).

IR (KBr): ν_{max} 3422, 3336, 1702, 1663, 1521 cm^{-1}.

^{1}H NMR (200 MHz, $CDCl_3$): δ 7.63 (s, 1H, NH); 7.34 (s, 5H, Z-CH phenyl); 7.09 (s, 1H, NH); 7.00 (s, 1H, NH); 6.70 (s, 1H, NH); 6.60 (s, 1H, NH); 5.85 – 5.75 (s, 1H, NH); 5.19 – 5.02 (m, 2H, Z-CH_2); 4.08 – 3.93 (m, 1H, CH Ala); 2.38 – 2.25 (m, 1H, β-CH); 2.18 – 2.07 (m, 1H, β-CH); 2.05 – 1.95 (m, 1H, β-CH); 1.94 – 1.82 (m, 1H, β-CH); 1.80 – 1.68 (m, 1H, β-CH); 1.52 – 1.35 [m, 24H, 15H α-CH_3 (αMe)Val, 9H *t*Bu-CH_3); 1.33 (d, 3H, CH_3 Ala); 1.05 – 0.75 (m, 30H, γ-CH_3 (αMe)Val).

Z-Ala-[(αMe)Val]$_5$-OH

To a solution of Z-Ala-[(αMe)Val]$_5$-O*t*Bu (76 mg, 0.0899 mmol) in 3 ml of CH_2Cl_2, cooled to 0 °C, 3 ml of TFA were added under stirring. After one hour the solvent was evaporated and the remaining traces of TFA removed by repetitive evaporations with Et_2O. The product was recrystallized from Et_2O. Yield: 95%.

M. p.: 223-225ºC.

Rf_1: 0.55; Rf_2: 0.90; Rf_3: 0.15.

$[\alpha]_D^{20}$ = 31.6; $[\alpha]_{578}^{20}$ = 33.3 (c = 0.5, $CHCl_3$).

IR (KBr): ν_{max} 3303, 1736, 1703, 1653, 1524 cm^{-1}.

^1H NMR (200 MHz, $CDCl_3$): δ 7.67 (1H, NH); 7.34 (s, 7H, 5H Z-CH phenyl, 2H, NH); 6.93 (s, 1H, NH); 6.87 (s, 1H, NH); 6.08 (s, 1H, NH); 5.18 – 5.02 (m, 2H, Z-CH_2); 4.05 – 3.93 (m, 1H, CH Ala); 2.40 – 2.22 (m, 1H, β-CH); 2.15 – 1.75 (m, 4H, β-CH); 1.50 – 1.30 [m, 18H, 15H α-CH_3 (αMe)Val, 3H CH_3 Ala); 1.15 – 0.78 (m, 30H, γ-CH_3 (αMe)Val).

Z-Ala-[(αMe)Val]$_5$-NH-C_6H_{10}-NH_2

A solution of Z-Ala-[(αMe)Val]$_5$-OH (58 mg, 0.0735 mmol) and EDC·HCl (21 mg, 0.1103 mmol) in acetonitrile was stirred 3 hours after that NH_2-C_6H_{10}-NH_2 (50 mg, 0.4410 mmol) was added. After tree days the solvent was evaporated to dryness, and the solid was redissolved in $CHCl_3$. The organic solution was washed with 5% $NaHCO_3$ and H_2O. The organic solution was dried over anhydrous Na_2SO_4 and the solvent was evaporated. Oil. Yield: 93%.

Rf_2: 0.85.

$[\alpha]_D^{20}$ = 12.8; $[\alpha]_{578}^{20}$ = 12.4 (c = 0.5, MeOH).

IR (film): ν_{max} 3316, 1703, 1656, 1521 cm^{-1}.

^1H NMR (200 MHz, $CDCl_3$): δ 7.45 (s, 1H, NH); 7.34 (s, 7H, 5H Z-CH phenyl, 2H, NH); 7.16 (s, 1H, NH); 6.83 (s, 1H, NH); 6.77 (s, 1H, NH); 6.32 (s, 1H, NH); 5.22 – 5.02 (m, 2H, Z-CH_2); 4.12 – 4.91 (m, 1H, CH Ala); 3.76 – 3.60 (m, 1H, CH cyclohexane ring); 3.28 – 3.12 (m, 1H, CH cyclohexane ring); 2.15 – 1.75 (m, 9H, 5H β-CH, 4H CH_2 cyclohexane ring); 1.55 – 1.22 [m, 22H, 15H α-CH_3 (αMe)Val, 4H CH_2 cyclohexane ring, 3H CH_3 Ala); 1.10 – 0.75 (m, 30H, γ-CH_3 (αMe)Val).

Z-Ala-[(αMe)Val]$_5$-NH-C_6H_{10}-NH-CO-TPP

To a solution of TPP-COOH (51 mg, 0.0773 mmol) and HATU (30 mg, 0.0773 mmol) in anhydrous CH_2Cl_2 cooled to 0°C, Z-Ala-[(αMe)Val]$_3$-NH-C_6H_{10}-NH_2 (57 mg, 0.0644

mmol) and NMM (10 µl, 0.0773 mmol) were added. The reaction mixture was stirred 24 hours. Then the solvent was evaporated to dryness and the product was purified by "flash chromatography" by eluting with CH_2Cl_2/EtOH (10/0; 10/0.2; 10/0.3; 10/0.4; 10/0.5) and recrystallized from EtOAc. Yield: 76%.

M. p.: 301-303ºC.

Rf_1: 0.75; Rf_2: 0.95; Rf_3: 0.40.

IR (KBr): ν_{max} 3321, 1704, 1658, 1522 cm^{-1}.

^1H NMR (200 MHz, $CDCl_3$): δ 8.95 – 8.72 (m, 8H, CH pyrrole); 8.35 – 8.12 (m, 10H, 8H *o*-CH phenyl, 2H *m*-CH phenyl); 7.91 – 7.65 (m, 9H, 3H *p*-CH phenyl, 6H *m*-CH phenyl); 7.62 (d, 1H NH); 7.35 (s, 5H, Z-CH phenyl); 7.29 (s, 1H, NH); 7.13 (s, 1H, NH); 6.74 (s, 1H, NH); 6.64 (s, 1H, NH); 6.32 (d, 1H, NH); 5.46 (d, 1H, NH); 5.19 – 5.02 (m, 2H, Z-CH_2); 4.27 – 4.05 (m, 2H, 1H CH Ala, 1H CH cyclohexane ring); 3.95 – 3.72 (m, 1H, CH cyclohexane ring); 2.36 – 1.85 (m, 5H, β-CH); 1.78 – 1.62 (m, 8H, CH_2 cyclohexane ring); 1.51 – 1.32 (m, 18H, 3H CH_3 Ala, 15H α-CH_3 (αMe)Val); 1.08 – 0.80 (m, 30H, γ-CH_3 (αMe)Val); -2.78 (s, 2H, NH pyrrole).

TPP-CO-Ala-[(αMe)Val]$_5$-NH-C_6H_{10}-NH-CO-TPP

To a solution of TPP-COOH (11 mg, 0.0173 mmol) and HATU (7 mg, 0.0173 mmol) in anhydrous CH_2Cl_2 cooled to 0°C, (H-Ala-[(αMe)Val]$_5$-NH-C_6H_{10}-NH-CO-TPP [obtained by catalytic hydrogenation with Pd/C of the corresponding Z-derivative (22 mg, 0.0144 mmol) in a mixture CH_2Cl_2/MeOH] were dissolved in CH_2Cl_2. NMM was added (2 µl, 0.0173 mmol) and the reaction mixture was stirred 24 hours at rt. Then the solvent was evaporated to dryness and the residue was purified by *flash* chromatography by eluting with CH_2Cl_2/EtOH (10/0; 10/0.1; 10/0.2; 10/0.3). Yield: 83%.

M. p.: 252-254ºC.

Rf_1: 0.85; Rf_2: 0.95; Rf_3: 0.45.

IR (KBr): ν_{max} 3423, 3319, 1656, 1521 cm^{-1}.

^1H NMR (200 MHz, $CDCl_3$): δ 8.93 – 8.72 (m, 16H, CH pyrrole); 8.39 – 8.05 (m, 20H, 16H *o*-CH phenyl, 4H *m*-CH phenyl); 7.81 – 7.62 (m, 18H, 6H *p*-CH phenyl, 12H *m*-CH phenyl); 7.45 (m, 2H, NH); 7.36 (m, 2H, NH); 7.16 (m, 2H, NH); 7.03 (s, 1H, NH); 6.50 (d, 1H, NH); 4.61 (m, 1H, CH Ala); 4.28 – 4.15 (m, 1H, CH cyclohexane

ring); 3.95 – 3.80 (m, 1H, CH cyclohexane ring); 2.40 – 1.95 (m, 9H, 5H β-CH, 4H CH_2 cyclohexane ring); 1.70 – 1.45 (m, 22H, 4H CH_2 cyclohexane ring, 15H α-CH_3 (αMe)Val, 3H CH_3 Ala); 1.20 – 1.05 (m, 30H, γ-CH_3 (αMe)Val); -2.79 (s, 4H, NH pyrrole).

3.2.4 Synthesis of TPP-CO-Ala-[(αMe)Val]$_6$-NH-C_6H_{10}-NH-CO-TPP

Z-Ala-[(αMe)Val]$_6$-O*t*Bu

$(Z\text{-Ala})_2O$ (140 mg, 0.3268 mmol) and H-[(αMe)Val]$_6$-O*t*Bu [obtained by catalytic hydrogenation with Pd/C of the corresponding Z-derivative (468 mg, 0.5275 mmol) in MeOH] were dissolved in anhydrous CH_2Cl_2. NMM was added (35 µl, 0.3162 mmol) and the reaction mixture was stirred 7 days at rt. During this period another 200 mg (0.467 mmol) of $(Z\text{-Ala})_2O$ and 30 µl of NMM were added to the reaction mixture. Then the solvent was evaporated, the oily residue was dissolved in EtOAc and the organic solution washed with 10% $KHSO_4$, H_2O, 5% $NaHCO_3$, and H_2O. The organic layer was dried over anhydrous Na_2SO_4, evaporated to dryness and recrystallized from EtOAc/PE. Yield: 90%.

M. p.: 205-207ºC.

Rf_1: 0.85; Rf_2: 0.95; Rf_3: 0.25.

$[\alpha]_D^{20}$ = 13.6; $[\alpha]_{578}^{20}$ = 14.5 (c = 0.5, MeOH).

IR (KBr): ν_{max} 3421, 3340, 1700, 1661, 1521 cm^{-1}.

^{1}H NMR (400 MHz, $CDCl_3$): δ 7.71 (s, 1H, NH); 7.36 (s, 5H, Z-CH phenyl); 7.20 (s, 2H, NH); 7.04 (s, 1H NH); 6.66 (s, 1H NH); 6.57 (s, 1H NH); 5.21 – 5.08 (m, 3H, 2H Z-CH_2, 1H, NH); 4.10 – 3.95 (m, 1H, CH Ala); 2.38 – 2.26 (m, 1H, β-CH); 2.20 – 2.12 (m, 1H, β-CH); 2.09 – 1.94 (m, 2H, β-CH); 1.93 – 1.75 (m, 1H, β-CH); 1.80 – 1.68 (m, 1H, β-CH); 1.52 – 1.35 [m, 30H, 18H α-CH_3 (αMe)Val, 9H *t*Bu-CH_3, 3H CH_3 Ala); 1.12 – 0.80 (m, 36H, γ-CH_3 (αMe)Val).

Z-Ala-[(αMe)Val]$_6$-OH

To a solution of Z-Ala-[(αMe)Val]$_6$-O*t*Bu (500 mg, 0.5218 mmol) in 3 ml of CH_2Cl_2, cooled to 0 °C, 3 ml of TFA were added under stirring. After one hour the solvent was evaporated and the remaining traces of TFA removed by repetitive evaporations with Et_2O. The product was recrystallized from Et_2O. Yield: 98%.

M. p.: 234-236ºC.

Rf_1: 0.60; Rf_2: 0.90; Rf_3: 0.15.

$[\alpha]_D^{20}$ = 25.3; $[\alpha]_{578}^{20}$ = 26.7 (c = 0.5, $CHCl_3$).

IR (KBr): ν_{max} 3302, 1737, 1704, 1652, 1524 cm^{-1}.

^{1}H NMR (200 MHz, $CDCl_3$): δ 7.63 (1H, NH); 7.36 (s, 7H, 5H Z-CH phenyl, 2H NH); 7.16 (s, 2H NH); 6.74 (s, 1H, NH); 5.18 – 5.05 (m, 3H, 2H Z-CH_2, 1H NH); 4.04 (m, 1H, CH Ala); 2.35 – 1.90 (m, 6H, β-CH); 1.50 – 1.35 [m, 21H, 18H α-CH_3 (αMe)Val, 3H CH_3 Ala); 1.15 – 0.80 (m, 36H, γ-CH_3 (αMe)Val).

Z-Ala-[(αMe)Val]$_6$-NH-C_6H_{10}-NH_2

A solution of Z-Ala-[(αMe)Val]$_6$-OH (414 mg, 0.4590 mmol) and EDC·HCl (132 mg, 0.6885 mmol) in acetonitrile was stirred 24 hours after that NH_2-C_6H_{10}-NH_2 (320 mg, 2.7960 mmol) was added. The reaction mixture was refluxed tree days. After that the solvent was evaporated to dryness, and the solid was redissolved in $CHCl_3$. The organic solution was washed with 5% $NaHCO_3$ and H_2O. The organic solution was dried over anhydrous Na_2SO_4 and the solvent was evaporated. Yield: 95%.

M. p.: 273-275ºC.

Rf_2: 0.90.

$[\alpha]_D^{20}$ = 9.1; $[\alpha]_{578}^{20}$ = 9.1 (c = 0.5, MeOH).

IR (KBr): ν_{max} 3316, 1703, 1656, 1524 cm^{-1}.

^{1}H NMR (600 MHz, $CDCl_3$): δ 7.51 (s, 1H, NH); 7.42 (d, 1H, NH); 7.36 (s, 5H, Z-CH phenyl); 7.32 (s, 1H, NH); 7.30 (s, 1H, NH); 7.17 (s, 1H, NH); 6.74 (s, 1H, NH); 6.69 (s, 1H, NH); 5.77 (s, 1H, NH); 5.22 – 5.08 (m, 2H, Z-CH_2); 4.02 (m, 1H, CH Ala); 3.68 (m, 1H, CH cyclohexane ring); 2.69 (m, 1H, CH cyclohexane ring); 2.12 – 1.71 (m, 14H, 6H β-CH, 8H CH_2 cyclohexane ring); 1.45 – 1.35 [m, 18H, α-CH_3 (αMe)Val); 1.25 – 1.15 (m, 3H, CH_3 Ala); 1.05 – 0.75 (m, 36H, γ-CH_3 (αMe)Val).

Z-Ala-[(αMe)Val]$_5$-NH-C$_6$H$_{10}$-NH-CO-TPP

To a solution of TPP-COOH (40 mg, 0.0607 mmol) and HATU (23 mg, 0.0607 mmol) in anhydrous CH_2Cl_2 cooled to 0°C, Z-Ala-[(αMe)Val]$_6$-NH-C$_6$H$_{10}$-NH$_2$ (73 mg, 0.0732 mmol) and NMM (8 μl, 0.0793 mmol) were added. The reaction mixture was stirred one week. Then the solvent was evaporated to dryness and the product was purified by *flash* chromatography by eluting with CH_2Cl_2/EtOH (10/0; 10/0.2; 10/0.3; 10/0.4; 10/0.5. Yield: 77%.

M. p.: 284-286ºC.

Rf_1: 0.80; Rf_2: 0.95; Rf_3: 0.40.

IR (KBr): ν_{max} 3320, 1704, 1658, 1521 cm^{-1}.

^{1}H NMR (400 MHz, $CDCl_3$): δ 8.90 – 8.76 (m, 8H, CH pyrrole); 8.32 – 8.12 (m, 10H, 8H *o*-CH phenyl, 2H *m*-CH phenyl); 7.77 (m, 9H, 3H *p*-CH phenyl, 6H *m*-CH phenyl); 7.61 (d, 1H NH); 7.52 (s, 1H, NH); 7.37 (s, 7H, 5H Z-CH phenyl, 2H NH); 7.15 (s, 1H, NH); 6.72 (s, 1H, NH); 6.61 (s, 1H, NH); 6.27 (d, 1H, NH); 5.25 – 5.05 (m, 3H, Z-CH_2, 1H NH); 4.29 – 4.00 (m, 2H, 1H CH Ala, 1H CH cyclohexane ring); 3.92 – 3.79 (m, 1H, CH cyclohexane ring); 2.36 – 1.80 (m, 14H, 6H β-CH, 8H CH_2 cyclohexane ring); 1.56 – 1.38 (m, 21H, 3H CH_3 Ala, 18H α-CH_3 (αMe)Val); 1.08 – 0.80 (m, 30H, γ-CH_3 (αMe)Val); -2.78 (s, 2H, NH pyrrole).

TPP-CO-Ala-[(αMe)Val]$_6$-NH-C$_6$H$_{10}$-NH-CO-TPP.

To a solution of TPP-COOH (25 mg, 0.0379 mmol) and HATU (15 mg, 0.0379 mmol) in anhydrous CH_2Cl_2 cooled to 0°C, (H-Ala-[(αMe)Val]$_6$-NH-C$_6$H$_{10}$-NH-CO-TPP [obtained by catalytic hydrogenation with Pd/C of the corresponding Z-derivative (67 mg, 0.0409 mmol) in a mixture CH_2Cl_2/MeOH] were dissolved in CH_2Cl_2. NMM was added (4 μl, 0.0379 mmol) and the reaction mixture was stirred two days at rt. Then the solvent was evaporated to dryness and the residue was purified by *flash* chromatography by eluting with CH_2Cl_2/EtOH (10/0; 10/0.1; 10/0.2; 10/0.3; 10/0.4; 10/0.5). Yield: 93%.

M. p.: 295-297ºC.

Rf_1: 0.85; Rf_2: 0.95; Rf_3: 0.45.

IR (KBr): ν_{max} 3316, 1655, 1520 cm^{-1}.

^{1}H NMR (400 MHz, $CDCl_3$): δ 8.90 – 8.72 (m, 16H, CH pyrrole); 8.39 – 8.10 (m, 20H, 16H *o*-CH phenyl, 4H *m*-CH phenyl); 7.81 – 7.62 (m, 20H, 6H *p*-CH phenyl, 12H *m*-CH phenyl, 2H NH); 7.58 (s, 1H, NH); 7.45 (s, 1H, NH); 7.43 (s, 1H, NH); 7.37 (s, 1H, NH); 7.21 (s, 1H, NH); 7.06 (s, 1H, NH); 6.34 (d, 1H, NH); 4.64 (m, 1H, CH Ala); 4.28 – 4.15 (m, 1H, CH cyclohexane ring); 3.95 – 3.78 (m, 1H, CH cyclohexane ring); 2.30 – 2.00 (m, 14H, 6H β-CH, 8H CH_2 cyclohexane ring); 1.55 – 1.45 (m, 18H, α-CH_3 (αMe)Val); 1.23 (m, 3H, CH_3 Ala); 1.17 – 0.96 (m, 36H, γ-CH_3 (αMe)Val); -2.79 (s, 4H, NH pyrrole).

3.2.5 Synthesis of TPP-CO-Ala-(αMe)Val-O*t*Bu

To a solution of TPP-COOH (100 mg, 0.1518 mmol) and HATU (57 mg, 0.1499 mmol) in anhydrous CH_2Cl_2 cooled to 0°C, (H-Ala-(αMe)Val-O*t*Bu [obtained by catalytic hydrogenation with Pd/C of the corresponding Z-derivative (45 mg, 0.1146 mmol) in MeOH solution] were dissolved in CH_2Cl_2. NMM was added (15 µl, 0.1499 mmol) and the reaction mixture was stirred one day at rt. Then the solvent was evaporated to dryness and the residue was purified by *flash* chromatography by eluting with CH_2Cl_2/EtOH (10/0; 10/0.2; 10/0.3). Yield: 89%.

M. p.: 136-138ºC.

Rf_1: 0.90; Rf_2: 0.95; Rf_3: 0.60.

IR (KBr): ν_{max} 3316, 1728, 1640, 1520 cm^{-1}.

^{1}H NMR (200 MHz, $CDCl_3$): δ 8.92 – 8.71 (m, 8H, CH pyrrol); 8.45 – 8.14 (m, 10H, 8H *o*-CH phenyl, 2H *m*-CH phenyl); 7.76 (m, 9H, 3H *p*-CH phenyl, 6H *m*-CH phenyl); 7.37 (d, 1H NH); 6.83 (s, 1H, NH); 4.91 (s, 1H, CH Ala); 2.34 (m, 1H, β-CH); 1.75 – 1.62 (m, 3H, α-CH_3 (αMe)Val); 1.53 (s, 9H, *t*Bu-CH_3); 1.50 (d, 3H, CH_3 Ala); 1.15 – 0.95 (m, 6H, γ-CH_3 (αMe)Val); -2.78 (s, 2H, NH pyrrol).

3.3 Synthesis of peptides for IR absorption spectroscopy studies

3.3.1 Synthesis of Ac-(Aib)$_2$-[D-(αMe)Val]$_2$-(Aib)$_2$-NH*i*Pr and its labelled analogue Ac-(Aib)$_2$-[L-(αMe)Val*]$_2$-(Aib)$_2$-NH*i*Pr.

[* indicates ^{13}C=O labeled]

Z-D-(αMe)Val-F

To a solution of Z-D-(αMe)Val-OH (1 g, 3.77 mmol) in anhydrous CH_2Cl_2, cooled to 0°C, pyridine (0.6 ml, 7.54 mmol) and cyanuric fluoride (1 g, 7.54 mmol) were added. The reaction mixture was stirred for two hours (with formation of an abundant precipitate) and then poured into a mixture of ice and water. The organic layer was separated and washed twice with cold water, dried over anhydrous Na_2SO_4, and evaporated to dryness. Oil. Yield: 85%.

Rf$_1$: 0.85; **Rf$_3$:** 0.85.

$[\alpha]_D^{20} = -2.7^o$ (c = 0.5, CH_2Cl_2).

IR (KBr): ν_{max} 3411, 3337, 1835, 1700, 1516 cm^{-1}.

^{1}H NMR (200 MHz, $CDCl_3$): δ 7.36 (m, 5H, Z-phenyl CH), 5.21 (s, 1H, NH), 5.11 (s, 2H, Z-CH_2), 1.59 (m, 1H, β-CH), 1.56 [d, 3H, β-CH_3), 1.05 – 0.95 (2d, 6H, γ-CH_3 (αMe)Val).

Z-L-(αMe)Val*-F was obtained as described above for Z-D-(αMe)Val-F.

Z-D-(αMe)Val-(Aib)$_2$-O*t*Bu

Z-D-(αMe)Val-F (668 mg, 2.52 mmol) and H-(Aib)$_2$-O*t*Bu [obtained by catalytic hydrogenation with Pd/C of the corresponding Z-derivative (1 g, 2.64 mmol) in MeOH] were dissolved in anhydrous CH_2Cl_2. Then NMM was added (280 µl, 2.54 mmol) and the reaction mixture was stirred seven days at room temperature. The solvent was evaporated, the oily residue was dissolved in EtOAc and the organic solution washed with 10% $KHSO_4$, H_2O, 5% $NaHCO_3$, and H_2O. The organic layer was dried over anhydrous Na_2SO_4 and evaporated to dryness. The product was purified by *flash*

chromatography by eluting with the mixture of PE/EtOAc (v/v 2:1) and recrystallized from EtOAc/PE. Yield: 90%.

M. p.: 141-142ºC.

Rf_1: 0.80; **Rf_2:** 0.90; **Rf_3:** 0.35.

$[\alpha]_{436}^{20}$ = -16.0; $[\alpha]_{578}^{20}$ = -8.8 (c = 0.5, MeOH).

IR (KBr): ν_{max} 3430, 3377, 3305, 1728, 1718, 1672, 1526, 1504 cm^{-1}.

^{1}H NMR (200 MHz, $CDCl_3$): δ 7.37 (s, 5H, Z- phenyl CH), 7.18 (s, 1H, NH), 6.45 (s, 1H, NH), 5.00 – 5.19 (m, 3H, 1H NH, 2H Z-CH_2), 2.02 – 2.09 (m, 1H, β-CH), 1.40 – 1.50 [m, 24H, 12H α-CH_3 Aib, 3H α-CH_3 (αMe)Val, 9H *t*Bu-CH_3), 0.91 – 0.97 (m, 6H, γ-CH_3 (αMe)Val).

Z-L-(αMe)Val*-(Aib)$_2$-O*t*Bu was prepared as described above for Z-D-(αMe)Val-(Aib)$_2$-O*t*Bu.

IR (KBr) (labelled): ν_{max} 3430, 3377, 3305, 1728, 1718, 1670, 1623, 1526, 1506 cm^{-1}.

Z-[D-(αMe)Val]$_2$-(Aib)$_2$-O*t*Bu

Z-D-(αMe)Val-F (568 mg, 2.14 mmol) and H-D-(αMe)Val-(Aib)$_2$-O*t*Bu [obtained by catalytic hydrogenation with Pd/C of the corresponding Z-derivative (1 g, 1.92 mmol) in MeOH] were dissolved in CH_2Cl_2. NMM was added (280 µl, 2.54 mmol) and the reaction mixture was stirred seven days at rt. The solvent was evaporated, the oily residue was dissolved in EtOAc and the organic solution washed with 10% $KHSO_4$, H_2O, 5% $NaHCO_3$, and H_2O. The organic layer was dried over anhydrous Na_2SO_4 and evaporated to dryness. The product was purified by *flash* chromatography by eluting with PE/EtOAc (v/v 2:1) and recrystallized from EtOAc/PE. Yield: 50%.

M. p.: 146-147ºC.

Rf_1: 0.80; **Rf_2:** 0.90; **Rf_3:** 0.30.

$[\alpha]_{436}^{20}$ = -79.8; $[\alpha]_{578}^{20}$ = -41.0 (c = 0.4, MeOH).

IR (KBr): ν_{max} 3444, 3345, 1732, 1670, 1656, 1520 cm^{-1}.

^{1}H NMR (200 MHz, $CDCl_3$): δ 7.51 (s, 1H, NH), 7.37 (s, 5H, Z- phenyl CH), 6.37 (1H, NH), 6.02 (s, 1H, NH), 5.10 (dd, 2H, Z-CH_2), 1.93 – 2.03 (m, 1H, β-CH), 1.41 – 1.50 [m, 28H, 12H 4α-CH_3 Aib, 6H 2α-CH_3 (αMe)Val, 1H β-CH, 9H *t*Bu-CH_3), 0.88 – 0.91 (m, 6H, γ-CH_3 (αMe)Val), 0.76 – 0.81 (m, 6H, γ-CH_3 (αMe)Val).

Z-[L-(αMe)Val*]$_2$-(Aib)$_2$-O*t*Bu was prepared as described above for Z-[D-(αMe)Val]$_2$-(Aib)$_2$-O*t*Bu.

IR (KBr) (labelled): ν_{max} 3443, 3345, 2980, 2934, 2878, 1732, 1705, 1656, 1631, 1527, 1513 cm^{-1}.

Z-[D-(αMe)Val]$_2$-(Aib)$_2$-OH

To a solution of Z-[D-(αMe)Val]$_2$-(Aib)$_2$-O*t*Bu (160 mg, 0.27 mmol) in 3 ml of CH_2Cl_2, cooled to 0°C, 3 ml of TFA were added under stirring. After two hours the solvent was evaporated and the remaining traces of TFA were removed by repetitive evaporations with Et_2O. The product was recristallized from Et_2O. Yield: 86%.

M. p.: 150-151ºC.

Rf$_1$: 0.50; **Rf$_2$:** 0.80; **Rf$_3$:** 0.10.

$[\alpha]_{436}^{20}$ = -87.2; $[\alpha]_{578}^{20}$ = -44.7 (c = 0.4, MeOH).

IR (KBr): ν_{max} 3434, 3322, 2980, 2940, 1740, 1702, 1663, 1523 cm^{-1}.

^{1}H NMR (200 MHz, $CDCl_3$): δ 7.61 (s, 1H, NH), 7.59 (s, 1H, NH), 7.37 (s, 5H, Z-phenyl CH), 6.38 (s, 1H, NH), 5.30 (s, 1H, NH), 5.10 (dd, 2H, Z-CH_2), 1.80 – 1.90 (m, 1H, β-CH), 1.39 – 1.56 [m, 19H, 12H α-CH_3 Aib, 6H α-CH_3 (αMe)Val, 1H β-CH), 0.97 – 1.00 (m, 6H γ-CH_3 (αMe)Val), 0.76 – 0.79 (m, 6H, γ-CH_3 (αMe)Val).

Z-[L-(αMe)Val*]$_2$-(Aib)$_2$-OH was prepared as described above for Z-[D-(αMe)Val]$_2$-(Aib)$_2$-OH.

IR (KBr) labeled: ν_{max} 3435, 3316, 2981, 2940, 1739, 1701, 1664, 1625 cm^{-1}.

Z-[D-(αMe)Val]$_2$-(Aib)$_2$-NH*i*Pr

EDC·HCl (40 mg, 0.21 mmol) was added to a suspension of Z-[D-(αMe)Val]$_2$-(Aib)$_2$-OH (115 mg, 0.21 mmol) in anhydrous CH_2Cl_2. After 1.5 hours the solution was washed with 10% $KHSO_4$ and H_2O. The organic layer was dried over anhydrous Na_2SO_4 and the organic solvent evaporated under reduced pressure. The oily product was dissolved in acetonitrile and isopropylamine (270 µl, 3.15 mmol) was added. After 1 hour the product was filtered, the solution was evaporated to dryness and the rest of

the product was purified by *flash* chromatography by eluting with step-gradient mixtures of $CHCl_3$/EtOH (v/v 10:0, 10:0.5, 10:1, 10:2). Yield: 85%.

M. p.: 235-237ºC.

Rf_1: 0.70; **Rf_2:** 0.90; **Rf_3:** 0.30.

$[\alpha]_{436}^{20}$ = -109.0; $[\alpha]_{578}^{20}$ = -55.7 (c = 0.4, MeOH).

IR (KBr): ν_{max} 3430, 3328, 1700, 1671, 1644, 1530 cm^{-1}.

^{1}H NMR (200 MHz, $CDCl_3$): δ 7.39 (s, 1H NH), 7.30 (s, 5H Z-phenyl CH), 7.19 (s, 1H NH), 7.13 (d, 1H NH), 6.25 (1H NH), 5.18 (s, 1H NH), 5.03 (dd, 2H Z-CH_2), 3.95 (m, 1H CH *i*Pr), 1.77 – 1.82 (m, 1H β-CH), 1.65 (s, 1H β-CH), 1.34 – 1.42 [m, 18H; 12H 4α-CH_3 Aib, 6H 2α-CH_3 (αMe)Val), 1.06 – 1.13 (m, 6H 2CH_3 *i*Pr), 0.89 – 0.91 (m, 6H 2γ-CH_3 (αMe)Val), 0.68 – 0.75 (m, 6H 2γ-CH_3 (αMe)Val).

Z-[L-(αMe)Val*]$_2$-(Aib)$_2$-NH*i*Pr was prepared as described above for Z-[D-(αMe)Val]$_2$-(Aib)$_2$-NH*i*Pr.

IR (KBr) (labelled) ν_{max} 3430, 3329, 2975, 2938, 1700, 1675, 1646, 1628, 1530 cm^{-1}.

Ac-(Aib)$_2$-OH

H-(Aib)$_2$-O*t*Bu [obtained by catalytic hydrogenation with Pd/C of the corresponding Z-derivative (150 mg, 0.40 mmol) in MeOH] was dissolved in the 3 ml of anhydrous CH_2Cl_2, 3 ml of Ac_2O were added under stirring. After 1 hour the solvent was evaporated, the rest was dissolved in the mixture of TFA/ CH_2Cl_2 (v/v 1:1) under cooling at 0°C. After 1 hour the solvent was evaporated and the remaining traces of TFA removed by repetitive evaporations with Et_2O. Yield: 95%.

M. p.: 141-142ºC.

Rf_1: 0.10; **Rf_2:** 0.55.

IR (KBr): ν_{max} 3390, 1714, 1662, 1627, 1559 cm^{-1}.

^{1}H NMR (200 MHz, DMSO): δ 7.18 (s, 1H, NH), 7.51 (s, 1H, NH), 1.81 (s, 3H, CH_3 acetyl), 1.30 – 1.32 (m, 12H, α-CH_3 Aib).

Ac-(Aib)$_2$-[D-(αMe)Val]$_2$-(Aib)$_2$-NH*i*Pr

EDC·HCl (40 mg, 0.20 mmol) was added to a suspension of Ac-$(Aib)_2$-OH (45 mg, 0.20 mmol) in anhydrous CH_2Cl_2. After 2 hours the solution was washed with 10% $KHSO_4$ and H_2O. The organic layer was dried over anhydrous Na_2SO_4 and the organic solvent was evaporated under reduced pressure. The oily product was dissolved in acetonitrile and H-[D-(αMe)Val]$_2$-$(Aib)_2$-NH*i*Pr [obtained by catalytic hydrogenation with Pd/C of the corresponding Z-derivative (58 mg, 0.10 mmol) in MeOH] was added. The reaction mixture was heated at 80°C for 3 days. Then the solvent was evaporated to dryness and the product was purified by *flash* chromatography by eluting with step-gradient mixtures of $CHCl_3$/EtOH (10:0, 10:2) and semi-preparative RP-HPLC (C_4 Vydac column, flow 2.5 ml/min, eluent A – 10% acetonitrile in water with 0.05% of TFA, eluent B – 90% acetonitrile in water with 0.05% TFA, gradient from 10 to 60% of eluent B in 20 min, t_r = 21.73 min) and lyophylized. Yield: 10%.

Rf_1: 0.40; **Rf_2:** 0.75; **Rf_3:** 0.05.

$[\alpha]_{436}^{20}$ = -17.9; $[\alpha]_{578}^{20}$ = -10.0 (c = 0.2, MeOH).

IR (KBr): ν_{max} 3437, 3319, 1656, 1532 cm^{-1}.

^{1}H NMR (200 MHz, $CDCl_3$): δ 7.59 (s, 1H, NH), 7.58 (s, 1H, NH), 7.45 (d, 1H, NH), 7.30 (s, 1H, NH), 7.19 (s, 1H, NH), 6.65 – 6.66 (m, 2H, NH), 4.02 (m, 1H, CH *i*Pr), 2.02 – 2.17 (m, 5H, 2H β-CH, 3H CH_3 acetyl), 1.25 – 1.49 [m, 30H, 24H α-CH_3 Aib, 6H α-CH_3 (αMe)Val), 1.04 – 1.23 (m, 6H, CH_3 *i*Pr), 0.99 – 1.04 (m, 6H, γ-CH_3 (αMe)Val), 0.92 – 1.00 (m, 6H, γ-CH_3 (αMe)Val).

Mass spectrometry (ESI-TOF): $[M+H]^+_{calc}$ = 668.90; $[M+H]^+_{exp}$ = 668.47.

Ac-$(Aib)_2$-[L-(αMe)Val*]$_2$-$(Aib)_2$-NH*i*Pr was prepared as described above for Ac-$(Aib)_2$-[D-(αMe)Val]$_2$-$(Aib)_2$-NH*i*Pr.

IR (KBr) (labelled): ν_{max} 3434, 3316, 2976, 2931, 1656, 1622, 1524 cm^{-1}.

Mass spectrometry (ESI-TOF): $[M+H]^+_{calc}$ = 670.90; $[M+H]^+_{exp}$ = 670.47.

3.3.2 Synthesis of Ac-D-[(αMe)Val]$_2$-(Aib)$_4$-NH*i*Pr and its labelled analogue Ac*-L-(αMe)Val*-L-(αMe)Val-(Aib)$_4$-NH*i*Pr

Z-D-(αMe)Val-(Aib)$_4$-O*t*Bu

Z-D-(αMe)Val-F (243 mg, 0.91 mmol) and H-(Aib)$_4$-O*t*Bu [obtained by catalytic hydrogenation with Pd/C of the corresponding Z-derivative (500 mg, 0.91 mmol) in MeOH] were dissolved in anhydrous CH_2Cl_2, cooled to 0°C. Then NMM (100 µl, 0.91 mmol) was added. The reaction mixture was stirred 6 days at room temperature. During this period another 114 mg (0.43 mmol) of Z-D-(αMe)Val-F were added. Then the solvent was evaporated, the oily residue was dissolved in EtOAc and the organic solution washed with 10% $KHSO_4$, H_2O, 5% $NaHCO_3$, and H_2O. The organic layer was dried over anhydrous Na_2SO_4 and evaporated to dryness. The product was purified by *flash* chromatography by eluting with the mixture of PE/EtOAc (v/v 10:1, 6:1, 4:1) and recrystallized from EtOAc. Yield: 63%.

M. p.: 217-218ºC.

Rf$_1$ = 0.60; **Rf$_2$** = 0.95; **Rf$_3$** = 0.30.

$[\alpha]_D^{20}$ = -31.3; $[\alpha]_{578}^{20}$ = -30.7 (c = 0.6, MeOH).

IR (KBr): ν_{max} 3429, 3327, 1728, 1703, 1667, 1530 cm^{-1}.

^{1}H NMR ($CDCl_3$, 200 MHz): δ 7.50 – 7.22 (m, 8H, 5H Z-phenyl CH, 3H NH); 6.24 (s, 1H, NH); 5.25 – 4.98 (m, 3H, 2H Z-CH_2, 1H NH); 2.00 – 1.85 [m, 1H, β-CH (αMe)Val)]; 1.55 – 1.38 [m, 33H, 24H CH_3 Aib, 9H CH_3 *t*Bu]; 1.21 (s, 3H, α-CH_3 (αMe)Val]; 1.05 – 0.93 [m, 6H, γ-CH_3 (αMe)Val].

Z-L-(αMe)Val-(Aib)$_4$-O*t*Bu was prepared as described above for Z-D-(αMe)Val-(Aib)$_4$-O*t*Bu.

Z-[D-(αMe)Val]$_2$-(Aib)$_4$-O*t*Bu

Z-D-(αMe)Val-F (124 mg, 0.46 mmol), H-D-(αMe)Val-(Aib)$_4$-O*t*Bu [obtained by catalytic hydrogenation with Pd/C of the corresponding Z-derivative (300 mg, 0.45 mmol) in MeOH] and NMM (50 µl, 0.46 mmol) were dissolved in anhydrous CH_2Cl_2 cooled to 0°C. The reaction mixture was stirred 10 days at room temperature. Then the solvent was evaporated, the oily residue was dissolved in EtOAc and the organic solution washed with 10% $KHSO_4$, H_2O, 5% $NaHCO_3$, and H_2O. The organic

layer was dried over anhydrous Na_2SO_4 and evaporated to dryness. The product was purified by *flash* chromatography by eluting with the mixture of PE/EtOAc (v/v 10:1, 5:1, 3:1, 2:1) and recrystallized from EtOAc. Yield: 70%.

M. p.: 176-177ºC.

Rf_1 = 0.50; **Rf_2** = 0.95; **Rf_3** = 0.35.

$[\alpha]_D^{20}$ = -44.9 (c = 0.6, MeOH).

IR (KBr): ν_{max} 3442, 2939, 1736, 1706, 1664, 1529 cm^{-1}.

^{1}H NMR ($CDCl_3$, 200 MHz): δ 7.75 (s, 1H, NH); 7.67 (s, 1H, NH); 7.45 (s, 1H, NH); 7.37 (s, 5H, Z-phenyl CH); 6.40 (s, 1H, NH); 5.87 (s, 1H, NH); 5.22 – 4.98 (m, 3H, 2H Z-CH_2, 1H NH); 2.05 – 1.85 [m, 2H, β-CH (αMe)Val)]; 1.55 – 1.38 [m, 39H, 24H CH_3 Aib, 9H CH_3 *t*Bu, 6H α-CH_3 (αMe)Val]; 1.05 – 0.93 [m, 6H, γ-CH_3 (αMe)Val]; 0.82 – 0.71 [m, 6H, γ-CH_3 (αMe)Val].

Z-L-(αMe)Val*-L-(αMe)Val-(Aib)$_4$-O*t*Bu was prepared as described above for Z-[D-(αMe)Val]$_2$-(Aib)$_4$-O*t*Bu.

IR (KBr) (labelled): ν_{max} 3441, 3329, 1735, 1703, 1664, 1529 cm^{-1}.

Z-[D-(αMe)Val]$_2$-(Aib)$_4$-OH

To a solution of Z-[D-(αMe)Val]$_2$-(Aib)$_4$-O*t*Bu (221 mg, 0.29 mmol) in 5 ml of CH_2Cl_2, cooled to 0°C, 5 ml of TFA were added under stirring. After one hour the solvent was evaporated and the remaining traces of TFA were removed by repetitive evaporations with Et_2O. The product was recristallized from Et_2O. Yield: 97%.

M. p.: 216-217ºC.

Rf_1 = 0.30; **Rf_2** = 0.95; **Rf_3** = 0.15.

$[\alpha]_D^{20}$ = -41.3; $[\alpha]_{578}^{20}$ = -39.7 (c = 0.4, MeOH).

IR (KBr): 3437, 3306, 1742, 1699, 1657, 1533 cm^{-1}.

^{1}H NMR ($CDCl_3$, 200 MHz): δ 8.03 (s, 1H, NH); 7.96 (s, 1H, NH); 7.84 (s, 1H, NH); 7.67 (s, 1H, NH); 7.37 (s, 5H, Z-phenyl CH); 6.53 (s, 1H, NH); 5.69 (s, 1H, NH); 5.22 – 4.98 (m, 2H, Z-CH_2); 2.00 – 1.85 [m, 1H, β-CH (αMe)Val)]; 1.58 – 1.38 [m, 31H, 24H CH_3 Aib, 6H α-CH_3 (αMe)Val), 1H β-CH (αMe)Val]; 1.05 – 0.93 [m, 6H, γ-CH_3 (αMe)Val]; 0.85 – 0.71 [m, 6H, γ-CH_3 (αMe)Val].

Z-L-(αMe)Val*-D-(αMe)Val-(Aib)$_4$-OH was prepared as described above for Z-[D-(αMe)Val]$_2$-(Aib)$_4$-OH.

IR (KBr) labeled: ν_{max} 3435, 3312, 2982, 2940, 1701, 1659, 1530 cm^{-1}.

Z-[D-(αMe)Val]$_2$-(Aib)$_4$-NH*i*Pr.

EDC·HCl (80 mg, 0.41 mmol) was added to a suspension of Z-[D-(αMe)Val]$_2$-(Aib)$_4$-OH (115 mg, 0.21 mmol) in anhydrous CH_2Cl_2. After 2 hours the solution was washed with 10% $KHSO_4$ and H_2O. The organic layer was dried over anhydrous Na_2SO_4 and the organic solvent evaporated under reduced pressure. The oily product was dissolved in acetonitrile and *i*Pr-NH_2 (215 µl, 2.51 mmol) and the reaction mixture was refluxed during one day. Since the oxazolone seemed to be hydrolysed (TLC), the solvent was evaporated, the oily residue was dissolved in CH_2Cl_2 and another 50 mg of EDC·HCl were added. The solution was washed with 10% $KHSO_4$ and H_2O, the organic layer was dried over anhydrous Na_2SO_4 and the organic solvent was evaporated under reduced pressure. The residue was dissolved in *i*Pr-NH_2 and the reaction mixture was refluxed two days. Then the solution was evaporated and the product was purified by *flash* chromatography by eluting with step-gradient mixtures of PE/EtOAc (v/v 10:1, 5:1, 3:1, 2:1). Yield: 35%.

M. p.: 241-243ºC.

Rf$_1$ = 0.70; **Rf$_2$** = 0.90; **Rf$_3$** = 0.25.

$[\alpha]_D^{20}$ = -51.9; $[\alpha]_{578}^{20}$ = -50.8 (c = 0.5, MeOH).

IR (KBr): 3428, 3372, 3328, 2980, 2939, 1697, 1663, 1531 cm^{-1}.

^{1}H NMR ($CDCl_3$, 200 MHz): δ 7.66 (s, 1H, NH); 7.62 (s, 1H, NH); 7.49 (s, 1H, NH); 7.30 (s, 5H, Z-phenyl CH); 7.24 (s, 1H, NH); 7.19 (s, 1H, NH); 6.31 (s, 1H, NH); 5.35 (s, 1H, NH); 5.22 – 4.95 (m, 2H, Z-CH_2); 4.05 – 3.85 (m, 1H, CH *i*Pr); 1.92 – 1.62 [m, 2H, β-CH (αMe)Val)]; 1.45 – 1.30 [m, 30H, 24H CH_3 Aib, 6H α-CH_3 (αMe)Val)]; 1.18 – 1.08 (m, 6H, CH_3 *i*Pr); 0.98 – 0.85 [m, 6H, γ-CH_3 (αMe)Val]; 0.78 – 0.65 [m, 6H, γ-CH_3 (αMe)Val].

Z-L-(αMe)Val*-L-(αMe)Val-(Aib)$_4$-NH*i*Pr was prepared as described above for Z-[D-(αMe)Val]$_2$-(Aib)$_4$-NH*i*Pr.

IR (KBr) (labelled): ν_{max} 3428, 3323, 2980, 2939, 1697, 1662, 1625, 1530 cm^{-1}.

Ac-[D-(αMe)Val]$_2$-(Aib)$_4$-NH*i*Pr

H-[D-(αMe)Val]$_2$-(Aib)$_4$-NH*i*Pr [obtained by catalytic hydrogenation with Pd/C of the corresponding Z-derivative (60 mg, 0.08 mmol) in MeOH] was dissolved in the 3 ml of

anhydrous CH_2Cl_2 and 3 ml of Ac_2O were added under stirring. After 1 hour the solvent was evaporated, the product was recrystallized from EtOAc. Yield: 80%.

Rf_1 = 0.40; **Rf_2** = 0.75; **Rf_3** = 0.10.

$[\alpha]_D^{20}$ = -48.9; $[\alpha]_{578}^{20}$ = -37.8 (c = 0.1, MeOH).

IR (KBr): 3446, 3303, 1658, 1534 cm^{-1}.

^{1}H NMR ($CDCl_3$, 400 MHz): δ 7.68 (s, 1H, NH); 7.64 (s, 1H, NH); 7.62 (s, 1H, NH); 7.26 (s, 1H, NH); 7.14 (d, 1H, NH); 6.22 (s, 1H, NH); 5.85 (s, 1H, NH); 4.05 – 3.85 (m, 1H, CH *i*Pr); 2.04 (s, 3H, CH_3 acetyl); 1.89 – 1.75 [m, 2H, β-CH (αMe)Val)]; 1.51 – 1.35 [m, 30H, 24H CH_3 Aib, 6H α-CH_3 (αMe)Val)]; 1.21 – 1.10 (m, 6H, CH_3 *i*Pr); 0.98 – 0 .85 [m, 12H, γ-CH_3 (αMe)Val].

Mass spectrometry (ESI-TOF): $[M+H]^+_{calc}$ = 668.90; $[M+H]^+_{exp}$ = 668.47.

Ac*-L-(αMe)Val*-L-(αMe)Val-(Aib)$_4$-NH*i*Pr was prepared as described above for Ac-[D-(αMe)Val]$_2$-(Aib)$_4$-NH*i*Pr.

IR (KBr) (labelled): ν_{max} 3446, 3301, 1660, 1626, 1534 cm^{-1}.

Mass spectrometry (ESI-TOF): $[M+H]^+_{calc}$ = 670.90; $[M+H]^+_{exp}$ = 670.49.

3.3.3 Synthesis of Ac-(Aib)$_4$-D-[(αMe)Val]$_2$-NH*i*Pr and its labelled analogue Ac-(Aib)$_4$-[L-(αMe)Val*]$_2$-NH*i*Pr

Z-[D-(αMe)Val]$_2$-O*t*Bu

Z-D-(αMe)Val-F (722 mg, 2.70 mmol) and H-D-(αMe)Val-O*t*Bu [obtained by catalytic hydrogenation with Pd/C of the corresponding Z-derivative (800 mg, 2.49 mmol) in MeOH] were dissolved in anhydrous CH_2Cl_2, cooled to 0°C. Then NMM (300 µl, 2.70 mmol) was added. The reaction mixture was stirred 6 days at room temperature. During this period another 342 mg (1.28 mmol) of Z-D-(αMe)Val-F were added. Then the solvent was evaporated, the oily residue was dissolved in EtOAc and the organic solution washed with 10% $KHSO_4$, H_2O, 5% $NaHCO_3$, and H_2O. The organic layer was dried over anhydrous Na_2SO_4 and evaporated to dryness. The product was purified by *flash* chromatography by eluting with the mixture of PE/EtOAc (v/v 15:1, 12:1, 10:1, 7:1). Yield: 61%.

M. p.: 91-92ºC.

Rf_1 = 0.95; **Rf_2** = 0.95; **Rf_3** = 0.70.

$[\alpha]_D^{20}$ = -15.6; $[\alpha]_{578}^{20}$ = -14.2 (c = 0.4, MeOH).

IR (KBr): 3315, 3033, 2971, 1721, 1701, 1673, 1509 cm^{-1}.

^{1}H NMR ($CDCl_3$, 200 MHz): δ 7.35 (s, 5H, Z-phenyl CH); 7.22 (s, 1H, NH); 5.28 (s, 1H, NH); 5.15 – 5.00 (m, 2H, Z-CH_2); 2.55 – 2.31 [m, 1H, β-CH (αMe)Val)]; 2.31 – 2.14 [m, 1H, β-CH (αMe)Val)]; 1.55 – 1.45 [m, 15H, 6H α-CH_3 (αMe)Val, 9H CH_3 *t*Bu]; 1.02 – 0.88 (m, 12H, γ-CH_3 (αMe)Val].

Z-[L-(αMe)Val*]$_2$-O*t*Bu was prepared as described above for Z-[D-(αMe)Val]$_2$-O*t*Bu.

IR (KBr) (labelled): ν_{max} 3390, 3304, 2976, 2876, 1721, 1679, 1617 cm^{-1}.

Z-Aib-[D-(αMe)Val]$_2$-O*t*Bu

To a solution of Z-Aib-OH (436 mg, 1.84 mmol), HOAt (250 mg, 1.84 mmol) and EDC·HCl (352 mg, 1.84 mmol) in anhydrous CH_2Cl_2 cooled to 0°C, H-[D-(αMe)Val]$_2$-O*t*Bu [obtained by catalytic hydrogenation with Pd/C of the corresponding Z-derivative (532 mg, 1.22 mmol) in MeOH] and NMM (200 µl, 1.84 mmol) were added. The reaction mixture was stirred 10 days at room temperature. Then the solvent was evaporated, the oily residue was dissolved in EtOAc and the organic solution washed with 10% $KHSO_4$, H_2O, 5% $NaHCO_3$, and H_2O. The organic layer was dried over anhydrous Na_2SO_4 and evaporated to dryness. The product was purified by *flash* chromatography by eluting with the mixture of PE/EtOAc (v/v 12:1, 10:1, 7:1, 4:1, 2:1). Yield: 55%.

M. p.: 102-103 ºC.

Rf_1 = 0.70; **Rf_2** = 0.95; **Rf_3** = 0.50.

$[\alpha]_D^{20}$ = -6.9; $[\alpha]_{578}^{20}$ = -5.3 (c = 0.6, MeOH).

IR (KBr): 3420, 3373, 1725, 1709, 1641, 1537 cm^{-1}.

^{1}H NMR ($CDCl_3$, 200 MHz): δ 7.32 (s, 5H, Z-phenyl CH); 6.75 (s, 1H, NH); 6.15 (s, 1H, NH); 5.15 – 4.95 (m, 3H, 2H Z-CH_2, 1H NH); 2.35 – 2.12 [m, 2H, β-CH (αMe)Val)]; 1.55 – 1.48 [m, 21H, 6H α-CH_3 (αMe)Val, 9H CH_3 *t*Bu, 6H CH_3 Aib]; 1.05 – 0.75 (m, 12H, γ-CH_3 (αMe)Val].

Z-Aib-[L-(αMe)Val*]$_2$-O*t*Bu was prepared as described above for Z-Aib-[D-(αMe)Val]$_2$-O*t*Bu.

IR (KBr) (labelled): ν_{max} 3420, 3373, 1709, 1695, 1682, 1601, 1527 cm^{-1}.

Z-(Aib)$_4$-[D-(αMe)Val]$_2$-O*t*Bu

To a solution of Z-(Aib)$_3$-O*t*Bu (400 mg, 0.86 mmol) in 5 ml of CH_2Cl_2, cooled to 0°C, 5 ml of TFA were added under stirring. After one hour the solvent was evaporated and the remaining traces of TFA were removed by repetitive evaporations with Et_2O. The residue was dissolved in CH_2Cl_2, and EDC·HCl (252 mg, 1.31 mmol) was added. After stirring during 1.5 hours the solution was washed with 10% $KHSO_4$, H_2O, 5% $NaHCO_3$, and H_2O. The organic layer was dried over anhydrous Na_2SO_4 and evaporated to dryness. Then the residue was dissolved in anhydrous acetonitrile and H-Aib-[D-(αMe)Val]$_2$-O*t*Bu [obtained by catalytic hydrogenation with Pd/C of the corresponding Z-derivative (330 mg, 0.64 mmol) in MeOH]. The reaction mixture was refluxed 8 days. Then the solvent was evaporated and the product was purified by *flash* chromatography by eluting with the mixture of PE/EtOAc (v/v 2:1, 1:1). Yield: 67%.

M. p.: 175-177ºC.

Rf$_1$ = 0.55; **Rf$_2$** = 0.90; **Rf$_3$** = 0.35.

$[\alpha]_D^{20}$ = -5.7; $[\alpha]_{578}^{20}$ = -4.1 (c = 0.6, MeOH).

IR (KBr): ν_{max} 3428, 3330, 1701, 1669, 1527 cm^{-1}.

^{1}H NMR ($CDCl_3$, 200 MHz): δ 7.53 (s, 1H, NH); 7.36 (s, 7H, 5H Z-phenyl CH, 2H NH); 7.05 (s, 1H, NH); 6.64 (s, 1H, NH); 6.22 (s, 1H, NH); 5.22 – 4.98 (m, 2H, Z-CH_2); 2.37 – 2.18 [m, 2H, β-CH (αMe)Val)]; 1.55 – 1.28 [m, 39H, 24H CH_3 Aib, 9H CH_3 *t*Bu, 6H α-CH_3 (αMe)Val]; 1.05 – 0.96 [m, 12H, γ-CH_3 (αMe)Val].

Z-(Aib)$_4$-[L-(αMe)Val*]$_2$-O*t*Bu was prepared as described above for Z-(Aib)$_4$-[D-(αMe)Val]$_2$-O*t*Bu.

IR (KBr) (labelled): ν_{max} 3428, 3332, 2982, 2938, 1668, 1526 cm^{-1}.

Z-(Aib)$_4$-[D-(αMe)Val]$_2$-OH

To a solution of Z-(Aib)$_4$-[D-(αMe)Val]$_2$-O*t*Bu (271 mg, 0.35 mmol) in 5 ml of CH_2Cl_2, cooled to 0°C, 5 ml of TFA were added under stirring. After two hours the solvent was evaporated and the remaining traces of TFA were removed by repetitive evaporations with Et_2O. The product was recristallized from Et_2O. Yield: 86%.

M. p.: 216-217ºC.

Rf$_1$ = 0.35; **Rf$_2$** = 0.30; **Rf$_3$** = 0.95.

$[\alpha]_D^{20}$ = -14.2; $[\alpha]_{578}^{20}$ = -12.5 (c = 0.5, MeOH).

IR (KBr): ν_{max} 3426, 3317, 1732, 1705, 1666, 1526, 1507 cm^{-1}.

^{1}H NMR ($CDCl_3$, 200 MHz): δ 7.68 (s, 1H, NH); 7.36 (s, 7H, 5H Z-phenyl CH, 2H NH); 6.79 (s, 1H, NH); 5.93 (s, 1H, NH); 5.22 – 4.98 (m, 3H, 2H Z-CH_2, 1H NH); 2.45 – 2.28 [m, 1H, β-CH (αMe)Val)]; 2.18 – 2.01 [m, 1H, β-CH (αMe)Val)]; 1.55 – 1.32 [m, 30H, 24H CH_3 Aib, 6H α-CH_3 (αMe)Val]; 1.10 – 0.94 [m, 12H, γ-CH_3 (αMe)Val].

Z-(Aib)$_4$-[L-(αMe)Val*]$_2$-OH was prepared as described above for Z-(Aib)$_4$-[D-(αMe)Val]$_2$-OH.

IR (KBr) (labelled): ν_{max} 3428, 3323, 2980, 2939, 1697, 1662, 1625, 1530 cm^{-1}.

Z-(Aib)$_4$-[D-(αMe)Val]$_2$-NH*i*Pr

EDC·HCl (100 mg, 0.53 mmol) was added to a suspension of Z-(Aib)$_4$-[D-(αMe)Val]$_2$-OH (250 mg, 0.35 mmol) in anhydrous CH_2Cl_2. After 1.5 hours the solution was washed with 10% $KHSO_4$ and H_2O. The organic layer was dried over anhydrous Na_2SO_4 and the organic solvent evaporated under reduced pressure. The oily product was dissolved in *i*Pr-NH_2 and the reaction mixture was refluxed during one day. The solution was washed with 10% $KHSO_4$ and H_2O, the organic layer was dried over anhydrous Na_2SO_4 and the organic solvent was evaporated under reduced pressure. The residue was dissolved in *i*Pr-NH_2 and the reaction mixture was refluxed two days. Then the solution was evaporated and the product was purified by *flash* chromatography by eluting with step-gradient mixtures of PE/EtOAc (v/v 10:1, 3:1, 2:1, 1:1) and recrystallized from EtOAc/PE. Yield: 32%.

M. p.: 210-212ºC.

Rf_1 = 0.70; **Rf_2** = 0.95; **Rf_3** = 0.35.

$[\alpha]_D^{20}$ = -26.0; $[\alpha]_{578}^{20}$ = -24.8 (c = 0.2, MeOH).

IR (KBr): ν_{max} 3428, 3327, 1705, 1663, 1527 cm^{-1}.

^{1}H NMR ($CDCl_3$, 200 MHz): δ 7.56 (s, 1H, NH); 7.37 (s, 6H, 5H Z-phenyl CH, 1H NH); 7.24 (s, 1H, NH); 7.19 (s, 1H, NH); 7.02 (s, 1H, NH); 6.57 (d, 1H, NH); 5.22-4.95 (m, 3H, 2H Z-CH_2, 1H NH); 4.05 – 3.89 (m, 1H, CH *i*Pr); 2.12 – 1.98 [m, 1H, β-CH (αMe)Val)]; 1.95 – 1.80 [m, 1H, β-CH (αMe)Val)]; 1.45 – 1.30 [m, 30H, 24H CH_3 Aib, 6H α-CH_3 (αMe)Val)]; 1.22 – 1.30 (m, 6H, CH_3 *i*Pr); 1.03 – 0.85 [m, 12H, γ-CH_3 (αMe)Val].

Z-(Aib)$_4$-[L-(αMe)Val*]$_2$-NH*i*Pr was prepared as described above for Z-(Aib)$_4$-[D-(αMe)Val]$_2$-NH*i*Pr.

IR (KBr) (labelled): ν_{max} 3428, 3325, 1704, 1665, 1527 cm^{-1}.

Ac-(Aib)$_4$-[D-(αMe)Val]$_2$-NH*i*Pr

H-(Aib)$_4$-[D-(αMe)Val]$_2$-NH*i*Pr [obtained by catalytic hydrogenation with Pd/C of the corresponding Z-derivative (50 mg, 0.07 mmol) in MeOH] was dissolved in the 3 ml of anhydrous CH_2Cl_2. Then 3 ml of Ac_2O were added under stirring. After 1 hour the solvent was evaporated, the product was purified by semi-preparative RP-HPLC (C_4 Vydac column, flow 2.5 ml/min, eluent A – 10% acetonitrile in water with 0.05% of TFA, eluent B – 90% acetonitrile in water with 0.05% TFA, gradient from 10 to 60% of eluent B in 30 min, t_r = 17.73 min) and lyophylized. Yield: 23%.

Rf$_1$ = 0.20; **Rf$_2$** = 0.80; **Rf$_3$** = 0.05.

$[\alpha]_D^{20}$ = -18.9; $[\alpha]_{578}^{20}$ = -11.8 (c = 0.2, MeOH).

IR (KBr): ν_{max} 3434, 3310, 1657, 1530 cm^{-1}.

^{1}H NMR ($CDCl_3$, 400 MHz): δ 7.50 (s, 1H, NH); 7.45 (s, 1H, NH); 7.19 (s, 2H, NH); 6.99 (s, 1H, NH); 6.37 (s, 1H, NH); 6.16 (s, 1H, NH); 4.05 – 3.92 (m, 1H, CH *i*Pr); 2.09 – 1.95 [m, 5H, 3H CH_3 Ac, 2H β-CH (αMe)Val)]; 1.48 – 1.27 [m, 30H, 24H CH_3 Aib, 6H α-CH_3 (αMe)Val)]; 1.21 – 1.13 (m, 6H, CH_3 *i*Pr); 0.98 – 0.85 [m, 12H, γ-CH_3 (αMe)Val].

Mass spectrometry (ESI-TOF): $[M+H]^+_{calc}$ = 668.90; $[M+H]^+_{exp}$ = 668.47.

Ac-Aib$_4$-[L-(αMe)Val]$_2$-NH*i*Pr was prepared as described above for Ac-(Aib)$_4$-[D-(αMe)Val]$_2$-NH*i*Pr.

IR (KBr) (labelled): ν_{max} 3435, 3310, 1663, 1622, 1529 cm^{-1}.

Mass spectrometry (ESI-TOF): $[M+H]^+_{calc}$ = 670.90; $[M+H]^+_{exp}$ = 670.48.

3.4 Synthesis of hhMag containing peptides for RCM experiments

3.4.1 Synthesis of Boc-hhMag-(Aib)$_2$-hhMag-Aib-OMe

Boc-hhMag-Aib-OMe

To a solution of Boc-hhMag-OH (500 mg, 1.94 mmol), HOAt (284 mg, 2.09 mmol) and EDC·HCl (400 mg, 2.09 mmol) in anhydrous CH_2Cl_2 cooled to 0^{o}C, HCl·H-Aib-OMe (400 mg, 2.60 mmol) and NMM (510 µl, 5.50 mmol) were added. The reaction mixture was stirred 5 days at rt. Then the solvent was evaporated, the oily residue was dissolved in EtOAc and the organic solution washed with 10% $KHSO_4$, H_2O, 5% $NaHCO_3$, and H_2O. The organic layer was dried over anhydrous Na_2SO_4 and evaporated to dryness. The product was purified by *flash* chromatography by eluting with step-gradient mixtures of PE/EtOAc (v/v 5:1, 4:1, 3:1). Yield: 51%.

M. p.: 87-88ºC.

IR (KBr): 3382, 3327, 3302, 1728, 1709, 1657, 1515 cm^{-1}.

^{1}H NMR ($CDCl_3$, 200 MHz): δ 6.93 (s, 1H, NH); 5.81 (m, 1H, ε-CH hhMag); 5.17 (s, 1H, NH); 5.12 – 4.95 (m, 2H, ζ-CH_2 hhMag); 3.76 (s, 3H, OCH_3); 2.22 – 1.71 (m, 6H, β-, γ-, δ-CH_2 hhMag); 1.65 – 1.41 (m, 18H, 6H CH_3 Aib, 3H CH_3 hhMag, 9H *t*Bu Boc).

Boc-Aib-hhMag-Aib-OMe

To a solution of Boc-Aib-OH (305 mg, 1.50 mmol), HOAt (220 mg, 1.62 mmol) and EDC·HCl (310 mg, 1.62 mmol) in anhydrous CH_2Cl_2 cooled to 0^{o}C, TFA·H-hhMag-Aib-OMe [obtained by the Boc-deprotection of Boc-hhMag-Aib-OMe (340 mg, 0.95 mmol) with 30% solution of TFA in CH_2Cl_2] and DIEA (400 µl, 2.45 mmol) were added. The reaction mixture was stirred 3 days at rt. Then the solvent was evaporated, the oily residue was dissolved in EtOAc and the organic solution washed with 10% $KHSO_4$, H_2O, 5% $NaHCO_3$, and H_2O. The organic layer was dried over anhydrous Na_2SO_4 and evaporated to dryness. The product was recrystallized from EtOAc/PE. Yield: 78%.

M. p.: 135-137ºC.

IR (KBr): 3376, 3305, 1728, 1689, 1660, 1529 cm^{-1}.

^{1}H NMR ($CDCl_3$, 200 MHz): δ 7.38 (s, 1H, NH); 6.53 (s, 1H, NH); 5.82 (m, 1H, ε-CH hhMag); 5.04 (s, 1H, NH); 5.01 – 4.90 (m, 2H, ζ-CH_2 hhMag); 3.69 (s, 3H, OCH_3); 2.12 – 1.65 (m, 6H, β-, γ-, δ-CH_2 hhMag); 1.59 – 1.39 (m, 24H, 12H CH_3 Aib, 3H CH_3 hhMag, 9H *t*Bu Boc).

Boc-$(Aib)_2$-hhMag-Aib-OMe

To a solution of Boc-Aib-OH (275 mg, 1.35 mmol), HOAt (220 mg, 1.62 mmol) and EDC·HCl (310 mg, 1.62 mmol) in anhydrous CH_2Cl_2 cooled to 0°C, TFA·H-Aib-hhMag-Aib-OMe [obtained by the Boc-deprotection of Boc-Aib-hhMag-Aib-OMe (320 mg, 0.90 mmol) with 30% solution of TFA in CH_2Cl_2] and DIEA (415 µl, 2.54 mmol) were added. The reaction mixture was stirred 5 days at rt. Then the solvent was evaporated, the oily residue was dissolved in EtOAc and the organic solution washed with 10% $KHSO_4$, H_2O, 5% $NaHCO_3$, and H_2O. The organic layer was dried over anhydrous Na_2SO_4 and evaporated to dryness. The product was purified by *flash* chromatography by eluting with CH_2Cl_2, then with the mixture of CH_2Cl_2/EtOH (v/v 10:0.1). Yield: 50%.

M. p.: 168-170ºC.

IR (KBr): 3329, 2984, 2940, 1734, 1687, 1527 cm^{-1}.

^{1}H NMR ($CDCl_3$, 200 MHz): δ 7.29 (s, 2H, NH); 6.53 (s, 1H, NH); 5.78 (m, 1H, ε-CH hhMag); 5.02 (s, 1H, NH); 4.98 – 4.87 (m, 2H, ζ-CH_2 hhMag); 3.69 (s, 3H, OCH_3); 2.20 – 1.69 (m, 6H, β-, γ-, δ-CH_2 hhMag); 1.59 – 1.30 (m, 30H, 18H CH_3 Aib, 3H CH_3 hhMag, 9H *t*Bu Boc).

Boc-hhMag-$(Aib)_2$-hhMag-Aib-OMe.

To a solution of Boc-hhMag-OH (120 mg, 0.46 mmol) and HATU (190 mg, 0.50 mmol) in anhydrous acetonitrile, cooled to 0°C, TFA·H-$(Aib)_2$-hhMag-Aib-OMe [obtained by the Boc-deprotection of Boc-$(Aib)_2$-hhMag-Aib-OMe (200 mg, 0.38 mmol) with 30% solution of TFA in CH_2Cl_2] and DIEA (746 µl, 7.38 mmol) were added. The reaction mixture was stirred 2 days at rt. Then the solvent was evaporated, the oily residue was dissolved in EtOAc and the organic solution washed with 10% $KHSO_4$, H_2O, 5% $NaHCO_3$, and H_2O. The organic layer was dried over anhydrous

Na_2SO_4 and evaporated to dryness. The product was purified by *flash* chromatography by eluting with $CHCl_3$, then with the mixture of $CHCl_3$/EtOH (v/v 10:0.1, 10:0.2) and recrystallized from EtOAc/PE. Yield: 51%.

M. p.: 227-229ºC.

IR (KBr): 3397, 3323, 1731, 1680, 1647, 1533 cm^{-1}.

^{1}H NMR ($CDCl_3$, 200 MHz): δ 7.78 (s, 1H, NH); 7.41 (s, 1H, NH); 7.18 (s, 1H, NH); 5.76 (m, 2H, ε-CH hhMag); 5.09 – 4.83 (m, 5H, 1H NH, 4H ζ-CH_2 hhMag); 3.68 (s, 3H, OCH_3); 2.18 – 1.61 (m, 12H, β-, γ-, δ-CH_2 hhMag); 1.52 – 1.30 (m, 33H, 18H CH_3 Aib, 6H CH_3 hhMag, 9H *t*Bu Boc).

3.4.2 Synthesis of Boc-hhMag-Aib-hhMag-(Aib)$_2$-OMe

Boc-hhMag-(Aib)$_2$-OMe

To a solution of Boc-hhMag-OH (400 mg, 1.55 mmol), HOAt (217 mg, 1.60 mmol) and EDC·HCl (307 mg, 1.60 mmol) in anhydrous CH_2Cl_2 cooled to 0ºC, H-(Aib)$_2$-OMe [obtained by catalytic hydrogenation with Pd/C of the corresponding Z-derivative (673 mg, 2.00 mmol) in MeOH] and DIEA (260 μl, 1.55 mmol) were added. The reaction mixture was stirred 5 days at rt. Then the solvent was evaporated and the product was purified by *flash* chromatography by eluting with step-gradient mixtures of PE/EtOAc (v/v 5:1, 4:1, 3:1, 2:1) and CH_2Cl_2/EtOH (v/v 10:0.5). Yield: 43%.

M. p.: 131-132ºC.

IR (KBr): 3349, 1745, 1693, 1666, 1525 cm^{-1}.

^{1}H NMR ($CDCl_3$, 200 MHz): δ 7.57 (s, 1H, NH); 6.50 (s, 1H, NH); 5.73 (m, 1H, ε-CH hhMag); 5.46 (s, 1H, NH); 5.02 – 4.89 (m, 2H, ζ-CH_2 hhMag); 3.67 (s, 3H, OCH_3); 2.12 – 1.95 (m, 6H, β-, γ-, δ-CH_2 hhMag); 1.55 – 1.38 (m, 24H, 12H CH_3 Aib, 3H CH_3 hhMag, 9H *t*Bu Boc).

Boc-Aib-hhMag-(Aib)$_2$-OMe

To a solution of Boc-Aib-OH (320 mg, 1.56 mmol), HOAt (255 mg, 1.87 mmol) and EDC·HCl (360 mg, 1.87 mmol) in anhydrous CH_2Cl_2, cooled to 0ºC, TFA·H-hhMag-(Aib)$_2$-OMe [obtained by the Boc-deprotection of Boc-hhMag-(Aib)$_2$-OMe (370 mg,

1.04 mmol) with 30% solution of TFA in CH_2Cl_2] and DIEA (480 µl, 2.90 mmol) were added. The reaction mixture was stirred 5 days at rt. Then the solvent was evaporated, the oily residue was dissolved in EtOAc and the organic solution washed with 5% $NaHCO_3$ and H_2O. The organic layer was dried over anhydrous Na_2SO_4 and evaporated to dryness. The product was purified by *flash* chromatography by eluting with $CHCl_3$, then with the mixture of $CHCl_3$/EtOH (v/v 10:0.1) and recrystallized from EtOAc/PE. Yield: 35%.

M. p.: 194-196ºC.

IR (KBr): 3377, 3336, 1728, 1691, 1672, 1655, 1524 cm^{-1}.

^{1}H NMR ($CDCl_3$, 200 MHz): δ 7.43 (s, 1H, NH); 7.35 (s, 1H, NH); 6.47 (s, 1H, NH); 5.73 (m, 1H, ε-CH hhMag); 5.10 – 4.91 (m, 3H, 1H NH, 2H ζ-CH_2 hhMag); 3.69 (s, 3H, OCH_3); 2.12 – 1.75 (m, 6H, β-, γ-, δ-CH_2 hhMag); 1.65 – 1.30 (m, 30H, 18H CH_3 Aib, 3H CH_3 hhMag, 9H *t*Bu Boc).

Boc-hhMag-Aib-hhMag-(Aib)$_2$-OMe

To a solution of Boc-hhMag-OH (132 mg, 0.51 mmol), HOAt (85 mg, 0.61 mmol) and EDC·HCl (120 mg, 0.61 mmol) in anhydrous acetonitrile, cooled to 0ºC, TFA·H-Aib-hhMag-(Aib)$_2$-OMe [obtained by the Boc-deprotection of Boc-Aib-hhMag-(Aib)$_2$-OMe (180 mg, 0.34 mmol) with 30% solution of TFA in CH_2Cl_2] and DIEA (100 µl, 0.61 mmol) were added. The reaction mixture was stirred 5 days at rt. Then the solvent was evaporated, the oily residue was dissolved in EtOAc and the organic solution washed with 10% $KHSO_4$, H_2O, 5% $NaHCO_3$, and H_2O. The organic layer was dried over anhydrous Na_2SO_4 and evaporated to dryness. The product was purified by *flash* chromatography by eluting with $CHCl_3$, then with the mixture of $CHCl_3$/EtOH (v/v 10:0.1, 10:0.2). Then it was purified by *flash* chromatography once more by eluting with EtOAc. Yield: 35%.

IR (KBr): 3323, 3302, 1733, 1678, 1653, 1532 cm^{-1}.

^{1}H NMR ($CDCl_3$, 200 MHz): δ 7.67 (s, 1H, NH); 7.49 (s, 1H, NH); 7.37 (s, 1H, NH); 6.69 (s, 1H, NH); 5.76 (m, 2H, ε-CH hhMag); 5.45 (s, 1H, NH); 5.10 – 5.81 (m, 4H, ζ-CH_2 hhMag); 3.68 (s, 3H, OCH_3); 2.15 – 1.71 (m, 12H, β-, γ-, δ-CH_2 hhMag); 1.58 – 1.30 (m, 33H, 18H CH_3 Aib, 6H CH_3 hhMag, 9H *t*Bu Boc).

3.4.3 Synthesis of Boc-hhMag-(Ala)$_2$-hhMag-Ala-OMe

Boc-hhMag-Ala-OMe

To a solution of Boc-hhMag-OH (2 g, 7.77 mmol) and HATU (3.6 g, 9.47 mmol) in anhydrous acetonitrile, cooled to 0^{o}C, HCl·H-Ala-OMe (1.31 g, 9.38 mmol) and DIEA (3.1 ml, 18.76 mmol) were added. The reaction mixture was stirred 5 days at rt. Then the solvent was evaporated, the oily residue was dissolved in EtOAc and the organic solution washed with 10% $KHSO_4$, H_2O, 5% $NaHCO_3$, and H_2O. The organic layer was dried over anhydrous Na_2SO_4 and evaporated to dryness. The product was purified by *flash* chromatography by eluting with step-gradient mixtures of PE/EtOAc (v/v 4:1, 3:1). Oil. Yield: 30%.

IR (in a film): 3321, 1754, 1685, 1653, 1524 cm^{-1}.

^{1}H NMR ($CDCl_3$, 200 MHz): δ 6.87 (d, 1H, NH); 5.75 (m, 1H, ε-CH hhMag); 5.12 (s, 1H, NH); 5.05 – 4.91 (m, 2H, ζ-CH_2 hhMag); 4.57 (m, 1H, CH Ala); 3.74 (s, 3H, OCH_3); 2.15 – 1.75 (m, 6H, β-, γ-, δ-CH_2 hhMag); 1.55 – 1.35 (m, 15H, 3H CH_3 Ala, 3H CH_3 hhMag, 9H *t*Bu Boc).

Boc-Ala-hhMag-Ala-OMe

To a solution of Boc-Ala-OH (904 mg, 4.78 mmol), HOAt (653 mg, 4.80 mmol) and EDC·HCl (920 mg, 4.80 mmol) in anhydrous acetonitrile, cooled to 0^{o}C, TFA·H-hhMag-Ala-OMe [obtained by the Boc-deprotection of Boc-hhMag-Ala-OMe (820 mg, 2.39 mmol) with 30% solution of TFA in CH_2Cl_2] and DIEA (4 ml, 24 mmol) were added. The reaction mixture was stirred one day at rt. Then the solvent was evaporated, the oily residue was dissolved in EtOAc and the organic solution washed with 10% $KHSO_4$, H_2O, 5% $NaHCO_3$ and H_2O. The organic layer was dried over anhydrous Na_2SO_4 and evaporated to dryness. The product was recrystallized from EtOAc/PE. Yield: 73%.

M. p.: 157-158ºC.

IR (KBr): 3294, 1744, 1682, 1646, 1529 cm^{-1}.

^{1}H NMR ($CDCl_3$, 200 MHz): δ 6.78 (m, 2H, NH); 5.76 (m, 1H, ε-CH hhMag); 5.03 (s, 1H, NH); 5.03 – 4.90 (m, 2H, ζ-CH_2 hhMag); 4.54 (m, 1H, CH Ala); 4.07 (m, 1H, CH

Ala); 3.74 (s, 3H, OCH_3); 2.20 – 1.75 (m, 6H, β-, γ-, δ-CH_2 hhMag); 1.55 – 1.35 (m, 18H, 6H CH_3 Ala, 3H CH_3 hhMag, 9H *t*Bu Boc).

Boc-$(Ala)_2$-hhMag-Ala-OMe

To a solution of Boc-Ala-OH (640 mg, 3.38 mmol), HOAt (460 mg, 3.38 mmol) and EDC·HCl (650 mg, 3.38 mmol) in anhydrous acetonitrile, cooled to 0°C, TFA·H-Ala-hhMag-Ala-OMe [obtained by the Boc-deprotection of Boc-Ala-hhMag-Ala-OMe (700 mg, 1.69 mmol) with 30% solution of TFA in CH_2Cl_2] and DIEA (2.8 ml, 17 mmol) were added. The reaction mixture was stirred 2 days at rt. Then the solvent was evaporated, the oily residue was dissolved in EtOAc and the organic solution washed with 10% $KHSO_4$, H_2O, 5% $NaHCO_3$ and H_2O. The organic layer was dried over anhydrous Na_2SO_4 and evaporated to dryness. The product was recrystallized from EtOAc/PE. Yield: 75%.

M. p.: 152-153ºC.

IR (KBr): 3368, 1748, 1662, 1500 cm^{-1}.

^{1}H NMR ($CDCl_3$, 200 MHz): δ 6.84 (m, 2H, NH); 6.63 (d, 1H, NH); 5.75 (m, 1H, ε-CH hhMag); 5.05 – 4.89 (m, 3H, 1H NH, 2H ζ-CH_2 hhMag); 4.54 (m, 1H, CH Ala); 4.34 (m, 1H, CH Ala); 4.13 (m, 1H, CH Ala); 3.74 (s, 3H, OCH_3); 2.15 – 1.75 (m, 6H, β-, γ-, δ-CH_2 hhMag); 1.55 – 1.35 (m, 21H, 9H CH_3 Ala, 3H CH_3 hhMag, 9H *t*Bu Boc).

Boc-hhMag-$(Ala)_2$-hhMag-Ala-OMe

To a solution of Boc-hhMag-OH (320 mg, 1.24 mmol), HOAt (200 mg, 1.47 mmol) and EDC·HCl (300 mg, 1.47 mmol) in anhydrous acetonitrile, cooled to 0°C, TFA·H-$(Ala)_2$-hhMag-Ala-OMe [obtained by the Boc-deprotection of Boc-$(Ala)_2$-hhMag-Ala-OMe (300 mg, 0.62 mmol) with 30% solution of TFA in CH_2Cl_2] and DIEA (1.2 ml, 7.5 mmol) were added. The reaction mixture was stirred one day at room temperature. Then the solvent was evaporated, the oily residue was dissolved in EtOAc and the organic solution washed with 10% $KHSO_4$, H_2O, 5% $NaHCO_3$, and H_2O. The organic layer was dried over anhydrous Na_2SO_4 and evaporated to dryness. The product was purified by *flash* chromatography by eluting with $CHCl_3$, then with the mixtures of $CHCl_3$/EtOH (v/v 10:0.1, 10:0.2) and recrystallized from EtOAc/PE. Yield: 78%.

IR (KBr): 3300, 1728, 1658, 1533 cm^{-1}.

^{1}H NMR ($CDCl_3$, 200 MHz): δ 7.76 (d, 1H, NH); 7.15 (d, 1H, NH); 6.96 (s, 1H, NH); 6.41 (d, 1H, NH); 5.77 (m, 2H, ε-CH hhMag); 5.09 – 4.85 (m, 5H, 1H NH, 4H ζ-CH_2 hhMag); 4.50 (m, 1H, CH Ala); 4.26 (m, 1H, CH Ala); 4.18 (m, 1H, CH Ala); 3.71 (s, 3H, OCH_3); 2.18 – 1.59 (m, 12H, β-, γ-, δ-CH_2 hhMag); 1.52 – 1.38 (m, 24H, 9H CH_3 Ala, 6H CH_3 hhMag, 9H *t*Bu Boc).

REFERENCES

1. Kotrotsiou, O.; Kotti, K.; Dini, E.; Kammona, O.; Kiparissides, C. *J. Phys.: Confer. Ser.* **2005**, *10*, 281.
2. Fairman, R.; Åkerfeldt, K. S. *Curr. Opin. Struct. Biol.* **2005**, *15*, 453.
3. Toniolo, C.; Crisma, M.; Formaggio, F.; Peggion, C.; Epand, R. F.; Epand, R. M. *Cell. Mol. Life Sci.* **2001**, *58*, 1179.
4. Ramachandran, G.N.; Sasisekharan, V. *Adv. Protein Chem.* **1968**, *23*, 283.
5. IUPAC-IUB Commission on Biochemical Nomenclature. *Biochemistry* **1970**, *9*, 3471.
6. Toniolo, C.; Benedetti, E. *Trends Biochem. Sci.* **1991**, *16*, 350.
7. Donohue, J. *Proc. Natl. Acad. Sci. USA*. **1953**, *39*, 470.
8. Ramachandran, G.N.; Venkatachalam, C.M.; Krimm, S. *Biophys. J*. **1966**, *6*, 849.
9. Baker, E.N.; Hubbard, E. *Prog. Biophys. Mol. Biol.* **1984**, *44*, 97**.**
10. Robbins, A.H.; Stout. C.D. *Protein Struct. Funct. Genet.* **1989**, *5*, 289.
11. Pathak, D.; Ollis, D. *J. Mol. Biol.* **1990**, *214*, 497.
12. Kostrikis, L.G.; Liu, D.J.; Day, L.A. *Biochemistry* **1994**, *33*, 1694.
13. Venkatachalam, C.M. *Biopolymers* **1968**, *6*, 1425.
14. Toniolo, C.; Crisma, M.; Formaggio, F.; Valle, G.; Cavicchioni, G.; Précigoux, G.; Aubry, A.; Kamphuis, J. *Biopolymers* **1993**, *33*, 1061.
15. Toniolo, C.; Crisma, M.; Formaggio, F.; Peggion, C. *Biopolymers (Pept. Sci.).* **2001**, *60*, 396.
16. Toniolo, C.; Crisma, M.; Formaggio, F.; Peggion, C.; Broxterman, Q. B.; Kaptein, B. *Biopolymers (Pept. Sci.)* **2004**, *76*, 162.
17. Toniolo, C.; Formaggio, F.; Tognon, S.; Broxterman, Q. B.; Kaptein, B.; Huang, R.; Setnicka, V.; Keiderling, T. A.; McColl, I. H.; Hecht, L.; Baron, L. D. *Biopolymers*. **2004**, *75*, 32.
18. Ramachandran, G. N.; Chandrasekharan, R. *Indian J. Biochem. Biophys*. **1972**, *9*, 1.
19. Burgess, A. W.; Leach, S. J. *Biopolymers*. **1973**, *12*, 2599.

20. Pavone, V.; Di Blasio, B.; Santini, A.; Benedetti, E.; Pedone, C.; Toniolo, C.; Crisma, M. *J. Mol. Biol.* **1990**, *214*, 633.
21. Toniolo, C.; Crisma, M.; Bonora, G.M.; Benedetti, E.; Di Blasio, B.; Pavone, V.; Pedone, C.; Santini, A. *Biopolymers* **1991**, *31*, 129.
22. Formaggio, F.; Crisma, M.; Rossi, P.; Scrimin, P.; Kaptein, P.; Broxterman, Q. B.; Kamphuis, J.; Toniolo, C. *Chem. Eur. J.* **2000**, *6*, 4498.
23. Polese, A.; Formaggio, F.; Crisma, M.; Valle, G.; Toniolo, C.; Bonora, G. M.; Broxterman, Q. B.; Kamphius, J. *Chem. Eur. J.* **1996**, *2*, 1104.
24. Toniolo, C.; Polese, A.; Formaggio, F.; Crisma, M.; Kamphuis, J. *J. Am. Chem. Soc.* **1996**, *118*, 2744.
25. Manning, M.; Woody, R. *Biopolymers* **1991**, *31*, 569.
26. Yoder, G.; Polese, A.; Silva, R. A. G. D.; Formaggio, F.; Crisma, M.; Broxterman, Q. B.; Kamphuis, J.; Toniolo, C.; Keiderling, T. A. *J. Am. Chem. Soc.* **1997**, *119*, 10278.
27. Mammi, S.; Rainaldi, M.; Bellanda, M.; Schievano, E.; Peggion, E.; Broxterman, Q. B.; Formaggio, F.; Crisma, M.; Toniolo C. *J. Am. Chem. Soc.* **2000**, *122*, 11735.
28. Bolin, K. A.; Millhauser, G. L. *Acc. Chem. Res*. **1999**, *32*, 1027.
29. Scarso, A.; Scheffer, U.; Gobel, M.; Broxterman, Q. B.; Kaptein, B.; Formaggio, F.; Toniolo, C.; Scrimin, P. *Proc. Natl. Acad. Sci. USA* **2002**, *99*, 5144.
30. Ide, T.; Tsutsui, H.; Kinugawa, S.; Utsumi, H.; Kang, D.; Hattori, N.; Uchida, K.; Arimura, K.; Egashira, K.; Takeshita A. *Circ. Res.* **1999**, 356.
31. Bott, A. W. *Curr. Separ.* **1999**, *18,* 47.
32. Wagner, R.W.; Lindsey, J. S. *J. Am. Chem. Soc*. **1994**, *116*, 9759.
33. Wagner, R.W.; Lindsey, J. S.; Seth, J.; Palaniappan, V.; Bocian, D. *J. Am. Chem. Soc.* **1996**, *118*, 3996.
34. Yanagisawa, K.; Morita, T.; Rimura, S. *J. Am. Chem. Soc.* **2004**, *126*, 12780.
35. Brea, R. J.; Castedo, L.; Granja, J. R.; Angeles Herranz, M.; Sanchez, L.; Martin, N.; Seitz, W.; Guldi, D. M. *Proc. Natl. Acad. Sci. USA* **2007**, *104*, 5291.
36. Yasutomi, S.; Morita, T.; Imanishi, Y.; Rimura, S. *Science* **2004**, *304*, 1944.
37. Beratan, D. N.; Betts, J. N.; Onuchic, J. N. *J. Phys. Chem*. **1992**, *96*, 2852.

38. Birch, D.; Coyle, J. D.; Hill, R. R.; Jeffs, G. E. *J. Chem. Soc., Chem. Commun*. **1986**, 293.
39. Ichinose, S.; Minato, T. *J. Phys: Condens. Matter* **1993**, *5*, 9145.
40. Clarke D. L.; Collins, M. A. *Biophys. J.* **1992**, *61*, 316.
41. Fukuzumi, S.; Yoshida, Y.; Okamoto, K.; Imahori, H.; Araki, Y.; Ito, O. *J. Am. Chem. Soc.* **2002**, *124*, 6794.
42. Whitesell, J. K.; Chang, H. K.; Fox, M. A.; Galoppini, E.; Watkins, D. M.; Fox**,** H.; Hong, B. *Pure & Appl. Chem.* **1996**, *68*, 1469.
43. Pistolis, G.; Andreopoulou, A.; Angelos Malliaris, K.; Kallitsis, J. K. *Macromolecules.* **2004**, *37,* 1524.
44. McGimpsey, W. G.; Samaniego, W. N.; Chen, L.; Wang, F. *J. Phys. Chem. A* **1998**, *45*, 8679.
45. Castellan, A.; Kessab, L.; Grelier, S.; Nourmamode, A. *J. Chem. Soc., Perkin Trans.* **1993**, 953.
46. Closs, G. L.; Johnson, M. D.; Miller, J. R.; Piotrowiak, P. J. *J. Am. Chem. Soc.* **1989**, *111*, 3751.
47. Tan, Z.; Kote, R.; Samaniego, W. N.; Weininger, S. J.; McGimpsey, W. G. *J. Phys. Chem. A.* **1999**, *103*, 7612.
48. Yeow, E. K. L.; Sintic, P. J.; Cabral, N. M.; Reek, J. N. H.; Crossley, M. J.; Ghiggino, K. P. *Phys. Chem. Chem. Phys.* **2000**, *2*, 4281.
49. Schmidt, J. A.; Siemiarczuk, A.; Weedon, A. C.; Bolton, J. R. *J. Am.Chem. Soc.* **1985**, *107*, 6112.
50. Anglos, D.; Bindra, V.; Kuki, A. *J. Chem. Soc., Chem. Commun.* **1994**, 213.
51. Ogawa, M. Y.; Fan, J.; Fedorova, A.; Hong, J.; Kharenko, O. A.; Kornilova, A. Y.; Lasey R. C.; Xie, F. *J. Braz. Chem. Soc.* **2006**, *17*, 1516.
52. Formaggio, F.; Crisma, M.; Scipionato, L.; Antonello, S.; Maran, F.; Toniolo, C. *Org. Lett.* **2004**, *6*, 2753.
53. Konishi, K.; Yokotake, Y.; Ishibashi, T. *J. Mass Spectrom. Soc. Jpn.* **2002**, *50*, 229.
54. Sisido, M.; Hoshino, S.; Kusano, H.; Kuragaki, M.; Makino, M.; Sasaki, H.; Smith, T. A.; Ghiggino, K. P. *J. Phys. Chem. B* **2001**, *105,* 10407.

55. Tamiaki, H.; Nomura, K.; Maruyama, K. *Bull. Chem. Soc. Jpn.* **1994**, *67*, 1863.
56. Pispisa, B.; Stella, L.; Venanzi, M.; Palleschi, A.; Viappiani, C.; Polese, A.; Formaggio, F.; Toniolo, C. *Macromolecules.* **2000,** *33,* 906.
57. Shin, Y. K.; Newton, M. D.; Isied, S. S. *J. Am. Chem. Soc.* **2003**, *125*, 3722.
58. Hol, W. G. J.; van Duijnen, P. T.; Berendsen, H. J. C. *Nature.* **1978**, *273*, 443.
59. Fox, M. A.; Galoppini, E. *J. Am. Chem. Soc.* **1997**, *119,* 5277.
60. Chiarani, S. Tesi di laurea. Università degli Studi di Padova. **2004**.
61. Murov, S. L.; Carmichael, I.; Gordon, L. H. Handbook of Photochemistry. Dekker, New York, **1993**, 2nd edition.
62. Berova, N.; Borhan, B.; Dong, J. G.; Guo, J.; Huang, X.; Karnaukhova, E.; Kawamura, A.; Lou, J.; Matile, S.; Nakanishi, K.; Rickman, K.; Su, J.; Tan, H; Zanze, I. *Pure & Appl. Chem.* **1998**, *70*, 377.
63. Matile, S.; Berova, N.; Nakanishi, K.; Fleischhauer, J.; Woody, R. W. *J. Am. Chem. Soc.* **1996,** *118*, 5198.
64. Berova, N.; Gargiulo, D.; Derguini, F.; Nakanishi, K.; Harada, N. *J. Am. Chem. Soc.* **1993**, *115*, 4769.
65. Cai, G.; Bozhkova, N.; Odingo, J.; Berova, N.; Nakanishi, K. *J. Am. Chem. Soc.* **1993**, *115*, 7192.
66. Harada, N.; Chen, S.-M. L.; Nakanishi, K. *J. Am. Chem. Soc.* **1975**, *97*, 5345.
67. Heyn, M. P. *J. Phys. Chem*. **1975**, *79*, 2424.
68. Chen, S. L.; Harada, N.; Nakanishi, K. *J. Am. Chem. Soc.* **1974**, *96*, 7352.
69. Canceill, J.; Collet, A.; Jacques, J. *J. Chem. Soc., Perkin Trans. II.* **1982**, 83.
70. Toniolo, C.; Formaggio, F.; Crisma, M.; Schoemaker, H. E.; Kamphuis, J. *Tetrahedron: Asymm.* **1994**, *5*, 507.
71. Nishino, N.; Mihara, H.; Hasegawa, R.; Yanai, T.; Fujimoto, T. *J. Chem. Soc., Chem. Commun.* **1992**, 692.
72. Redl, F. X.; Lutz, M.; Daub, J. *Chem. Eur. J.* **2001**, *7*, 5350.
73. Ribo, J. M.; Bofill, J. M.; Crusats J.; Rubires, R. *Chem. Eur. J.* **2001**, *7*, 2733.

74. Tanaka, K.; Itagaki, Y.; Satake, M.; Naoki, H.; Yasumoto, T.; Nakanishi, K.; Berova, N.; *J. Am. Chem. Soc.* **2005**, *127*, 9561.
75. Borovkov, V. V.; Hembury, G. A.; Inoue, Y. *Acc. Chem. Res*. **2004**, *37*, 449.
76. Paolesse, R.; Monti, D.; La Monica, L.; Venanzi, M.; Frosio, A.; Nardis, S.; Di Natale, C.; Martinelli, E.; D'Amico, A. *Chem. Eur. J.* **2002**, *8*, 2476.
77. Borovkov, V. V.; Lintuluoto, J. M.; Sugiura, M.; Inoue, Y.; Kuroda, R. *J. Am. Chem. Soc.* **2002**, *124*, 11282.
78. Borovkov, V. V.; Fujii, I.; Muranaka, A.; Hembury, G.; Tanaka, T.; Ceulemants, A.; Kobayashi, N.; Inoue, Y. *Angew. Chem. Int. Ed.* **2004**, *43*, 5481.
79. Huang, X.; Rickman, B. H.; Borhan, B.; Berova, N.; Nakanishi, K. *J. Am. Chem. Soc.* **1998**, *120,* 6185.
80. Borovkov, V. V.; Lintuluolo, J.; Fujiki, M.; Inoue, Y. *J. Am. Chem. Soc.* **2000**, *122,* 4403.
81. Huang, X.; Fujioka, N.; Pescitelli, G.; Koehn, F. E.; Williamson, R. T.; Nakanishi, K.; Berova, N. *J. Am. Chem. Soc.* **2002**, *124*, 10320.
82. Borovkov, V. V.; Lintuluolo, J.; Inoue, Y. *J. Phys. Chem. A* **2000**, *104,* 9213.
83. Borovkov, V. V.; Hembury, G. A.; Yamamoto, N.; Inoue, Y. *J. Phys. Chem. A* **2003**, *107,* 8677.
84. Borovkov, V. V.; Lintuluoto, J.; Hembury, G. A.; Sugiura, M.; Arakawa, R.; Inoue Y. *J. Org. Chem.* **2003**, *68*, 7176.
85. Lintuluolo, J.; Borovkov, V. V.; Inoue, Y. *J. Am. Chem. Soc.* **2002**, *124*, 13676.
86. MacMillan, J. B.; Molinski, T. F. *J. Am. Chem. Soc.* **2004**, *126*, 9944.
87. Balaz, M.; Holmes, A. E.; Benedetti, M.; Rodriguez, P. C.; Berova, N.; Nakanishi, K.; Proni, G. *J. Am. Chem. Soc.* **2005**, *127*, 4172.
88. Jiang, H.; Huang, X.; Nakanishi, K.; Berova N. *Tetrahedron Lett.* **1999**, *40*, 7645.
89. Formaggio, F.; Crisma, M.; Toniolo, C. *Biopolymers.* **1996**, *38*, 301.
90. Cammidge, A. N.; Scaife, P. J.; Berber, G.; Hughes, D. L. *Org. Lett.* **2005**, *7*, 3417.
91. Imahori, H.; Sekiguchi, Y.; Ito, O.; Sakata, Y.; Fukuzumi, S. *J. Am. Chem. Soc.* **2002**, *124*, 5165.

92. Kashiwada, A.; Takeuchi, Y.; Watanabe, H.; Mizuno, T.; Yasue, H.; Kitagawa, K.; Iida, K.; Wang, Z.; Nozawa, T.; Kawai, H.; Nagamura, T.; Kurono, Y.; Nango M. *Tetrahedron Lett.* **2000**, *41*, 2115.
93. Ogawa, T.; Nishimoto, Y.; Yoshida, N.; Ono, N.; Osuka, A. *Angew. Chem. Int. Ed.* **1999**, *38*, 176.
94. Shi, X.; Liebeskind, L. S. *J. Org. Chem*. **2000**, *65*, 1665.
95. Cho, H. S.; Song, N. W.; Kim, Y. H.; Jeoung, S. C.; Hahn, S.; Kim, D.; Kim, S. K.; Yoshida, N.; Aratani, N.; Osuka, A. *J. Phys. Chem. A* **2000**, *104*, 3287.
96. Yoshida N.; Osuka, A. *Org. Lett.* **2000,** *2*, 2963.
97. Fujitsuka, M.; Okada, A.; Tojo, S.; Takei, F.; Onitsuka, K.; Takahashi, S.; Majima, T.; *J. Phys. Chem. B.* **2004,** *108,* 11935.
98. Fujitsuka, M.; Hara, M.; Tojo, S.; Okada, A.; Troiani, V.; Solladie, N.; Majima, T. *J. Phys. Chem. B.* **2005**, *109*, 33.
99. Dunetz, J. R.; Sandstrom, C.; Young, E. R.; Baker, P.; Van Name, S. A.; Cathopolous, T.; Fairman, R.; de Paula, J. C.; Åkerfeldt, K. S. *Org. Lett.* **2005**, *7*, 2559.
100. Pasternack, R. F.; Giannetto, P.; Gibbs, E. J. *J. Am. Chem. Soc.* **1991**, *113*, 7799.
101. Arutyunyan, A. M.; Rafikova, E. R.; Drachev, V. A.; Dob, E. N. *Biochemistry (Moscow)* **2001**, *66*, 1378.
102. Arai, T.; Inudo, M.; Ishimatsu, T.; Akamatsu, C.; Tokusaki, Y.; Sasaki, T.; Nishino, N. *J. Org. Chem.* **2003**, *68*, 5540.
103. Tamiaki, H.; Suzuki, S.; Maruyama, K. *Bull. Chem. Soc. Jpn.* **1993**, *66*, 2633.
104. Tamiaki, H.; Nomura, K.; Maruyama, K. *Bull. Chem. Soc. Jpn.* **1993**, *66*, 3062.
105. Arai, T.; Maruo, N.; Sumida, Y.; Korosue C.; Nishino N. *J. Chem. Soc., Chem. Commun.* **1999**, 1503.
106. Jeong, D. H.; Jang, S. M.; Hwang, I.-W.; Kim, D.; Yoshida, N.; Osuka, A. *J. Phys. Chem. A* **2002,** *106,* 11054.
107. Ema, T.; Nemugaki, S.; Tsuboi, S.; Utaka M. *Tetrahedron Lett.* **1995**, *36*, 5905.
108. Huang, X.; Nakanishi, K.; Berova, N. *Chirality.* **2000**, *12*, 237.
109. Oancea, S.; Formaggio, F.; Campestrini, S.; Broxterman, Q. B.; Kaptein, B.; Toniolo, C. *Biopolymers (Biospectroscopy)* **2003**, *72*, 105.

110. Minaev, B.; Ågren, H. *Chem. Phys.* **2005**, *315*, 215.
111. Polese, A.; Formaggio, F.; Crisma, M.; Valle, G.; Toniolo, C.; Bonora, G. M.; Broxterman, Q. B.; Kamphuis, J. *Chem. Eur. J.* **1996**, *2*, 1104.
112. Mihara, H.; Nishino, N.; Hasegawa, R.; Yanai, T.; Fujimoto, T. *Chem. Lett.* **1992**, 1805.
113. Kim, S.; Ayala, I.; Steenhuis, J. J.; Gonzalez, E. T.; Barry, B. A. *Biochim. Biophys. Acta* **1998**, *1364*, 337.
114. Wojciechowska, E.; Włochowicza, A.; Wysockib, M.; Pielesza, A.; Wesełucha-Birczynska, A. *J. Mol. Struct.* **2002**, *614*, 355.
115. Ludlam, C. F. C.; Arkin, I. T.; Liu, X.-M.; Rothman, M. S.; Rath, P.; Aimoto, S.; Smith, S. O.; Engelman, D. M.; Rothschild, K. J. *Biophys. J.* **1996**, *70*, 1728.
116. Wang, R.; Sivakumar, V.; Wade Johnson, T.; Hastings, G. *Biophys. J.* **2004**, *86*, 1061.
117. Fang, C.; Wang, J.; Charnley, A.K.; Barber-Armstrong, W.; Smith III, A. B.; Decatur, S. M.; Hochstrasser, R.M. *Chem. Phys. Lett.* **2003**, *382*, 586.
118. Barber-Armstrong, W.; Donaldson, T.; Wijesoorija, H.; Silva, D.; Decatur, S. M. *J. Am. Chem. Soc.* **2004**, *126*, 2339.
119. Huang, R.; Kubelka, J.; Barber-Armstrong, W.; Silva, R. A. G. D.; Decatur, S. M.; Keiderling, T. A. *J. Am. Chem. Soc.* **2004**, *126*, 2346.
120. Decatur, S. M. *Biopolymers*. **2000**, *54*, 180.
121. Volk, M.; Pozo Ramajo A.; Petty, S. A.; Starzyk, A.; Decatur, S. M. *Central Laser Facility Annu. Report* **2004**/**2005**, 173.
122. Silva, R. A. G. D.; Barber-Armstrong, W.; Decatur, S. M. *J. Am. Chem. Soc.* **2003**, *125*, 13674.
123. Gordon, L. M.; Mobley, P. W.; Lee, W.; Eskandary, S.; Kaznessis, Y N.; Sherman, M. A.; Waring A. J. *Protein Sci.* **2004**, *13*, 1012.
124. Abell, A. D. *Lett. Pep. Sci.* **2002**, *8*, 267.
125. Smith, A. B.; Hirschmann, R.; Pasternak, A.; Guzman, M. C.; Yokohama, A.; Sprengeler, P. A.; Darke, P. L.; Emini, E. A.; Schleif, W. A. *J. Am. Chem. Soc.* **1995**, *117*, 11113.

126. Kim, E. E.; Baker, C. T.; Dwyer, M. D.; Murcko, M. A.; Rao, B. G.; Tung, R. D.; Navia, M. A. *J. Am. Chem. Soc*. **1995**, *117*, 1181.
127. ten Brink, H. T.; Rijkers, D. T. S.; Kemmink, J.; Hilbers, H. W.; Liskamp, R. M. J. *Org. Biomol. Chem.* **2004**, *2*, 2658.
128. Tong, Y.; Olczak, J.; Zabrocki, J.; Gershengorn, M. C.; Marshall G. R.; Moeller K. D. *Tetrahedron* **2000**, *56*, 9791.
129. Dekker, F. J.; de Mol, N. J.; Fischer, M. J. E.; Kemmink, J.; Liskamp, R. M. J. *Org. Biomol. Chem.* **2003**, *1*, 3297.
130. Flink, B. E.; Kym, P. R.; Katzenellenbogen, J. A. *J. Am. Chem. Soc*. **1998**, *120*, 4334.
131. Bijani, C.; Varray, S.; Lazaro, R.; Martinez, J.; Lamatya, F.; Kiefferb, N. *Tetrahedron Lett.* **2002**, *43*, 3765.
132. Wei, Q.; Harran, S.; Harran, P. G. *Tetrahedron* **2003**, *59*, 8947.
133. Lambert, J. N.; Mitchell, J. P.; Roberts, K. D. *J. Chem. Soc*., *Perkin Trans. 1*. **2001**, 471.
134. Hebach C.; Kazmaier U. *J. Chem. Soc., Chem. Commun*. **2003**, 596.
135. Scholtz, J. M.; Qian, H.; Robbins, V. H.; Baldwin, R. L. *Biochemistry* **1993**, *32*, 9668.
136. Ghadiri, M. R.; Fernholz, A. K. *J. Am. Chem. Soc.* **1990**, *112*, 9633.
137. Ruan, F.; Chen, Y.; Hopkins, P. B. *J. Am. Chem. Soc.* **1990**, *112*, 9403.
138. Camarero, J. A.; Giralt, E.; Andrei, D. *Tetrahedron Lett.* **1995**, *7*, 1137.
139. Galande, A. K.; Trent, J. O.; Spatola, A. F. *Biopolymers*. **2003**, *71*, 534.
140. Fujimoto, K.; Oimoto, N.; Katsuno K.; Inouye M. *J. Chem. Soc., Chem. Commun.* **2004**, 1280.
141. Grubbs, R. H. *Tetrahedron*. **2004**, *60*, 7117.
142. Grubbs, R. H.; Chang, S. *Tetrahedron.* **1998**, *54*, 4413.
143. Chatterjee, A. K.; Morgan, J. P.; Scholl, M.; Grubbs, R. H. *J. Am. Chem. Soc.* **2000,** *122*, 3783.
144. Pschirer, N. G.; Fu, W.; Adams, R. D.; Bunz, U. H. F. *Chem. Commun.* **2000**, 87.
145. Biagini, S.; Gibson, S. E.; Keen, S. P. *J. Chem. Soc., Perkin Trans. 1* **1998**, 2485.
146. Gilliom, L. R.; Grubbs, R. H. *J. Am. Chem. Soc.* **1986**, *108*, 733.

147. Hofmann, M.; Puskas, J. E.; Weiss, K. *Eur. Polymer J.* **2002**, *38*, 19.
148. Trnka, T. M.; Morgan, J. P.; Sanford, M. S.; Wilhelm, T. E.; Scholl, M; Choi, T.-L.; Ding, S.; Day, M. W.; Grubbs, R. H. *J. Am. Chem. Soc.* **2003**, *125*, 2546.
149. Melis, K.; De Vos, D.; Jacobs, P.; Verpoort, F. *J. Mol. Catalysis A: Chem.* **2001**, *169*, 47.
150. Fürstner, A.; Ackermann L. *J. Chem. Soc., Chem. Commun.* **1999**, 95.
151. Hoveyda, A. H.; Zhugralin, A. R. *Nature.* **2007**, *450*, 243.
152. Aldhart, C.; Chen, P. *J. Am. Chem. Soc.* **2004**, *126*, 3496.
153. Yamamoto, K.; Biswas, K.; Gaula, C.; Danishefskya, S. J. *Tetrahedron Lett.* **2003**, *44*, 3297.
154. Thanh, G. V.; Loupy, A. *Tetrahedron Lett.* **2003**, *44*, 9091.
155. Kotha, S.; Sreenivasachary, N.; Mohanraja K.; Durani S. *Bioorg. Med. Chem. Lett.* **2001**, *11*, 1421.
156. Osipov, S. N.; Dixneuf, P. *Russ. J. Org. Chem.* **2003**, *39,* 1211.
157. Hammer, K.; Romming, C.; Undheim, K. *Tetrahedron*. **1998**, *54*, 10837.
158. Tjen, K. C. M. F.; Kinderman, S. S.; Schoemaker, H. E.; Hiemstra H.; Rutjes, F. P. J. T. *J. Chem. Soc., Chem. Commun.* **2000**, 699.
159. Rutjes, F. P. J. T.; Wolf, L. B.; Schoemaker, H. E. *J. Chem. Soc*., *Perkin Trans. 1*. **2000**, 4197.
160. Conde-Frieboes, K.; Andersen S.; Breinholt J. *Tetrahedron Lett.* **2000**, *41*, 9153.
161. Piscopio, A. D.; Miller, J. F.; Koch, K. *Tetrahedron.* **1999**, *55*, 8189.
162. Pernerstorfer, J.; Schuster M.; Blechert S. *J. Chem. Soc., Chem. Commun*. **1997**, 1949.
163. Sastry, T. V. R. S.; Banerji, B.; Kiran Kumar, S.; Kunwar, A. C.; Das, J.; Nandya J. P.; Iqbal, J. *Tetrahedron Lett.* **2002**, 43, 7621.
164. Chapman, R. N.; Dimartino, G.; Arora, P. S. *J. Am. Chem. Soc.* **2004**, *126*, 12252.
165. Qian, H.; Schellman, J. A. *J. Phys. Chem.* **1992**, *96*, 3987.
166. Reichwein, J. F.; Wels, B.; Kruijtzer, J. A. W.; Versluis C.; Liskamp, R. M. J. *Angew. Chem. Int. Ed.* **1999**, *38*, 3684.

167. Prabhakaran, E. N.; Rajesh, V.; Dubey S.; Iqbal, J. *Tetrahedron Lett.* **2001**, *42*, 339.

168. Blackwell, H. E.; Grubbs, R. H. *Angew. Chem., Int. Ed.* **1998**, *37*, 3281.

169. Saviano, M.; Benedetti, E.; Vitale, R. M.; Kaptein, B; Broxterman, Q. B.; Crisma, M.; Formaggio, F.; Toniolo, C. *Macromolecules*. **2002**, *35*, 4204.

170. von Arx, E.; Faupel, M.; Brugger, M. *J. Chromatogr.* **1976**, *120*, 224.

171. Connel, E.; Dixon, G.H.; Hones, C.S. *Can. J. Biochem. Physiol*. **1985**, *33*, 416.

ACKNOWLEDGEMENTS

Though there were many people around me to help, to give an advise, to make the time unforgettable and the life unpredictable, there are two persons I would like to thank especially. Actually, it is difficult to imagine one without another. The first one is Prof. C. Toniolo, whose knowledges in the field of peptide chemistry are almost unlimited, and whose ability to head the laboratory and organize its work make a really great impression. The second one is Prof. F. Formaggio. He was the first Italian I have meet and who made a lot, though he could not know it, to drastically change my way of thinking. These two persons gave me a possibility to acquire important knowledges and precious experience useful both for the future work and carrier, and in the life. In addition, they gave me an opportunity to see Italy "from inside", and I am very grateful for this.

Everytime in the lab there were many people, not only Italians but also coming from all the world. And for sure the central person was Dr. A. Moretto, who looked after everything. He created a friendly atmosphere and with his huge practical experience helped to everyone needed in an advise.

Though being completely emerged in a work, Dr. P. Geotti-Bianchini gave me a part of his time. I am very grateful for his friendship. A possibility to share a lunch in mensa gave me a chance to know more about Italians and their life.

I would like to thank also Dr. C. Peggion, Dr. M. De Zotti and Dr. M. Crisma for the readiness to help whenever I came.

My greatest appreciations go to my russian friends in Padova who made me feel home and foreigners who gave me an opportunity to have an idea about the world.